

**Lyotropic liquid crystals as templates for advanced materials**

Journal:	<i>Journal of Materials Chemistry A</i>
Manuscript ID	TA-REV-04-2021-002748.R1
Article Type:	Review Article
Date Submitted by the Author:	15-Jun-2021
Complete List of Authors:	Saadat, Younes; New Mexico State University, Chemical and Materials Engineering Imran, Omar; Yale University, Chemical and Environmental Engineering; University of Pennsylvania, Chemical and Biomolecular Engineering Osuji, Chinedum; University of Pennsylvania, Chemical and Biomolecular Engineering; Yale University, Chemical and Environmental Engineering Foudazi, Reza; New Mexico State University, Chemical and Materials Engineering

Lyotropic liquid crystals as templates for advanced materials

Younes Saadat ¹, Omar Q. Imran ^{2,3}, Chinedum O. Osuji ^{3*}, Reza Foudazi ^{1†}

¹ Department of Chemical and Materials Engineering, New Mexico State University, Las Cruces, NM 88003, USA

² Department of Chemical and Environmental Engineering, Yale University, New Haven CT 06520

³ Department of Chemical and Biomolecular Engineering, University of Pennsylvania, Philadelphia, Pennsylvania 19104, USA

Abstract

Lyotropic liquid crystals (LLCs) have drawn attention in numerous technical fields as they feature a variety of nanometer-scale structures, processability, and diverse chemical functionality. However, they suffer from poor mechanical properties and thermal stability. Polymerization in LLCs, referred to as LLC templating, is an effective approach to overcome this issue. While the templating approach results in robust mechanical, physical, and thermal properties, retention of the parent LLC structure after polymerization has been a major concern in the field. Therefore, there have been several efforts to introduce new materials and techniques to preserve the native LLC nanostructure after polymerization. In this review, we survey the efforts put in this area along with the applications of the obtained materials from LLC templating, after providing a brief introduction of LLC structures. Moreover, polymerization kinetics in different LLC structures, as a key player in the structure retention, are analyzed. Furthermore, we discuss the outlook of the field and available opportunities.

Keywords: *Lyotropic liquid crystals, Self-assembly, Templating, Membrane, Mesophases*

1. Introduction

Nanostructured materials have attracted the attention of scientific communities as well as industries world-wide because of their unique properties which make them applicable in a variety of technical fields including biomedical devices,^{1,2} light scattering,³ membranes,^{4,5} energy storage devices,⁶ and so forth. Precise control of the structure in the nanometer scale is the key to improve the functionality of such materials and thus to guarantee their applicability in each field. Process-ability and chemical functionality of the components are other important factors when it comes to the large scale production of nanostructured substances.⁷ As an example, inorganic materials such as zeolites that are widely used for separation in molecular scale suffer from challenging process-ability as well as limited range of chemistry (e.g., chemical functionality), resulting in restricted application as highly selective membranes.⁷

* Corresponding author. Email: cosuji@seas.upenn.edu.

† Corresponding author. Email: rfoudazi@nmsu.edu.

35 The “bottom-up” approach, which works based on self-arrangement in the atomic, molecular or
36 colloidal scales, is the common method used in nanotechnology for the fabrication of precisely
37 designed nanostructures.⁸ Amongst the huge diversity of materials employed in this technique,
38 the components that form liquid crystalline structures (LCs) through a molecular self-assembly
39 process (supramolecular chemistry) have received a great deal of attention.⁸ LCs have both
40 ordered and disordered regions in their structures. These structures, also called mesophases,
41 offer some of the properties of liquids and solid simultaneously (e.g., fluidity coupled with
42 optical anisotropy). Many organic compounds show LC behavior under certain conditions. LC
43 behavior can be observed in the molten state (thermotropic LCs), or in the presence of a solvent
44 as in lyotropic LCs (LLCs).⁹ In both cases, molecular self-assembly, liquidity and diverse
45 chemistry not only provide an opportunity to precisely control the nanostructure, but also result
46 in the ease of processing as well as a wide range of chemical functionality.⁷

47 Amphiphilic molecules, which have lipophilic tail(s) and hydrophilic head(s), are used to form
48 LLCs in the presence of water, as the commonly used solvent. Assembly in non-aqueous phases
49 has also been studied^{10–12} but our primary concern here is for aqueous LLCs. Molecular self-
50 assembly of these substances results in several LLC nanostructures such as normal (oil-in-water)
51 micelles (L_1), normal discontinuous cubic (I_1), normal hexagonal (H_1), lamellar (L_α), normal
52 bicontinuous cubic (Q_1), reverse (water-in-oil) bicontinuous cubic (Q_2), reverse hexagonal (H_2),
53 reverse discontinuous cubic (I_2), and reverse micelles (L_2), which all are shown schematically in
54 Fig. 1. In this review, we have assigned I_α , H_α , and Q_α as the general signs for discontinuous cubic,
55 hexagonal and bicontinuous cubic phases regardless of the type of each structure. Temperature,
56 pressure, light, and magnetic field are some of the external factors which can affect the phase
57 structure of LLCs. In addition, there are other factors including concentration, chemistry and shape
58 of the amphiphilic molecules, water content, and additives (e.g., in the oil phase) that can influence
59 the formation of a particular nanostructure. The LLC structural transitions, which are controlled
60 by aforementioned parameters, are explained via the critical packing parameter (CPP). CPP is
61 defined as:

$$62 \quad CPP = \frac{V}{al} \quad (1)$$

63 Where V , a , and l represent the lipophilic tail volume, ‘effective’ cross-sectional area of the
64 hydrophilic head group, and extended lipophilic chain length, respectively. Although the
65 parameter a is sometimes interpreted in LLC literature as a measure of the physical/geometric
66 cross-sectional area of the surfactant headgroup, it is in fact an effective thermodynamic
67 quantity,¹³ which encapsulates various conditions, such as charge, solvent ionic strength,
68 temperature, and additives.¹⁴ Free energy minimum models for calculating a have been developed
69 at various levels of complexity. However, examples exist in literature where simply estimating a_e
70 as the geometrical cross-sectional area¹⁵ of the charged headgroup still leads to excellent matching
71 between theory and experiment.

72 As shown in Fig. 1, when the cross-sectional area of hydrophilic group is larger than that of
73 lipophilic tails ($CPP < 1$), mean curvature is positive, resulting in the formation of normal phases.
74 When $CPP > 1$, negative mean curvature is present, resulting in inverted nanostructures (inverse

75 phase). Lamellar structures are obtained when the mean curvature is zero ($CPP = 1$), meaning that
76 the cross-sectional area of the polar head group and the tail are almost equal. Therefore, the CPP
77 concept is a powerful semi-quantitative lens for understanding type and stability of LLC phases
78 of amphiphiles. The solvent(s) content is the leading factor which can induce a transition in the
79 structure as schematically shown in Fig. 1. Common techniques used for the characterization of
80 LLC structures include Cross Polarized Light Microscopy (CPLM), Small-Angle X-ray Scattering
81 (SAXS), X-ray Diffraction (XRD), and Nuclear Magnetic Resonance (NMR). Among commonly
82 encountered LLC structures, only the lamellar and hexagonal phases are optically birefringent. H_α
83 mesophases typically show a fan-like texture in CPLM, while L_α typically exhibit streaky-oil
84 textures. Fig. 2a shows examples of these typical textures. Cubic systems lack birefringence due
85 to the isometric nature of the system, and therefore appear dark in CPLM. This includes I_α and Q_α ,
86 e.g. body-centered cubic (*BCC*) or face-centered cubic (*FCC*) packings of micelles, and the gyroid,
87 double diamond, and primitive bicontinuous cubic mesophases. Likewise, disordered micellar
88 systems (L_1 and L_2) are also optically isotropic and appear dark in CPLM. In conjunction with
89 CPLM, the relative position of Bragg peaks obtained from XRD or SAXS measurements is the
90 most common method to identify the phase of LLCs.¹⁶ The typically observed X-ray
91 crystallographic features of each structure, presented in Fig. 2, will be discussed in section 2.

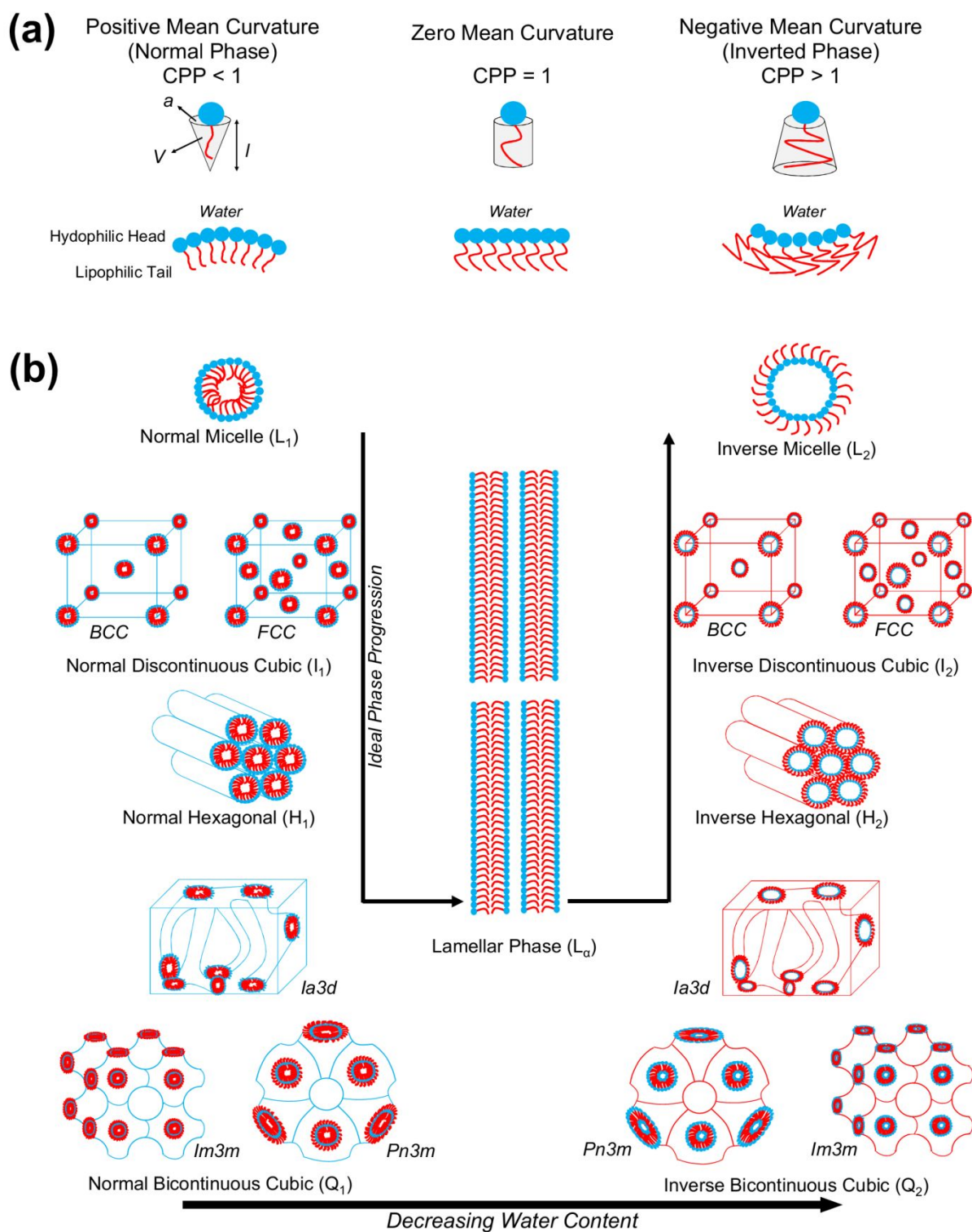
92

93

94

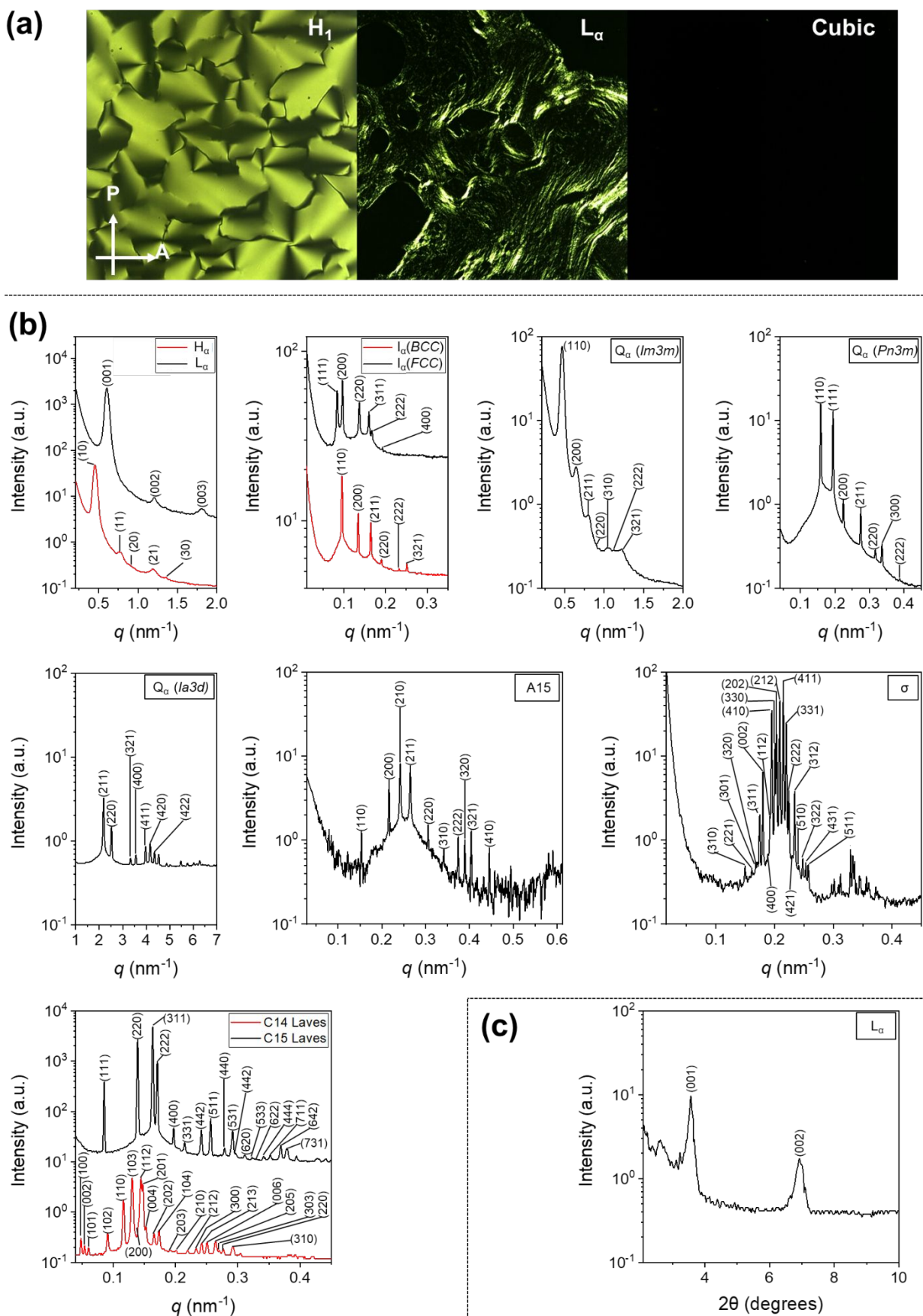
95

96



97

98 **Fig. 1.** (a) The schematic representation of CPP and its corresponding favorable structure. (b) Schematic
 99 diagram of common LLC structures.^{9,16–18} Addition/removal of solvents, such as decreasing water content
 100 can drive the phase transition.



101
102
103

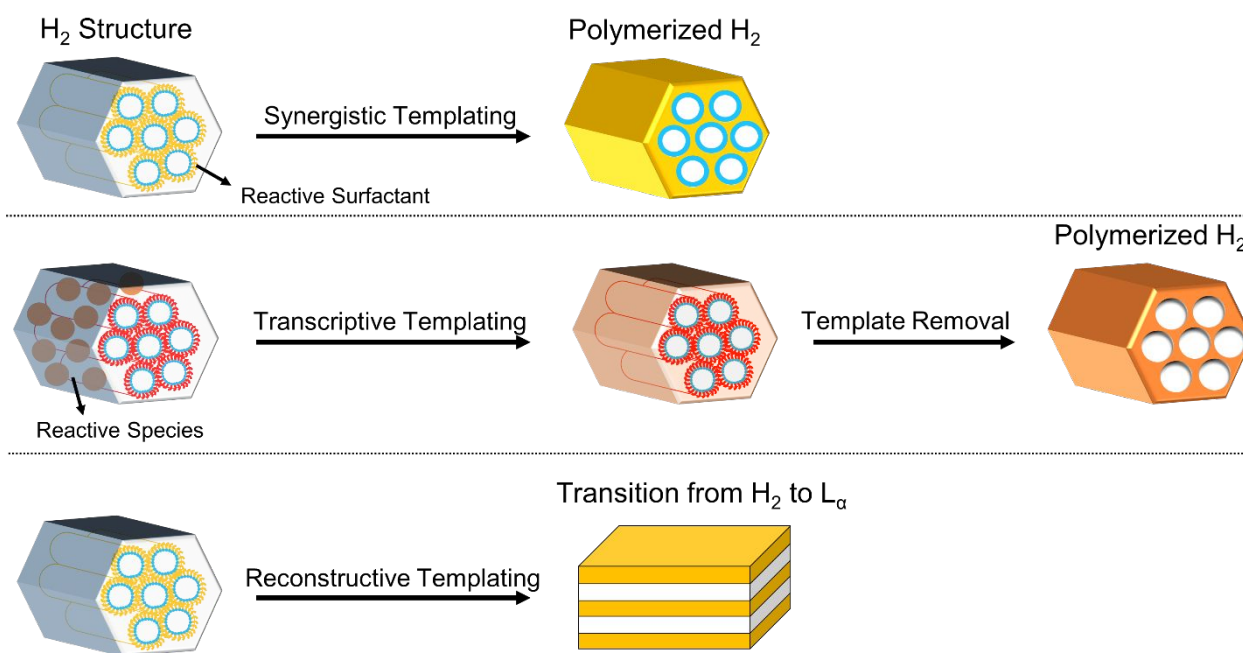
Fig. 2. (a) Typical CPLM Textures for LLC Mesophases – Representative micrographs for various LLC mesophases when samples are observed in a light microscope with a 90° difference in the Polarizer (P) and

104 Analyzer (A) directions. Birefringent ‘fan-like’ and ‘oily-streak’ textures are observed for the normal
105 cylinder (H_1) and lamellar sheet L_α mesophases. No birefringence is observed for any of the cubic phases
106 i.e. $Im3m$, $Pn3m$, $Ia3d$, BCC , and FCC . (b) Typical 1D SAXS profiles and corresponding assigned
107 diffraction planes observed for L_α ,¹⁹ H_α ,¹⁹ I_α (FCC ²⁰ and BCC ²⁰), Q_α ($Im3m$,¹⁹ $Pn3m$,²¹ and $Ia3d$ ²²)
108 and Frank-Kasper phases ($A15$,²³ σ ,²³ $C14$ Laves,²¹ and $C15$ Laves²¹). (c) Representative example
109 of results acquired from XRD for an L_α LLCs.²⁴

110 Even though LLC phases offer several advantages as previously mentioned, they still suffer from
111 poor mechanical and thermal properties which reduce their suitability in many applications. The
112 predominant method to circumvent these limitations is to use LLCs as a template to synthesize
113 polymers known as polyLLCs, with the desired nanostructure and chemical properties. Such
114 templating is approached via two common routes: synergistic and transcriptive templating. In the
115 former method, the organic component forming the LLC is polymerized, resulting in a cured
116 template. In the transcriptive approach, the desired material is formed (e.g., via polymerization)
117 in the nano-confinement of the LLC template, resulting in the formation of a one-to-one replica.
118 The main challenge in the transcriptive method is to preserve the parental template nanostructure.
119 If the structure is not retained, the method is instead referred to as reconstructive templating and
120 the final product may have a higher or lower order compared to the parent LLC, as shown
121 schematically for the H_2 phase in Fig. 3. Having a precisely controlled structure has led almost all
122 of the studies to focus on high-fidelity retention of the parental nanostructure, which is considered
123 successful LLC templating.²⁵ There are several reports on using LLC templating for fabrication
124 of organic (e.g., polymers),²⁶ inorganic (e.g., silica and mesoporous metal and alloys),²⁷ and
125 organic/inorganic hybrid^{28,29} nanostructures. However, LLC templating through the
126 polymerization of organic compounds is the focus of this review since the templating of inorganic
127 species is usually carried out to fabricate nanostructured inorganic materials²⁷ rather than
128 improving the properties of LLC templated materials.

129

130



131

132 **Fig. 3.** Schematic illustration of typical synergistic, transcriptive, and reconstructive LLC templating using
 133 H₂ structure. The reconstructive templating may lead to various structures and the lamellar structure shown
 134 here is just one example of the phase transition possible in this method.

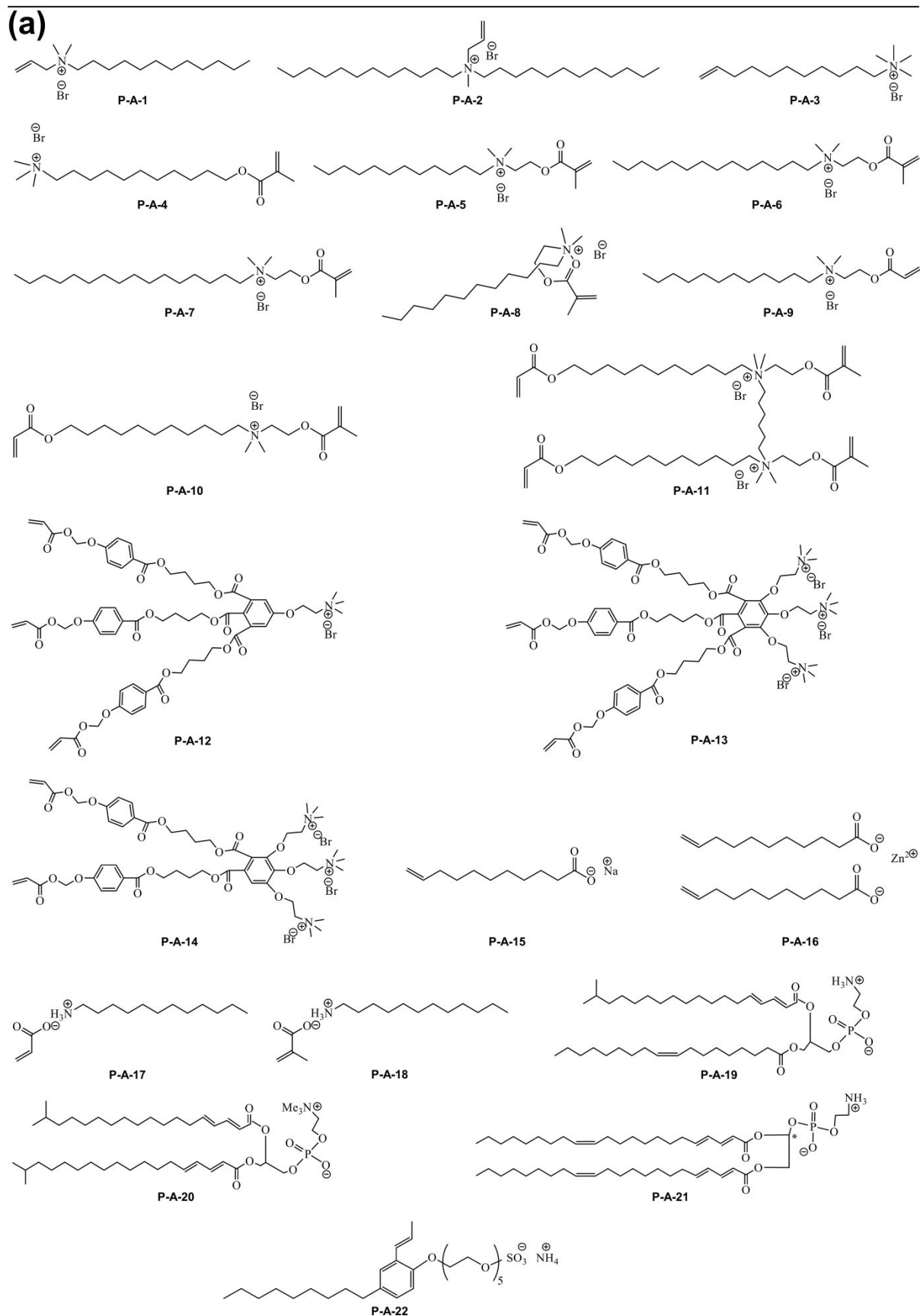
135 Thanks to the diversity in nanostructures with 1-10 nm length scale, the fabricated polyLLCs not
 136 only are applicable in a wide variety of technical applications, but also can provide enhanced
 137 properties compared to common materials. For instance, the membranes obtained from polyLLC
 138 technology show an enhanced permeability, selectivity, and fouling resistance compared to the
 139 current industry standard.³⁰⁻³⁴ Furthermore, the LLC-templated hydrogels offer an excellent
 140 balance of water uptake, swelling/de-swelling rate, and mechanical properties while preserving
 141 key characteristics including biocompatibility, biodegradability, and stimuli-responsiveness.³⁵⁻⁴⁵
 142 For body motion sensors, LLC templating has provided an opportunity to fabricate conductive
 143 materials with improved mechanical properties over non-LLC counterparts.⁴⁶⁻⁴⁸ Additionally,
 144 distinctive catalytic activity/selectivity compared to commercially used catalysts has been reported
 145 for the catalytic systems fabricated through LLC templating approach.^{28,49} Unique light emitting
 146 properties are another advantage of LLC-templated products over non-LLC materials.^{50,51} There
 147 are many other potential applications (e.g., energy storage devices⁵²) for polyLLCs which will be
 148 further discussed in section 7.

149 The interesting properties of polyLLCs have promoted the LLC templating approach for a variety
 150 of organic compounds since the first trials of synergistic templating by Luzzati and coworkers in
 151 the 1960s.⁵³ In-lab synthesized reactive surfactants have been used in almost all of the synergistic
 152 templating studies. For the case of transcriptive templating, there have been several reports
 153 concerning the polymerization of widely available (co)monomers and/or cross-linkers in LLC
 154 structures created by the solution self-assembly of commercially produced non-reactive surfactant
 155 molecules. In the latter case, the cross-linker is used to prevent structure loss during
 156 polymerization by kinetically trapping the formed polymer chains and therefore avoiding phase
 157 separation/inversion.^{54,55} The chemistry, polarity, shape, and concentration of LLC components

158 are not only key factors for preserving the structure, but also determine the reaction kinetics as
159 well as the properties of the final nano-structure.²⁶ Hence, a wide variety of reactive amphiphiles
160 and different combinations of non-reactive surfactants/(co)monomers have been used to perform
161 successful synergistic and transcriptive LLC templating as listed in Fig. 4 and Fig. 5, respectively.

162 Formation of polymer and thus increasing the molecular weight of the monomer phase results in
163 an increase in the thermodynamic penalty of mixing. Additionally, surface energy of the
164 polymerizing phase changes upon the synthesis of polymer chains. Furthermore, the density
165 increases (shrinkage of polymerizing phase takes place) due to the formation of polymer network.
166 The combination of these phenomena can result in a change in the domain size and even phase
167 separation/inversion, and thus loss of the structure.³¹ Therefore, in addition to the
168 surfactant,(co)monomer and cross-linker, the polymerization initiation system has an important
169 role on retention of the structure since it affects the polymerization kinetics and therefore controls
170 the formation rate of cross-linked network. According to literature reports, fast polymerization
171 rate increases the chance of structure retention due to the rapid cross-linking of polymer network.
172 As a rule of thumb, when the reaction rate is faster than the time scale required for demixing of
173 growing polymer chains, the structure will most probably be preserved.²⁶ In addition,
174 polymerization near room temperature decreases the risk of structure disturbance.^{26,56} Therefore,
175 photoinitiated polymerization, which typically delivers a fast polymerization rate at room
176 temperature, has been the top choice in most of the studies.²⁶ A variety of photoinitiators have
177 been employed for LLC templating, as listed in Fig. 6. Nevertheless, there are some studies which
178 have successfully carried out templating by using other initiation systems (e.g., thermal⁵⁷ and
179 redox⁵⁸), as presented in Fig. 6. For enhancing readability and simplifying chemical references
180 throughout the paper for readers, we have coded the large variety of key components used in LLC
181 templating (as seen in Fig. 4-6), with the names or chemical formulae of the component tabulated
182 in Table S1.

183 Following the above introduction on the basic concepts of LLC templating, the remainder of this
184 article is outlined as follows. First, characteristics of common LLC structures used in LLC
185 templating will be presented. Then, the available literature on synergistic templating will be
186 reviewed based on the structure of the LLC template. A similar survey will be presented for
187 transcriptive templating afterward. In each section, the efficiency of the templated products will
188 be analyzed in the application(s) they are designed for (e.g., membranes, hydrogels, energy storage
189 devices, light emitting components, catalyst support, tissue engineering scaffolds, and
190 compatibilizers of immiscible monomers). These sections will be followed by a summary of
191 polymerization kinetics in nanostructured LLCs as well as a concise comparison between
192 synergistic and transcriptive templating techniques. The outlook of the field and available
193 opportunities will be summarized at the end of the review.



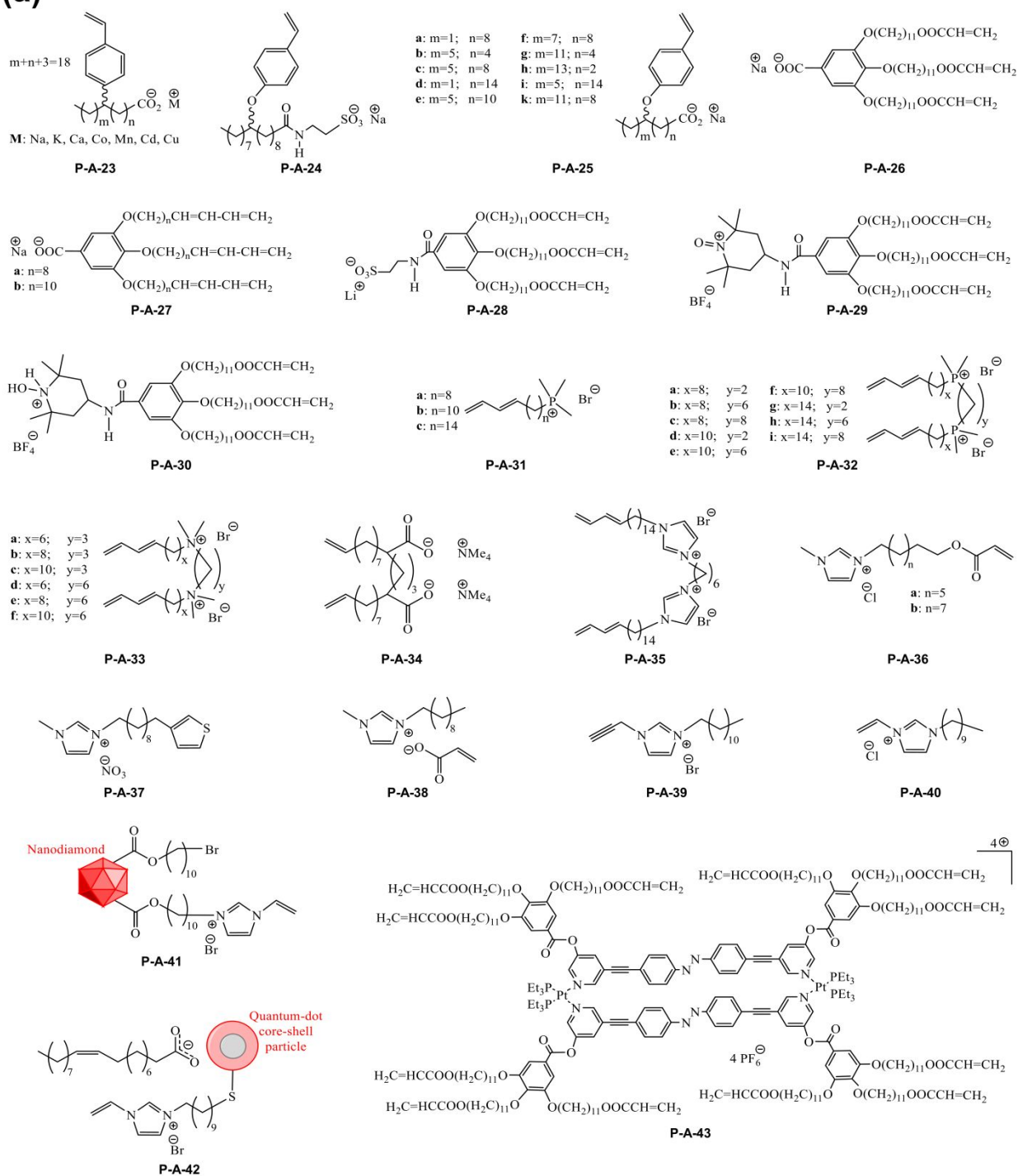
194

195

196

Fig. 4. Chemical structure of (a) polymerizable ionic, (b) polymerizable non-ionic and (c) non-polymerizable amphiphiles used for LLC templating.

(a)



197

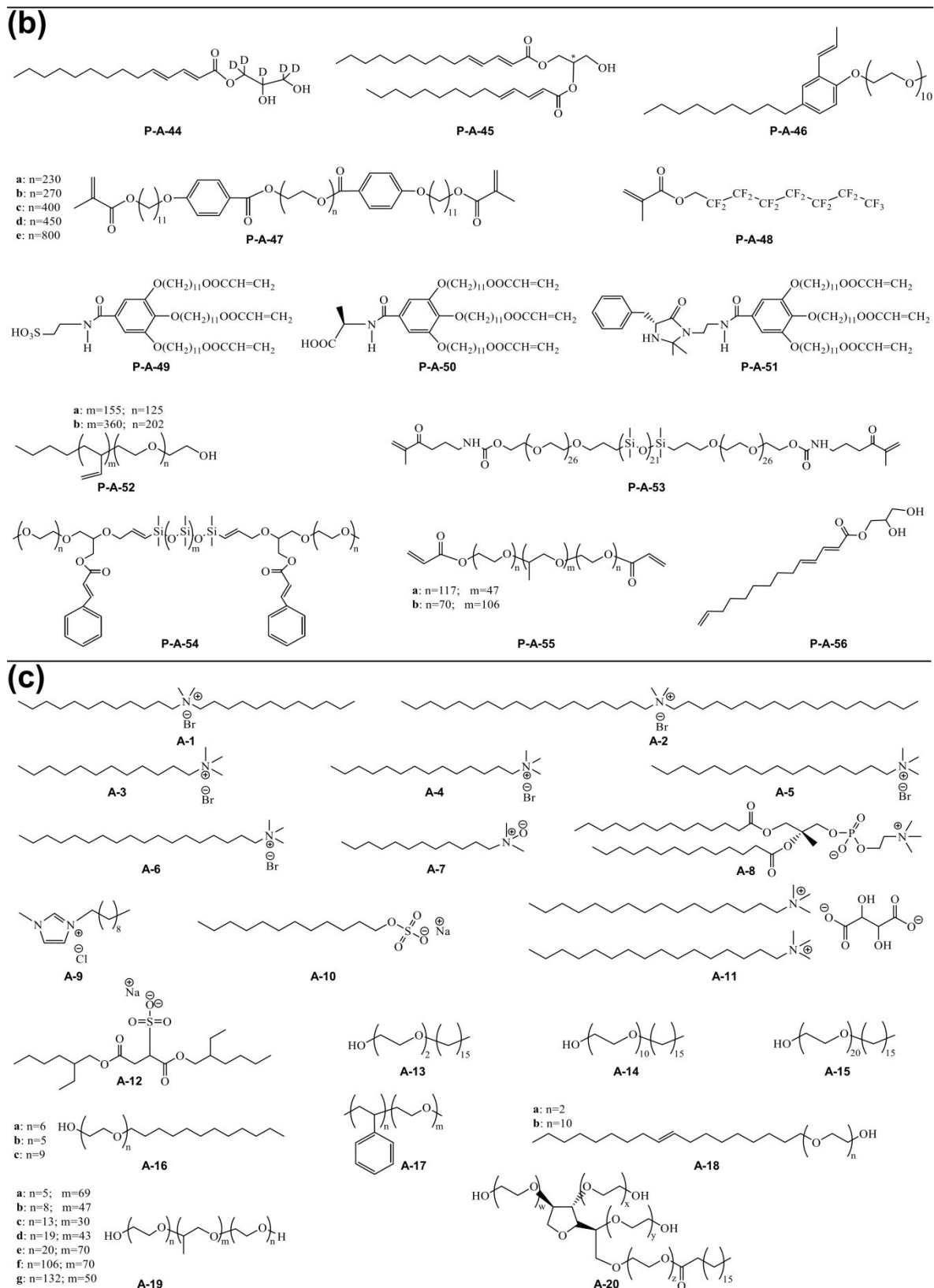
198

199

Fig. 4. Chemical structure of (a) polymerizable ionic, (b) polymerizable non-ionic and (c) non-polymerizable amphiphiles used for LLC templating.

200

201



202
203
204

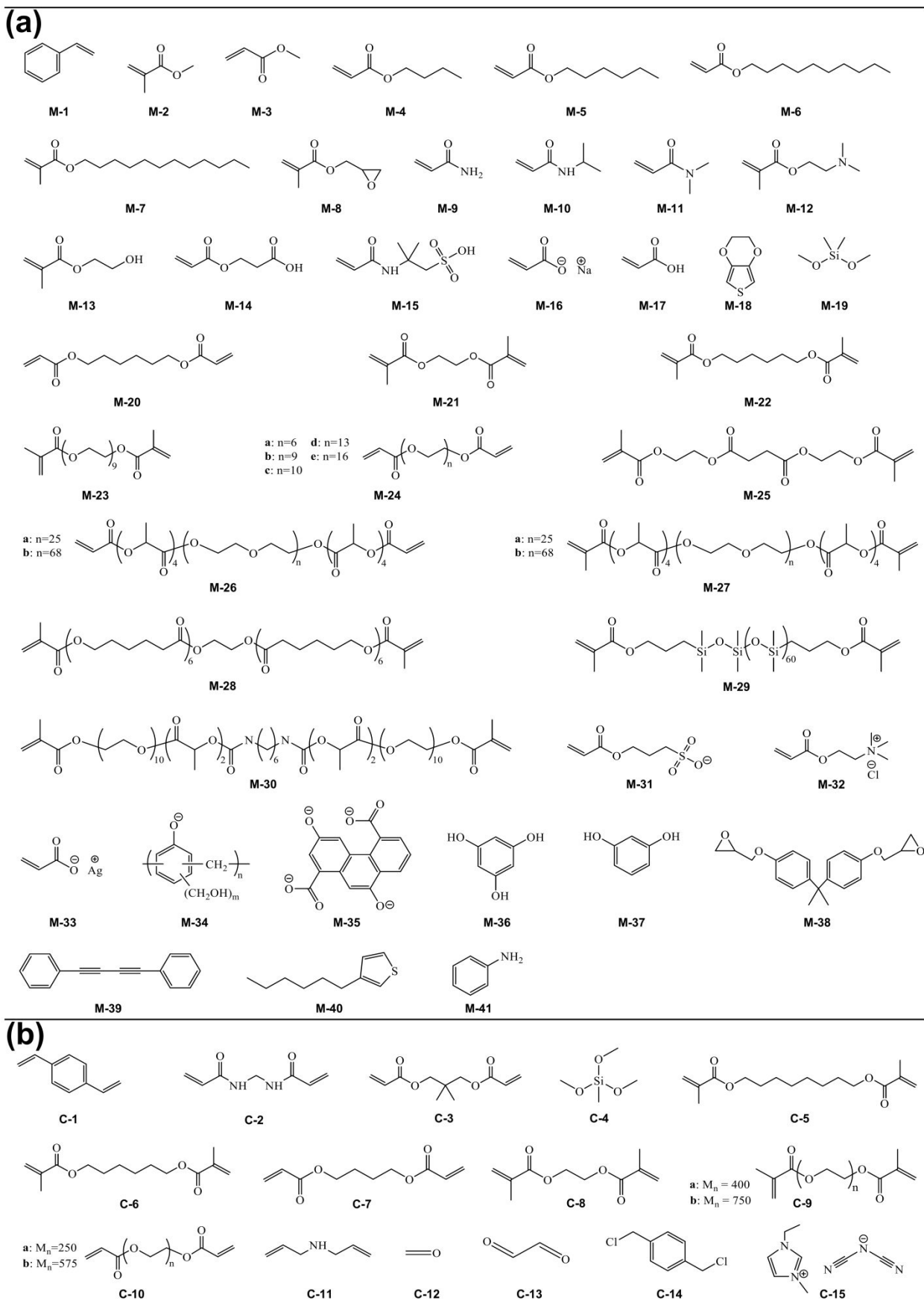
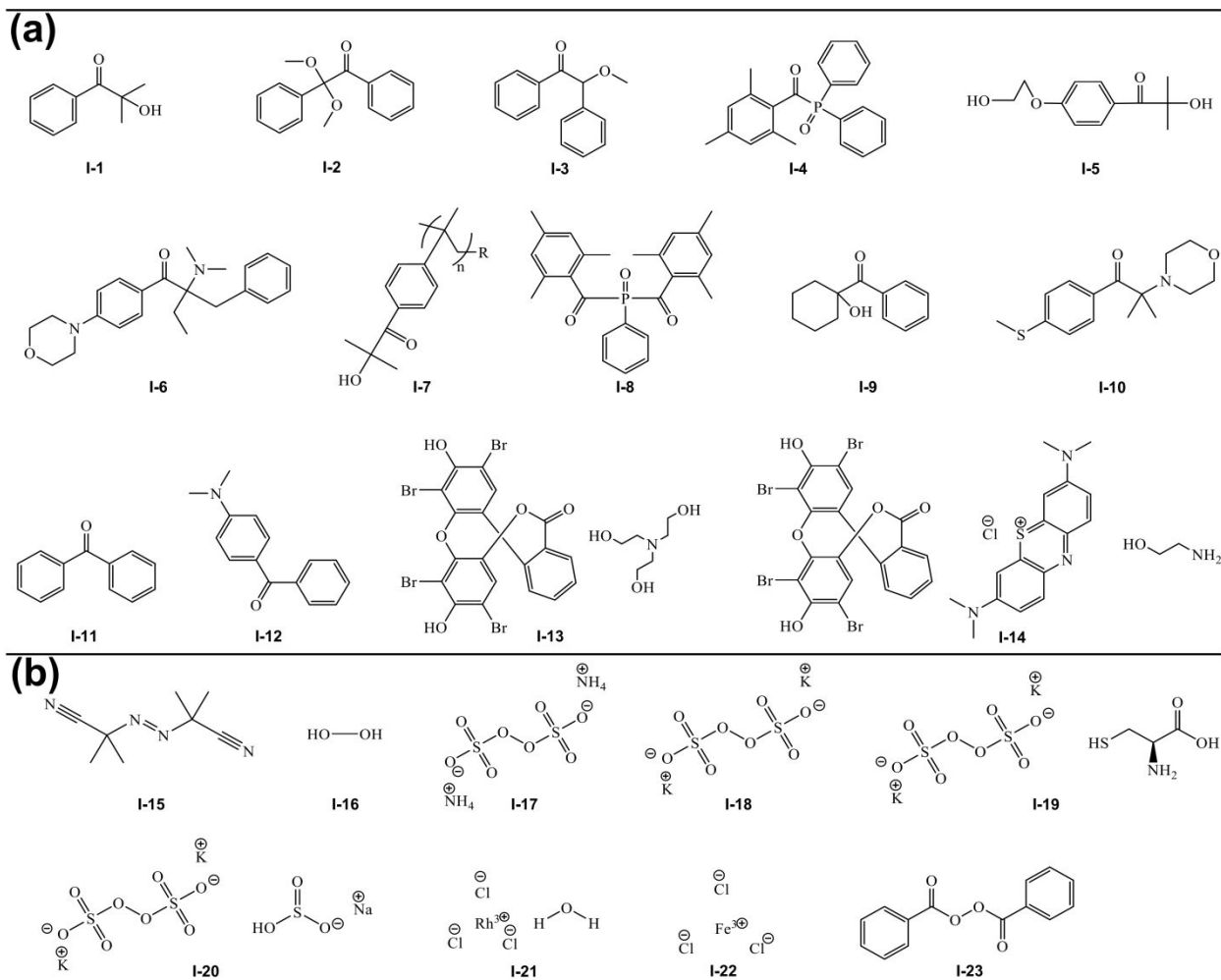
205
206

Fig. 5. Chemical structure of (a) (co)monomers and (b) cross-linkers used for LLC templating.



207

208 **Fig. 6.** Chemical structure of the polymerization initiators used for LLC templating: (a) photoinitiators and
 209 (b) other (i.e. thermal and ionic) commonly used initiator.

210

211 2. Characteristics of LLC structures

212 As shown in Fig. 1, a variety of LLC nanostructured phases can be obtained from LLC templating
 213 processes. Hence, methods for distinguishing different phases/structures are central to verifying a
 214 successful templating. X-ray crystallographic studies are the primary tool of choice for LLC
 215 structure characterization. In this section, we discuss key geometric characteristics of different
 216 LLC structures, which can be revealed via X-ray crystallographic studies. The characteristic
 217 period for commonly studied LLC mesophases (~2-5 nm) is amenable to study by X-ray
 218 scattering. Both small-angle X-ray scattering (SAXS) and conventional X-ray diffraction (XRD)
 219 are used for this purpose, though the latter is typically better suited for elucidating structures at
 220 even smaller length scales. A summary of LLC structural characteristics is presented in Table 1.

221

222

Table 1. Characteristics of LLC structures used is LLC templating.

LLC structure	CPLM	X-ray Bragg Peak Ratios	Lattice parameter
Hexagonal	Fan-like texture	1:√3:2:√7:3:√12:√13...	$a = \frac{2}{\sqrt{3}}d, d = \frac{2\pi}{q_{10}}$
Lamellar	Oily-streak texture	1:2:3:4:5:6...	$d = \frac{2\pi}{q_1}$
Bicontinuous cubic	Not birefringent	<i>Im3m</i> : √2:√4:√6:√8:√10... <i>Pn3m</i> : √2:√3:√4:√6:√8:√9... <i>Ia3d</i> : √6:√8:√14:√16:√18:√20...	1/a = Slope of 1/d _{hkl} vs (h ² + k ² + l ²) ^{1/2}
Discontinuous cubic	Not birefringent	<i>BCC</i> : 1:√2:√4:√6:√8:√10... <i>FCC</i> : 1:√3:√4:√8:√11:√12...	1/a = Slope of 1/d _{hkl} vs (h ² + k ² + l ²) ^{1/2}
Frank-Kasper phases	Not birefringent	A15: 1:√2:√4:√5:√6:√8:√10:√12... C15: 1:√3:√8:√11:√12:√16:√19...	1/a = Slope of 1/d _{hkl} vs (h ² + k ² + l ²) ^{1/2}

223

224 2.1. Hexagonal (H_α)

225 The hexagonal columnar structure is one of the most studied phases in LLC templating. H_α consists
 226 of closely packed cylindrical micelles arranged in a hexagonal lattice. Depending on the curvature,
 227 the hydrophilic head of the surfactant is located on the external or internal surface of the micelles
 228 to be in contact with water in H₁ or H₂ structure, respectively. As shown in Fig. 7, there are
 229 multiple parameters of interest in the hexagonal phase structure: *d* is the distance between the
 230 planes passing by two adjacent rows of cylinders or *d*-spacing, *a* is the center to center distance of
 231 two adjacent cylinders or lattice parameter, *R_m* is the radius of micelle, *R_c* is the radius of confined
 232 phase in micelle, *D_m* is the intermicellar distance, and *R_{h,max}* is the radius of the largest circle
 233 trapped between the micelles.⁵⁶ Bragg peaks with relative positions at the ratios of
 234 1:√3:2:√7:3:√12:√13... (corresponding to the d₁₀, d₁₁, d₂₀, d₂₁, d₃₀, ... diffraction planes) are the
 235 characteristic signature of the hexagonal structure in X-ray measurements (see Fig. 2b).¹⁷ The *d* is
 236 calculated from Eq. (2) by using the position of the first Bragg peak from SAXS measurement,
 237 *q*₁₀. The lattice parameter can be calculated from Eq. (3) based on the obtained value of *d*.¹⁷

$$238 \quad d = \frac{2\pi}{q_{10}} \quad (2)$$

$$239 \quad a = \frac{2}{\sqrt{3}}d \quad (3)$$

240 To calculate *R_c*, the following equation is used. In this equation, *φ* is the volume fraction of the
 241 dispersed phase (i.e., the phase confined in the cylindrical micelles).¹⁷

$$242 \quad R_c = a \left(\frac{\sqrt{3}}{2\pi} \phi \right)^{1/2} \quad (4)$$

243 The radius of micelle R_m is calculated using Eq. (5). Here, ϕ_t is the volume fraction of the
244 confined phase plus the volume fraction of the surfactant.

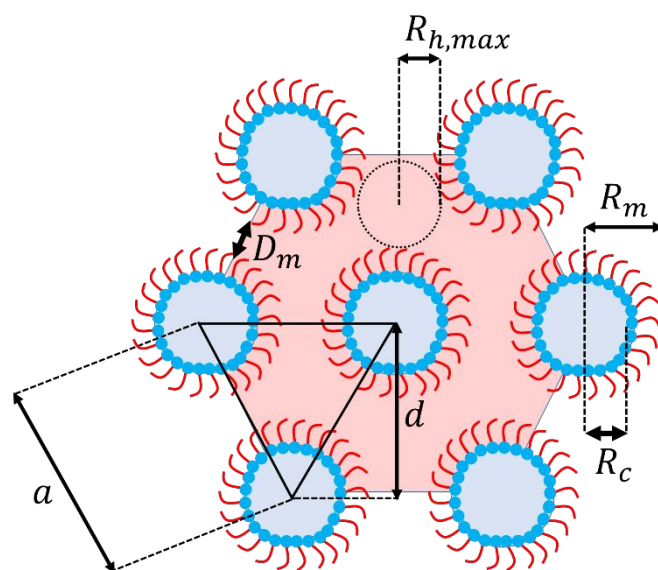
$$245 \quad R_m = a \left(\frac{\sqrt{3}}{2\pi} \phi_t \right)^{1/2} \quad (5)$$

246 The intermicellar distance for H_2 phase D_m , is obtained using Eq. (6). Moreover, the size of the
247 nanoconfinement cavity between micelles can be estimated from the radius of the biggest circle
248 trapped between the micelles $R_{h,max}$. Eq. (7) and (8) can be used for this estimation.

$$249 \quad D_m = a - 2R_m \quad (6)$$

$$250 \quad R_{h,max} = \sqrt{\frac{A_h}{\pi}} \quad (7)$$

$$251 \quad A_h = a^2 \frac{\sqrt{3}}{4} - \pi \frac{(R_m)^2}{2} \quad (8)$$



252

253 **Fig. 7.** Typical schematic of H_2 structure with d -spacing (d), lattice parameter (a), radius of micelle (R_m),
254 radius of confined phase in micelle (R_c), intermicellar distance (D_m), and radius of the biggest circle trapped
255 between the micelles ($R_{h,max}$). In this case, ϕ is the volume fraction of the polar phase.

256 In the broader mesophase literature, other columnar mesophases have been studied which exhibit
257 non-circular cross-sections and/or non-hexagonal packing of the columns. These LLC phases are
258 sometimes termed ‘ribbon’ phases, and include lattices of rectangularly or obliquely packed
259 mesogen columns.⁵⁹ However, they have generally not been studied in the polyLLC context. There

260 are studies of rectangular columnar phases for thermotropic LCs,⁶⁰ but for lyotropic LCs
 261 hexagonal columns are the predominantly observed and studied columnar mesophase.

262 2.2. Lamellar (L_a)

263 The lamellar phase is formed under zero mean curvature. The hydrophilic heads of the amphiphile
 264 molecules assemble toward the water, while lipophilic tails remain away from water. As shown in
 265 Fig. 8, L_a has various characteristic dimensions; d is the repeating distance of bilayers or lattice
 266 parameter, δ_1 is the thickness of the apolar domain, δ_2 is the thickness of the polar domain, D_1 is
 267 the intermicellar distance in apolar phase, D_2 is the intermicellar distance in polar domain, and
 268 $R_{1,max}$ and $R_{2,max}$ are the radii of the largest circles trapped between the micelles in apolar and polar
 269 domains, respectively.⁵⁶ As shown in Fig. 2b, The lamellar phase structure shows a sequence of
 270 Bragg peaks in integer ratios of 1:2:3:4:5:6...¹⁷ (corresponding to the d_{001} , d_{002} , d_{003} , d_{004} , d_{005} ,
 271 d_{006} , ... diffraction planes) in X-ray crystallographic studies. The position of the first Bragg peak
 272 in SAXS measurement (q_1) is used to calculate d , δ_1 and δ_2 via the following equations,
 273 respectively. In these equations, ϕ_1 and ϕ_2 are the volume fraction of the apolar and polar domains,
 274 respectively. In other words, ϕ_1 is the volume fraction of oil phase plus surfactant hydrophobic
 275 moiety, whereas ϕ_2 is the volume fraction of aqueous phase plus the surfactant hydrophilic
 276 segment.

$$277 \quad d = \frac{2\pi}{q_1} \quad (9)$$

$$278 \quad \delta_1 = d\phi_1 \quad (10)$$

$$279 \quad \delta_2 = d\phi_2 \quad (11)$$

280 To calculate D_1 and D_2 , Eq. (12) and (13) can be used. The average intermicellar distance in
 281 lamellar structure D_L is obtained via Eq. (14). In these equations, ϕ' and ϕ'' are the volume fraction
 282 of the phases confined in the apolar and polar domains, respectively

$$283 \quad D_1 = d\phi' \quad (12)$$

$$284 \quad D_2 = d\phi'' \quad (13)$$

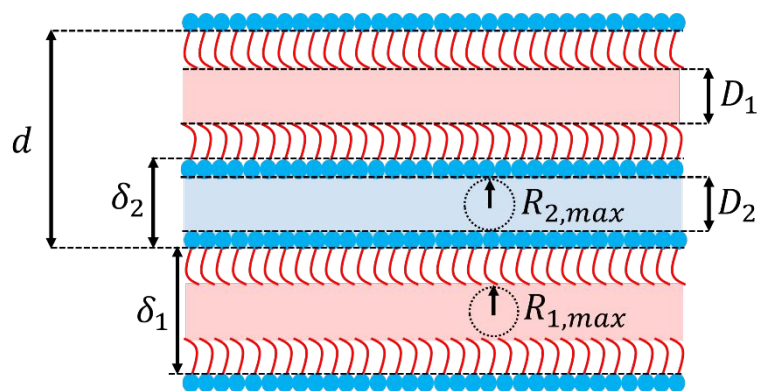
$$285 \quad \frac{1}{D_L^3} = \frac{1}{D_1^3} + \frac{1}{D_2^3} \quad (14)$$

286 $R_{1,max}$ and $R_{2,max}$ are obtained using Eq. (15) and (16).

$$287 \quad R_{1,max} = \frac{D_1}{2} \quad (15)$$

$$288 \quad R_{2,max} = \frac{D_2}{2} \quad (16)$$

289



290

291

292

293

294

Fig. 8. Typical schematic of L_{α} structure showing lattice parameter d , δ_1 is the thickness of the apolar domain, δ_2 is the thickness of the polar domain, D_1 is the intermicellar distance in apolar phase, D_2 is the intermicellar distance in polar domain, and $R_{1,max}$ and $R_{2,max}$ are the radii of the biggest circles trapped between the micelles in apolar and polar domains, respectively.

295

296 2.3. Bicontinuous cubic (Q_{α})

297

298

299

300

301

302

303

304

305

306

307

308

309

310

311

312

313

314

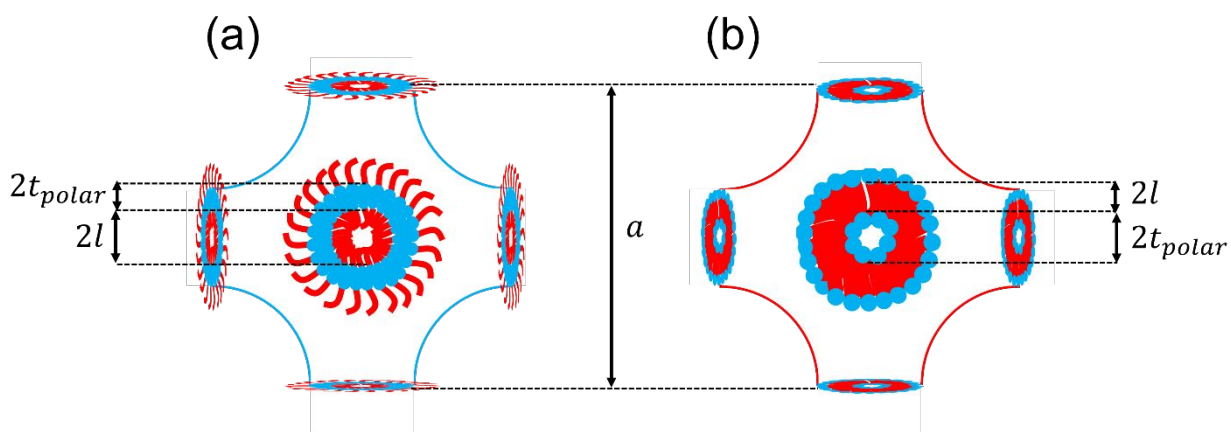
315

316

317

318

Bicontinuous cubic phases are some of the more interesting but uncommon LLC structures which have been studied for LLC templating. These structures, which are usually obtained by using precisely designed amphiphiles in typically very narrow amphiphile/water weight ratio ranges, consist of continuous but non-intersecting nanochannels separated by a curved bicontinuous layer. Depending on the mean curvature, the bicontinuous bilayer can be hydrophobic tail or polar head (see Fig. 1).¹⁶ Interconnected pores make these structures perfect candidates for a variety of applications, particularly molecular separations because the pores/channels do not require structural alignment. X-ray crystallographic studies typically encounter Q_{α} structures of three main types, namely the primitive lattice ($Im3m$, Q_{229}), the double-diamond lattice ($Pn3m$, Q_{224}) and the gyroid lattice ($Ia3d$, Q_{230}), as schematically shown in Fig. 1.^{9,16,18} The important dimensional parameters of the primitive type are presented schematically in Fig. 9. $2l$ represents the thickness of the apolar domain (including the surfactant tail), $2t_{polar}$ is the polar domain thickness (including the surfactant headgroup), and a is the lattice parameter.⁹ In X-ray crystallographic studies, the peak ratios for $Im3m$, $Pn3m$ and $Ia3d$ are $\sqrt{2}:\sqrt{4}:\sqrt{6}:\sqrt{8}:\sqrt{10}...$ (corresponding to the d_{110} , d_{200} , d_{211} , d_{220} , d_{310} , ... diffraction planes),⁶¹ $\sqrt{2}:\sqrt{3}:\sqrt{4}:\sqrt{6}:\sqrt{8}:\sqrt{9}...$ (corresponding to the d_{110} , d_{111} , d_{200} , d_{211} , d_{220} , d_{221} (or d_{300}), ... diffraction planes),⁶¹ and $\sqrt{6}:\sqrt{8}:\sqrt{14}:\sqrt{16}:\sqrt{18}:\sqrt{20}...$ (corresponding to the d_{211} , d_{220} , d_{321} , d_{400} , d_{411} (or d_{330}), d_{420} , ... diffraction planes),⁶¹ respectively.^{9,16} Typical SAXS profiles for different Q_{α} structures are shown in Fig. 2b. Calculation of these parameters for Q_{α} structure from X-ray studies is not as simple as for H_{α} and L_{α} . To calculate the lattice parameter a , the reciprocal spacings, $1/d_{hkl}$, of the peaks in the X-ray measurement are plotted versus the sum of the Miller indices, $(h^2 + k^2 + l^2)^{1/2}$.¹⁷ The $1/a$ is equal to the slope of the line passing through the data points.



319

320

321

Fig. 9. Typical schematic of (a) normal and (b) reverse primitive Q_α structure with lattice parameter (a) and the thickness of the polar ($2t_{polar}$) and apolar domains ($2l$).

322

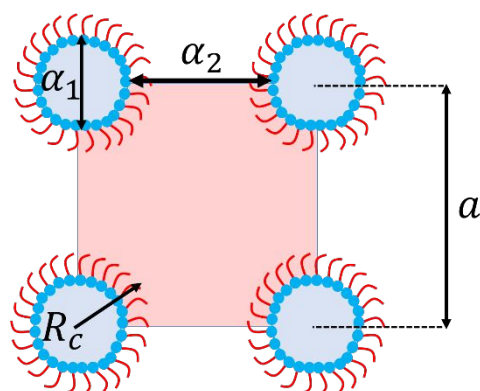
323 2.4. Discontinuous cubic (I_a)

324 The discontinuous cubic phases, which are also called micellar cubic, consist of micelles arranged
 325 in a cubic lattice. There are two types of cubic lattices for this structure, body-centered cubic
 326 (BCC) and face-centered cubic (FCC), as presented in Fig. 1. In the X-ray measurements, the
 327 characteristic peak ratio for BCC and FCC phases are $1:\sqrt{2}:\sqrt{4}:\sqrt{6}:\sqrt{8}:\sqrt{10}\dots$ (corresponding to the
 328 $d_{100}, d_{110}, d_{200}, d_{211}, d_{220}, d_{310}, \dots$ diffraction planes)⁶² and $1:\sqrt{3}:\sqrt{4}:\sqrt{8}:\sqrt{11}:\sqrt{12}\dots$ (corresponding
 329 to the $d_{100}, d_{111}, d_{200}, d_{220}, d_{311}, d_{222}, \dots$ diffraction planes),⁶² respectively (see Fig. 2b).⁹ To
 330 calculate the lattice parameter (see Fig. 10), a procedure similar to the one for bicontinuous cubic
 331 structures is used.⁶² Polar domain size α_1 and apolar domain size α_2 of BCC lattice can be estimated
 332 via Eq. (17) and Eq. (18), respectively.⁶³ In these equations, R_c is the radius of the spherical
 333 micelles and ϕ , which is obtained by Eq. (19), is the volume fraction of continuous domain.

$$334 \quad \alpha_1 = 2R_c \quad (17)$$

$$335 \quad \alpha_2 = 2a \left(\frac{3\phi}{8\pi} \right)^{\frac{1}{3}} \quad (18)$$

$$336 \quad \phi = 1 - 2 \frac{\frac{4}{3} \pi R_c^3}{a^3} \quad (19)$$

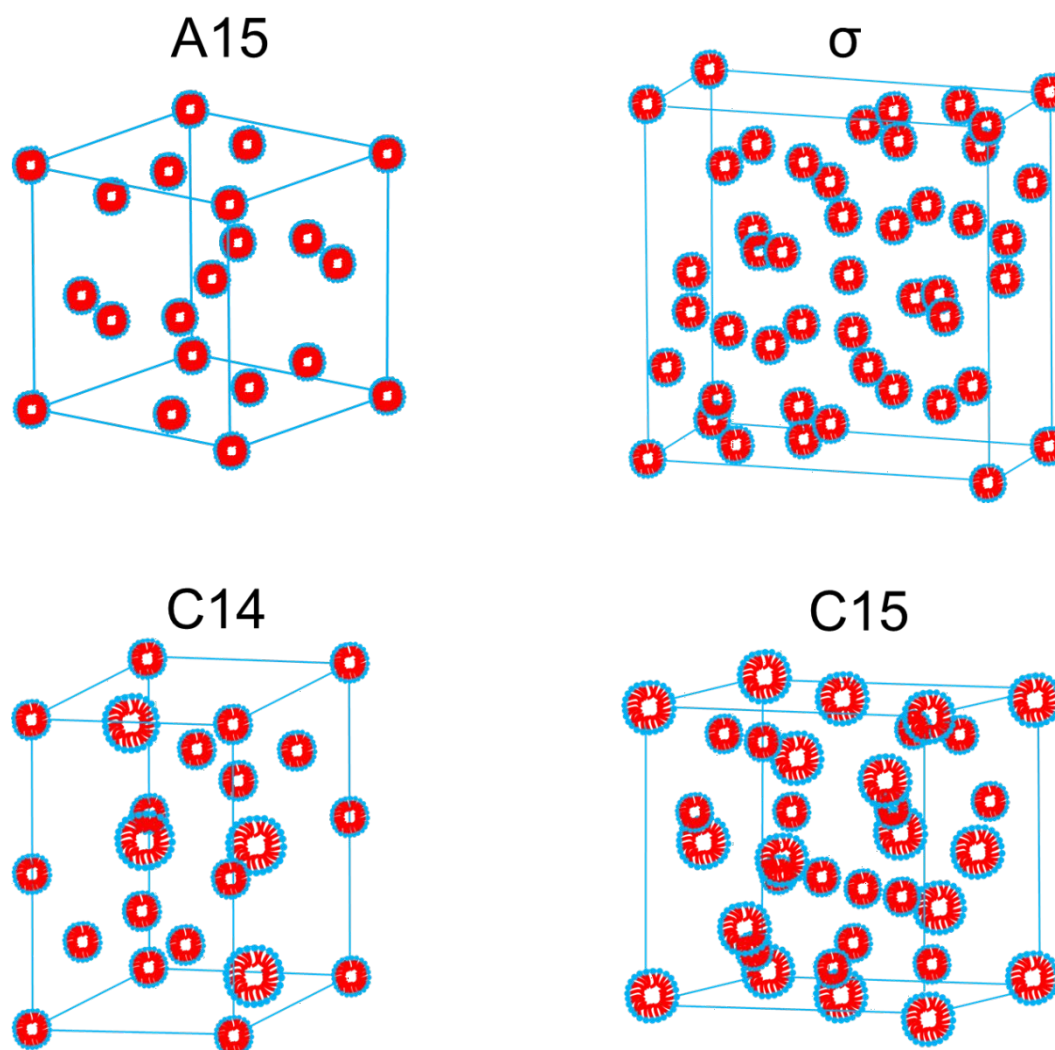


337

338 **Fig. 10.** Typical schematic of inverse *BCC* discontinuous cubic structure with lattice parameter (a), radius
 339 of spherical micelles (R_c), polar domain size (α_1) and apolar domain size (α_2).

340 2.5. Other LLC structures

341 So far, we have discussed the LLC structures which are commonly observed in different LLC
 342 formulations. However, quasi-crystal structures, such as Frank-Kasper (F-K) phases, are also
 343 reported for lyotropic systems.^{20,21,23,64} F-K phases, which exhibit tetrahedrally close-packed
 344 structures, were discovered for metal alloys more than 50 years ago.^{65,66} Since then, more than
 345 twenty different types of F-K phases have been experimentally observed in metal alloys. Amongst
 346 such variety, A15, Laves, σ , μ , M, P, R, and Z phases are the most common ones.⁶⁷ In the case of
 347 LLCs, formation of A15,^{20,23,64} Laves (e.g., C14 and C15)²¹ and σ ^{23,64} phases have been reported
 348 in the literature. The LLC with A15 structure contains 8 quasispherical micelles per unit cell with
 349 two different types of coordination environments.^{20,23,64} The C15 Laves phase includes eight
 350 quasispherical micelles located at the positions of a cubic diamond lattice and tetrahedral
 351 groupings of smaller micelles fill the remaining tetrahedral interstitial sites.²¹ In the case of C14
 352 Laves phase, the micelles are located on the sites of the hexagonal diamond structure.²¹ The
 353 lyotropic σ mesophase consists of a primitive tetragonal unit cell with 30 quasispherical micelles
 354 which belong to five different symmetry-equivalent classes.^{23,64} The common F-K phase reported
 355 for LLCs are schematically shown in Fig. 11. As with other mesophases, X-ray analysis is used to
 356 characterize these structures. Accordingly, as presented in Fig. 2b, the characteristic peak ratio of
 357 $1:\sqrt{2}:\sqrt{4}:\sqrt{5}:\sqrt{6}:\sqrt{8}:\sqrt{10}:\sqrt{12}\dots$ (corresponding to the d_{100} , d_{110} , d_{200} , d_{210} , d_{211} , d_{220} , d_{310} , d_{222}, \dots
 358 diffraction planes) and $1:\sqrt{3}:\sqrt{8}:\sqrt{11}:\sqrt{12}:\sqrt{16}:\sqrt{19}\dots$ (corresponding to the d_{100} , d_{111} , d_{220} , d_{311} ,
 359 d_{222} , d_{400} , d_{331} , ... diffraction planes) is observed for A15^{20,23,64} and C15²¹ Laves phases,
 360 respectively. In the case of C14 Laves²¹ and σ ^{23,64} phases, Bragg peaks corresponding to the d_{100} ,
 361 d_{002} , d_{101} , d_{102} , d_{110} , d_{103} , d_{200} , d_{112} , d_{201} , d_{004}, \dots and the d_{310} , d_{221} , d_{301} , d_{320} , d_{311} , d_{002} , d_{400} , d_{112} or
 362 d_{321} , d_{410} , d_{330}, \dots diffraction planes have been reported, respectively. Although these LLC phases
 363 have not yet been applied in LLC templating, they seem to have excellent potential in fabrication
 364 of nanostructured species with unique properties (see the discussion in section 3.4).



365

366 **Fig. 11.** Typical schematics of different F-K phases observed for LLCs including A15, C14 and C15 Laves,
367 and σ phases.

368 For the sake of completeness, it should be mentioned that there are other occasionally observed
369 LLC structures which are variously described as ‘intermediate’, ‘transition’ or ‘irregular’
370 mesophases. One such mesophase is the L_3 ‘sponge’ phase, which has an overall lamellar
371 structural motif, but the spacing of solvent domains is irregular. This polydispersity in feature
372 spacing manifests itself as a broad primary peak in L_3 X-ray diffractograms.^{68,69} Another example
373 are the ‘ribbon’ phases, which are transition/intermediate structures typically observed between
374 hexagonal and lamellar phases.⁷⁰ As the focus of this review, and of polyLLC focused research
375 efforts in general, is to obtain regular and well-ordered nanofeatures, these miscellaneous
376 mesophases are understudied in polyLLC literature, likely because they lack any immediately
377 apparent utility because of their non-uniform order and/or transitory nature.

378 3. Synergistic LLC templating

379 Since the first works on synergistic LLC templating in 1960s,⁵³ there have been several successful
380 LLC templating efforts. Early studies suffered from the inability to retain the parent LLC
381 structures after polymerization and/or rather low extents of polymerization/conversion.^{57,71–76}

382 These issues were partly resolved by the introduction of novel reactive amphiphiles, employing
383 highly efficient polymerization initiation systems, and developing new LLC formulations.^{7,26}
384 However, the major concern was still to expand the available variety of LLC nanostructures
385 accessible for a successful templating. The performance of different polyLLCs in desired
386 applications is highly dependent on the structures. For instance, in molecular separation
387 applications (e.g., water filtration), permeability, selectivity, and fouling resistance have to be
388 optimized simultaneously.⁴ While Q₂ structures offer such opportunity, they are not easily
389 accessible. Moreover, due to the high tortuosity of this structure, cleaning the nanochannels
390 blocked by foulants is highly challenging. On the other hand, H₂ and L_α phases, while easily
391 achievable LLC structures, need further processing steps (e.g., pore/channel alignment by
392 magnetic field) to decrease the tortuosity, thus optimizing the aforementioned membrane
393 characteristics.³⁰ Similar examples concerning the differences among LLC structures and obtained
394 polyLLCs provide the motivation to classify the following discussion based on the LLC
395 nanostructures.

396

397 3.1. Hexagonal (H_α)

398 A summary of reports in the current literature on synergistic templating of H_α structures is listed
399 in Table 2. As shown in the table, the lattice parameter reported for this structure typically ranges
400 from ~ 3 to ~ 11 nm. The lattice parameter is controlled by the geometric characteristics of the
401 employed reactive amphiphile such as the molecular size and shape, ionic charge, the position of
402 the polymerizable group, and so forth. As an example, P-A-13 which has a 3-head/3-tail structure,
403 results in a larger lattice parameter compared to P-A-12 and P-A-14 with 1-head/3-tail and 3-
404 head/2-tail structures, respectively.⁷⁷ P-A-26 is another example for which the *d*-spacing decreases
405 when the hydrophilic head contains trivalent lanthanide salts instead of sodium ion.⁷⁸ In addition
406 to the lattice parameter, the accessibility of H_α is also determined by the type of the surfactant. For
407 instance, to form LLC from the mixture of P-A-29 and P-A-30 in water, addition of P-A-50 is
408 crucial.⁷⁹ Moreover, specific compositions of amphiphiles in mixture are required to obtain the
409 intended structure. Change in the lattice parameter after polymerization is another important result
410 in most of the studied cases. If the structure is retained, dimensional changes due to the formation
411 of the polymer network^{41,56} and formation of a hexagonal structure with different *d*-spacing are
412 believed to be the main reasons for changes in the lattice parameter.

413 Enhanced thermal stability,^{58,61,73,80–88} swelling behavior,^{58,76,86–90} and mechanical
414 properties^{81,87,90,91} of polyLLC are the common outcomes of a successful synergistic templating
415 process. However, as listed in Table 2, there are some reports on the enhanced properties of
416 polyLLCs in particular applications such as molecular separation membrane,^{30,92–94}
417 catalysis,^{49,79,95} and light emitting materials.^{50,78} As described by Osuji and co-workers,
418 synergistic LLC templating by polymerization of H₁ structure has outstanding potential as
419 membranes in water purification application because such polyLLC membranes offer low
420 tortuosity without requiring any structural alignment. According to their results,³⁰ it is possible to
421 fabricate a membrane with an excellent permeability coupled with proper selectivity and
422 biofouling resistance by polymerizing H₁ template created from self-assembly of P-A-6 in water.

423 Using one oil- and one water-soluble cross-linker simultaneously in the mesophase formulation is
424 one promising technique for creating an interconnected network among nanocylinders and
425 therefore fabricating a mechanically robust membrane.

426 Gin and co-workers have focused on the preparation of molecular separation membranes (e.g., for
427 water purification and gas separation) based on synergistic LLC templating with H₂ structure.^{92–}
428 ⁹⁴ Although they have obtained promising results demonstrating the higher efficiency of the
429 polyLLC specimens over non-LLC ones, there are still some modifications required (e.g.,
430 alignment of the nanochannels) due to the performance mismatch between permeability and
431 selectivity metrics. In addition to the membrane applications, polyLLCs from synergistic H₂
432 templating have been used as catalyst support in reactions, such as alcohol oxidation⁷⁹ and
433 esterification.⁹⁵ The reported results show that polyLLC-based catalysts exhibit an improved
434 selectivity and activity comparable to the industrially used catalysts.^{49,79,95} In another application,
435 a H₂ template has been used to fabricate a nanocomposite containing poly(*p*-phenylenevinylene)
436 (PPV) inside the nanochannels, resulting in a durable material with higher light emission
437 capabilities compared to pure PPV.^{50,78}

438

439

440 3.2. Lamellar (L_α)

441 As summarized in Table 2, several studies have used L_α structures in synergistic templating.
442 Depending on the amphiphile(s) and LLC formulation, lattice parameters in the range of ~ 3 to ~
443 12 nm have been obtained. In addition, in most of the cases, L_α is obtained at relatively high
444 surfactant concentrations (~ > 70 wt%).^{51,73,81,96–102} Similar to the hexagonal structure, changes in
445 the lattice dimension are typically observed after polymerization, attributed to the formation of a
446 polymer network as well as the production of L_α structures with different *d*-spacings. Another
447 notable point here is the formation of a unique structure called hexagonal perforated lamellar
448 (HPL) which is a hybrid lamellar-hexagonal structure made from sheets that have in-plane
449 aqueous perforations arranged on a hexagonal lattice. HPL is formed when structural changes
450 from L_α to Q_α takes place during LLC formation or after the polymerization. HPL has been
451 commonly observed in LLCs based on amphiphilic imidazolium-based ionic liquids.¹⁰³ HPL is
452 considered to be a necessary kinetic pathway for the existence of Q_α phase.¹⁰⁴

453 As mentioned in the Introduction section, improving the thermal, mechanical, and physical
454 properties of nanostructured polymers are the primary goals of polymerization of LLC phases.
455 Therefore, the majority of the reported works on synergistic templating of the L_α phase have
456 focused on proving this concept in addition to studying the polymerization kinetics, which will be
457 discussed in a later section.^{58,61,73,80,81,86,87,101,103,105,106} As an example, Firestone et al. have
458 performed several studies to cure L_α and HPL structures made by reactive amphiphilic
459 imidazolium-based ionic liquids to produce a robust ion gels without sacrificing the conductivity
460 of the parent LLC phases.^{86,87,103,105}

461

462 3.3. Bicontinuous cubic (Q_α)

463 LLCs with Q_α structures having lattice parameters of ~ 5 to ~ 13.5 nm have been used in
464 synergistic templating efforts (see Table 2). The accessibility of Q_α phase before polymerization
465 is the most important challenge in templating process. Due to the relative scarcity of Q_α phases,
466 researchers have generally focused their efforts in synthesizing new reactive amphiphiles and
467 formulations design and optimizations.¹⁰⁷ For instance, the formation of Q_α phases is less
468 challenging in binary phases rather than in ternary ones.¹⁰⁷ On the other hand, the shape of the
469 amphiphilic monomer (e.g., the volume of the lipophilic tail, the ‘effective’ area of the hydrophilic
470 head, and the extended lipophilic chain length) dictates the type of the LLC structure. As an
471 example, monomers with small hydrophilic head and a broad flattened hydrophobic tail (tapered
472 shape) tend to form H_2 structure, whereas amphiphilic monomers with cylindrical shape tend to
473 form lamellar phase.⁸³ O’Brian and co-workers were pioneers in designing reactive surfactants
474 that form Q_2 structure.^{58,82,108–111} The Gin group have added a considerable body of knowledge on
475 synergistic templating of Q_α structures. Among other contributions, they have shown that Gemini-
476 structured reactive amphiphiles which have low critical micelle concentration (CMC) are reliable
477 species for obtaining Q_1 structures.^{32,33,52,112–121}

478 Efforts by the Gin group are not limited to design and synthesis of new monomers for LLC
479 templating in bicontinuous cubic structures, but also include investigations of the efficiency of the
480 polymerized LLCs in different applications. In one trial, they have shown that polymerized Q_2
481 structure of P-A-28/Li salt solution of propylene carbonate shows a conductivity similar to the
482 liquid-like electrolytes while maintaining high flexibility even at temperatures as low as -35 °C.¹¹⁶
483 In another series of works, they have used Q_1 phases obtained from P-A-32 to fabricate membranes
484 with different applications. As breathable barrier materials for chemical agent protection, the
485 produced butyl rubber (BR) incorporated membranes (LLC/BR composite) with Q_1 structure show
486 improved water vapor permeability/selectivity over LLC/BR composite membranes with H_2
487 structure.¹¹⁵ On the other hand, the water filtration performance of the membranes fabricated with
488 the Q_1 LLC lies in between that of conventional nanofiltration (NF) and reverse osmosis (RO)
489 membranes.^{33,119} They have also shown the possibility to modify/reduce the pore size of the final
490 product by atomic layer deposition (ALD) and therefore to increase the efficiency of light gas
491 separations.¹¹⁷ In another effort, Gin and co-workers decreased the production cost of Q_1 -based
492 water filtration membranes by using P-A-33 instead of P-A-32 while maintaining the same
493 efficiency.¹¹⁸ To further examine the performance of this structure, the team has used a mixture of
494 P-A-35 in glycerol to obtain Q_1 -based membranes having a thin active layer (< 0.1 micrometer)
495 as a thin film composite (TFC). The generated membranes show a water flux comparable to the
496 industrially used NF and RO membranes, salt rejection in between of them, and higher fouling
497 resistance and flux recovery.^{32,114,120,121} Furthermore, the fabricated membranes exhibit an
498 improved water/chemical agent molar vapor selectivity over Q_1 LLC/BR membranes created by
499 P-A-32 while requiring lower production costs.¹¹² Modification of ion sorption and pore transport
500 properties via polymerization of an ionic monomer inside the membrane pores has also been
501 explored to modify the performance of the Q_1 -based membranes.¹¹³ Finally, they have reported a
502 higher dehydration and resistivity of the Q_1 -based anion exchange membrane (AEM) in dilute
503 $FeCl_3$ solutions compared to amorphous AEMs thanks to closer spacing of ion exchange sites.⁵²

504

505 **3.4. Discontinuous cubic**

506 Discontinuous cubic phases have mainly been used in synergistic templating to study the
507 polymerization kinetics in LLCs,^{98,122} which will be discussed later. However, Lopez-Barron et
508 al. have used a P-A-55 directed FCC type discontinuous cubic structure to fabricate a cross-linked
509 ion gel with lattice parameter spanning from 15 to 30 nm. Partially deuterated ionic liquid
510 (ethylammonium nitrate) has been used instead of water to fabricate the LLC. By controlling the
511 LLC composition, they have been able to fabricate ion gels having highly viscoelastic or
512 elastomeric behavior with excellent mechanical properties, conductivity, and mechano-electrical
513 responses.^{46,48} They have also shown that the produced ultrastretchable iono-elastomers can be
514 used as a motion sensor as well as a temperature sensor with sufficient sensitivity and accuracy.
515 Impressive mechanical properties of such discontinuous cubic structures, in which discrete
516 micelles (spheres) are cross-linked, can indicate opportunities in other technical fields (e.g.,
517 membrane application) which require robust materials.⁴⁷ The mentioned properties can possibly
518 be further improved if the F-K phases are employed in the synergistic templating instead of
519 common discontinuous cubic structures.

520

521

522

523

524

Table 2. Summary of the reported results for synergistic LLC templating.

* Calculated d-spacing for the primary reflection in the SAXS profile; Dis. Cube: Discontinuous Cube; BR: Butadiene rubber; TDS: Total dissolved solid; DOC: Dissolved organic carbon; FW: Flow back water; PDA: Polydopamine; CEES: 2-Chloroethyl ethyl sulfide; DMMP: Dimethyl methylphosphonate; DOP: Dioctyl phthalate; ChO: Chemical oxidation; HPL: Hexagonal perforated lamellar; PPV: Poly(p-phenylenevinylene); ADL: Atomic layer deposition

Amphiphile	Cross-linker	Initiation system	Reaction temperature [°C]	Amphiphile concentration [wt%]	Structure before polymerization	Structure after polymerization	Lattice parameter before reaction [nm]	Lattice parameter after reaction [nm]	Application characteristics of the product	Polymerization kinetics	Remarks	Ref.
P-A-1	-	I-15 or UV	RT - 60	48 - 83 (H ₁) 83 - 92 (Q ₁) > 94 (L _α)	H ₁ , Q ₁ , L _α	Retention of the structures	4 (H ₁), 7.21 (Q ₁), 3.02 (L _α)	4.08 (H ₁), 7.57 (Q ₁), 2.95 (L _α)	20 °C higher thermal stability of the cured LLC	Conversion of ~ 30%	-	73
P-A-2	-	I-15 or UV	RT - 60	>75	L _α	-	2.5 - 2.97	-	-	Polymerization was not successful	-	73
P-A-3	-	I-15 or UV	60	50 - 60 (L ₁) 63 - 80 (H ₁)	L ₁ , H ₁	Retention of the structures	3.57 (H ₁)	3.57 (H ₁)	No difference in thermal stability after templating	Conversion of ~ 45%	-	75
P-A-4	-	γ-ray radiation	RT	58 - 65	H ₁	Retention of the structures	3.98	-	Swelling with polar and nonpolar solvents	Higher reaction rate than non-LLC sample but lower conversions than P-A-5 (conversion of ~ 60%)	Reactive group in the tail resulted in an incomplete reaction	76
	-	I-2 or I-5	RT	60 - 79 (H ₁) > 82 (L _α)	H ₁ , L _α	Complete structure lose with I-5 and limited retention of H ₁ with I-2	4.157 (H ₁), 3.05 (L _α)	-	-	Polymerization rate: L _α < H ₁ < non-LLC Higher polymerization rate with I-2 Lower reaction rate compared to P-A-5	To prepare H ₁ and L _α , 10-29 and 32-40 wt% A-3 was used, respectively with respect to the total surfactant content	96
P-A-5	-	γ-ray radiation	RT	50 - 60 (L ₁) 60 - 83 (H ₁) 83 - 90 (Q ₁)	L ₁ , H ₁ , Q ₁	Retention of the structures	3.56 (H ₁), 7.3 ± 0.7 (Q ₁)	3.83 (H ₁)	Higher toluene uptake for H ₁ over Q ₁ Higher water uptake for Q ₁ over H ₁	Polymerization rate: non-LLC < Q ₁ < L ₁ < H ₁ Almost complete conversion for LLC samples	The order of the structures were changed by swelling	76
	-	I-5	RT - 55	60 - 80 (H ₁) 80 - 90 (Q ₁) > 90 (L _α)	H ₁ , Q ₁ , L _α	Retention of the structures	3.71 (H ₁), 3.03 (Q ₁)*	3.71 (H ₁), 3.3 (Q ₁)*	-	Polymerization rate: H ₁ < Q ₁ < Q ₁ + L _α < L _α	-	97
	-	I-5	RT	50 (Dis. Cube) 60 - 78 (H ₁) > 90 (L _α)	Dis. Cube, H ₁ , L _α	H ₁ changed to L _α L _α is retained	3.55 (H ₁)	3.7 (H ₁)	-	Polymerization rate: Dis. Cube = Dis. Cube/H ₁ < H ₁ < L _α	H ₁ structure was highly prone to phase transition	98
P-A-5	-	I-2 or I-5	RT	60 - 79 (H ₁) 79 - 82 (Q ₁) > 82 (L _α)	H ₁ , Q ₁ , L _α	structure retention in higher reaction rates	3.84 (H ₁), 3.2 (Q ₁)*, 3.07 (L _α)	3.88 (H ₁)	-	Polymerization rate: non-LLC < H ₁ = Q ₁ < L _α Higher polymerization rate with I-2	To prepare H ₁ , Q ₁ and L _α , 10-29, 29-32 and 32-40 wt A-3 was used, respectively with respect to the total surfactant content	96
	-	I-5	RT	50 (Dis. Cube) 60 - 78 (H ₁) > 90 (L _α)	Dis. Cube, H ₁ , L _α	H ₁ changed to L _α L _α is retained	4.32 (H ₁)	4.18 (H ₁)	-	Polymerization rate: Dis. Cube < Dis. Cube/H ₁ < H ₁ < L _α	The polymerization rate of P-A-6 was lower than P-A-5	98
C-6	I-5	RT	70	H ₁	H ₁ is retained when more than 5.9% C-6 is used	(in 0 - 8.34% of C-6)	4.32 - 4.1	-	Higher water uptake when H ₁ structure is retained	Polymerization rate was the highest when transition from H ₁ to L _α happened (C-6 content of less than 3.5%)	Higher water uptakes at higher cross-linker contents was in contrary with the behavior of the non-LLC samples	89
P-A-6	C-8 / C-9-b	I-3	RT	55-80	H ₁	Retention of the structure	4.16	4.16	Thickness-normalized water permeability of ~10 liters m ⁻² hour ⁻¹ bar ⁻¹ μm The molecular weight cut off and size cut off for the charged solutes were ~350 Da and 1 nm Antifouling properties toward biofouling and antimicrobial properties due to the presence of quaternary ammonium groups	-	Using the oil- and water-soluble cross-linkers resulted in excellent mechanical properties and prevented phase transition Alignment was not required	30
P-A-7	-	I-5	RT	50 (Dis. Cube) 60 - 78 (H ₁)	Dis. Cube, H ₁	H ₁ changes to L _α	4.8 (H ₁)	4.64 (H ₁)	-	Polymerization rate: Dis. Cube < Dis. Cube/H ₁ < H ₁	-	98
P-A-8	-	I-15 or UV	RT - 60	40 - 57 (L ₁) 70 - 73 (H ₂) 80.7 (Q ₁)	L ₁	-	-	-	-	More than 95% conversion in 15 min with I-15	P-A-8 formed H ₁ , Q ₁ and L _α , but polymerization was not successful for these structures	123
P-A-9	This reactive surfactant has been used for transcriptive templating. Please see Table 3/M-9 section.											
P-A-10 or P-A-11	C-3	I-2	RT	-	-	-	-	-	Water contents of around 40% can be tolerated with the transparent polymers	-	The presence of methacrylate at the hydrophilic head group and low cross-linker content resulted in phase transition	124
P-A-12	C-3	I-2	RT	81	H ₂	Retention of H ₂ at 10 wt% C-3	6.53	7.1	-	-	The structure cannot be retained at 30 wt% C-3	77
P-A-13	C-3	I-2	RT	28 (Dis. Cube) 54 (H ₂)	Dis. Cube, H ₂	Disordered structure at 30 and 12 wt% C-3 for H ₂ and Dis. Cube, respectively	8.65 (H ₂)	9.62 (H ₂)	-	Incomplete conversion due to the chains mobility restriction in cross-linked network	-	77

525

526

527

528

Table 2. Summary of the reported results for synergistic LLC templating (continue).

Amphiphile	Cross-linker	Initiation system	Reaction temperature [°C]	Amphiphile concentration [wt%]	Structure before polymerization	Structure after polymerization	Lattice parameter before reaction [nm]	Lattice parameter after reaction [nm]	Application characteristics of the product	Polymerization kinetics	Remarks	Ref.
P-A-14	C-3	I-2	RT	54	H ₁	Structure Retention at 30 wt% C-3	7.61	7.82	-	-	-	77
	-	I-17	60	47 - 59	H ₁	Disordered structure at high temperature	4.192 (H ₁)	2.883 (L _α)	-	-	After polymerization, L _α was seen when the temperature was decreased to 20 °C	57,71
P-A-15	-	γ-ray radiation	30 - 60	40 - 60	H ₁	Probable change to L _α	-	-	-	Conversion of ~ 20 - 40% The highest polymerization rate happened in LLC structure	-	72
	-	I-15 or UV	RT - 60	< 38 (L ₁) 42 - 55 (H ₁)	L ₁ , H ₁	Retention of the structures	4.5 (H ₁)	3.7 (H ₁)	-	Conversion of less than 30% Conversion in non-LLC phase was ~ 80%	-	74
P-A-16	-	γ-ray radiation	0 - 70	-	-	-	-	-	-	Conversion of less than 30%	This mixture can form L _α at temperatures more than 100 °C	72
P-A-17	C-1	I-3	RT	80	L _α	Retention of the structure	3.56	3.62	Insolubility in water and organic solvents even without cross-linker	Almost complete conversion	-	106
P-A-18	C-1	I-3	RT	20 (Q ₁) 80 (L _α)	Q ₁ , L _α	L _α was retained but Q ₁ changed to L _α	2.58 (L _α), 10.47 - 11.59 (Q ₁)*	2.93 (L _α), 3.33 - 3.45 (Q ₁)*	Insolubility in water and organic solvents even without cross-linker	Almost complete conversion	Q ₁ changed to L _α with or without using C-1	106
P-A-19 / P-A-20	-	I-20	60 - 65	2.5 - 50	H ₂ , L _α , Q ₂	Retention of H ₂	5.5 (L _α), 6.5 (H ₂)	6.75 (H ₂)	Improved thermal stability Not soluble in organic solvents	Conversion of more than 80%	H ₂ and L _α were seen at temperatures higher and lower than 60 °C, respectively Q ₂ structure was obtained via low concentrations of P-A-19/P-A-20 in water (25 - 100 mg/ml)	58
P-A-21	-	I-16 or I-19	60	50	H ₂	Retention of the structure	7.26	7.06	Improved thermal stability	Conversion of more than 90%	The presence of H ₂ + Q ₂ phase was detected for the LLC before polymerization when the temperature was less than 40 °C	82
P-A-22	This reactive surfactant has been used for transcriptive templating. Please see Table 3/M-4 section.											
P-A-23	C-1	I-1	RT	87	H ₂ , L _α	Retention of the structures	3.2 - 4.24 (H ₂), 3.82 (L _α)	3.24 - 4.12 (H ₂), 3.82 (L _α)	Precipitation of CdS particles inside the cadmium containing pores by exposure to H ₂ S	Almost complete conversion	L _α was obtained when the metal ion was potassium <i>d</i> -spacing depends on the type of metal ion incorporated in the structure of P-A-23 This structure can also be used for in-situ synthesis of ~ 2 wt% silica in the pores	51,100
P-A-24	C-1	I-1	RT	86	H ₂	Retention of the structure	4.71	4.35	The formed catalyst afforded condensation products with consistent syn/anti diastereoselectivity ratios of ~ 2/1 in Mukaiyama aldol and Mannich reactions in water	-	The structure underwent a slight distortion due to Sc(III) ion exchange	49
P-A-25	-	I-1	RT	82	H ₂	Retention of the structure	2.87 - 5.33	2.92 - 5.35	Higher thermal stability	Conversion of ~ 80%	High water content can change H ₂ to L _α	83
	-	I-1	RT	80	H ₂	Retention of the structure	4.04	3.98	Higher light emission of the nanocomposite compared to pure PPV Longer stability of PPV in polymerized LLC due to the isolation from oxygen	Almost complete conversion	PPV was in-situ formed as a filler in the pores of H ₂ structure	50
P-A-26	-	I-1	RT	85	H ₂	Retention of the structure	3.62 - 4.3	3.49 - 4.13	When PPV was incorporated in trivalent Eu containing polymerized LLC, a new intense emission band appeared compared to sodium ion	Almost complete conversion	Same metal ion charge resulted in same <i>d</i> -spacings Trivalent lanthanide salts showed lower spacings	78
	-	I-1	RT	88	H ₂	Retention of the structure	4.25	4.18	-	-	Xylene solution of initiator was used in LLC preparation	84
	-	I-1	RT	80	H ₂	Retention of the structure	4.04	3.98	Water flux of 0.3 ± 0.1 L m ⁻² h ⁻¹ at 50 psi The pore size of 1.2 nm based on the molecular weight cut off	Conversion of less than 30% in air Almost complete conversion in nitrogen	To prepare the membrane, a solution of LLC in methanol was used for roll-casting	93

529

530

531

532

Table 2. Summary of the reported results for synergistic LLC templating (continue).

Amphiphile	Cross-linker	Initiation system	Reaction temperature [°C]	Amphiphile concentration [wt%]	Structure before polymerization	Structure after polymerization	Lattice parameter before reaction [nm]	Lattice parameter after reaction [nm]	Application characteristics of the product	Polymerization kinetics	Remarks	Ref.
P-A-26	-	I-1	RT	25 - 73.5	H ₂	Retention of the structure	4.22 (at 13.8 wt% BR)	4.1	The prepared membrane of polymerized LLC/BR composite resulted in water vapor flux of 438 g m ⁻² day Additional BR phase vulcanization step was used to improve CEES rejection	Conversion of ~ 79%	Blending with 25 wt% BR increased <i>d</i> -spacing to 3.95 H ₂ structure was achieved when up to 75 wt% BR was used BR solution in <i>n</i> -hexane was used for blending	92
	-	I-1	RT	80	H ₂	Retention of the structure	-	4.03	The membrane of the polymerized LLC significantly influenced the solubility of CO ₂ and retarded the diffusion for all gases	Almost complete conversion	To prepare the membrane, a solution of LLC in ethyl acetate was used for casting	94
	-	I-4	RT	88.5	H ₂	Retention of the structure	-	-	-	-	Magnetic field was used to successfully align the nano-channels before polymerization 8 wt% of M-4 was also used as the oil phase in LLC	125
P-A-27	-	I-1	RT	86	H ₂	Retention of the structure	3.84 (P-A-27a) 4.14 (P-A-27b)	3.77 (P-A-27a) 3.98 (P-A-27b)	Higher thermal stability	-	<i>n</i> -Dodecane initiator solution was used in LLC preparation	84
P-A-28	-	I-1	RT	84	Q ₂	Retention of the structure	8.87	8.29	The polymerized LLC showed a conductivity similar to the liquid-like electrolytes while maintaining high flexibility even at temperatures as low as -35 °C	Conversion of ~ 85 - 95%	Li salt solution of the liquid electrolyte, propylene carbonate (PC) was used instead of water to prepare LLC Crude P-A-28 containing 0.87 wt% (LiCl + NaCl) free salt contaminants with 15 wt% PC showed L _g structure	116
P-A-29 / P-A-30	-	UV	RT	95	H ₂	Retention of the structure	4.91	4.85	The polyLLC-based catalyst showed higher activity compared to industrially available TEMPO-based catalysts Lower catalyst activity toward alcohols with bigger molecules The catalyst can be reused without major loss of activity	Almost complete conversion	19 wt% of amphiphile was a mixture of P-A-29 and P-A-30 The remaining 76 wt% was P-A-50 The polymerized LLC film was powdered and sieved for 75 - 150 μm particle sizes for catalysis experiments	79
P-A-31	C-1	I-2	RT	50 - 75 (H ₁) 75 - 85 (Q ₂) 85 - 95 (L _a)	H ₁	Retention of the structure	4.57	4.5	Higher thermal stability for the sample containing C-1	Conversion of ~ 90%	It was possible to retain the structure without using a cross-linker The results are for P-A-31b	85
	-	I-2	≥ RT	45 - 85 (H ₁) 80 - 90 (Q ₁) 50 - 98 (L _a)	H ₁ , Q ₁ , L _a	Retention of the structures	3.44 - 4.91 (H ₁) 2.92 - 4.41 (L _a) 7.92 (Q ₁)	3.39 - 4.88 (H ₁) 3.03 - 4.53 (L _a) 7.67 (Q ₁)	Excellent thermal stability in air	Conversion of ~ 23 - 71%	The same conversion range was achieved without initiator LLC formulation and structure characteristics depend on x and y	61
	-	I-1	65	80	Q ₁	Retention of the structure	-	7.23	Thickness-normalized water permeability of ~ 0.089 liters m ⁻² hour ⁻¹ bar ⁻¹ μm Full water flux recovery (> 95%) and less than 15% water flux loss after contact with salty water Membrane pore size of 0.75 nm based on rejection tests	Conversion of more than 90%	P-A-32e was used in this study	33
P-A-32	-	I-1	70	73.9	Q ₁	Retention of the structure	8.86 (at 8.2 wt% BR)	8.52	Higher water vapor permeability compared to the membrane with H ₂ structure prepared via P-A-26 while maintaining proper CEES rejection	Conversion of more than 95%	P-A-32e was used in this study BR solution in <i>n</i> -hexane was used for blending Broader Q ₁ range in phase diagram in the presence of BR (44.7 - 76.4 wt% P-A-32e)	115
	-	I-1	65	80	Q ₁	Retention of the structure	-	8.73 before ALD ~ 8.52 after 5 cycles ALD ~ 6.21 after 10 cycles ALD	After 10 cycles of ALD, the gas selectivity of hydrogen/nitrogen increased from 12 to 65 while gas permeability decreased ~ 40%	Conversion of more than 90%	P-A-32e was used in this study ALD of alumina was carried out to modify/reduce the pore size	117
	-	I-1	65	80	Q ₁	Retention of the structure	-	-	Water filtration performance in between that of conventional NF and RO membranes Low water flux due to high thickness Higher resistance against chlorine degradation	-	P-A-32e was used in this study	119
P-A-33	-	I-1	60	84.2	Q ₁	Retention of the structure	4.95 - 6.73	7.35 - 9.46	The prepared membrane showed water flux and permeability comparable to the membrane prepared by P-A-32	Conversion of more than 95%	Only P-A-33e and P-A-33f can produce Q ₁ structure P-A-33 is cheaper than P-A-32 to be produced	118
P-A-34	This reactive surfactant has been used for transcriptive templating. Please see Table 3/M-22 section.											

533

534

Table 2. Summary of the reported results for synergistic LLC templating (continue).

Amphiphile	Cross-linker	Initiation system	Reaction temperature [°C]	Amphiphile concentration [wt%]	Structure before polymerization	Structure after polymerization	Lattice parameter before reaction [nm]	Lattice parameter after reaction [nm]	Application characteristics of the product	Polymerization kinetics	Remarks	Ref.
P-A-35	-	I-1	70	79.7	Q ₁	Retention of the structure	8.71	9.34	Thickness-normalized water permeability of ~ 0.066 liters m ⁻² hour ⁻¹ bar ⁻¹ μm Water flux was comparable to the industrially used NF and RO membranes Salt rejection was between NF and RO Partial ion exchange can result in a reversible change in water flux Unique selectivity toward TDS and DOC under different FW pH Higher fouling resistance and flux recovery compared to industrially used membranes	Conversion of more than 90%	Glycerol was used instead of water for the formation of LLC To prepare the membrane, a solution of LLC in methanol was used for roll-casting Ion exchange did not affect <i>d</i> -spacing	32,11 4,120,1 21
	-	I-1	70	79.4	Q ₁	Retention of the structure	-	4.03 *	Higher water/CEES and water/DMMP molar vapor selectivity compared to previously reported LLC based membranes	Almost complete conversion	Glycerol was used instead of water for the formation of LLC The prepared membrane was cheaper than the BR/LLC system in same application The membrane did not have appropriate selectivity toward water over CEES without addition of a PDA layer on the surface of the membrane	112
	-	I-1	52.5	79.4	Q ₁	Retention of the structure	-	-	Eternal presence of anionic polymer inside the pores resulted in significant changes in ion sorption and pore transport properties	Almost complete conversion	Glycerol was used instead of water for the formation of LLC The internal surface of the pores was modified by polymerization of M-31 inside the pores	113
	-	I-1	52.5	79.4	Q ₁	Retention of the structure	-	10.57	Higher dehydration and resistivity of Q ₁ AEM in dilute FeCl ₃ solutions compared to amorphous AEMs thanks to closer spacing of ion exchange sites	Almost complete conversion	Glycerol was used instead of water for the formation of LLC The prepared membrane was used as anion exchange membrane (AEM)	52
P-A-36a	-	UV	RT	78 ± 3	No structure	Formation of L _α	-	2.8	Proper thermal stability and high swelling capacity via water and polar hydrogen-bonding solvents	Conversion of more than 98% Thermal polymerization resulted in a limited conversion	Reversible swellability of the polymer and insolubility in organic solvents were signs of cross-linked network Both thermal and photopolymerization were carried out without initiator	86,87
P-A-36b	-	UV and I-1	RT	60 - 70 (H ₂)	H ₂	Formation of Q _α at low water contents Retention of H ₂	3.23 (H ₂)	3.78 (H ₂) 4.3 - 7.97 (Q _α)	Enhanced mechanical properties and insolubility in a variety of solvents were the key characteristics of the obtained compatible IPN	-	Mechanically robust gel was obtained through production of IPN via swelling the polymerized LLC by M-33 and then photopolymerization initiated by I-1 The structure changed to L _α after formation of the IPN (lattice parameter of 3.3 nm)	87,90
P-A-37	-	ChO	RT	> 85	H ₂	Disordered structure	3.41	-	-	-	Anion-exchange to a divalent anion (sulfate and sulfite) and difficulty of controlling the regio-regularity during the polymerization of thiophene were the reason of losing the structure after polymerization	126
P-A-38	C-10b	I-1	RT	87.9	H ₂	Formation of HPL structure	3.12	-	Relatively low T _g , high thermal stability, and high resistance toward swelling by in organic solvents and water were the important features of the product	Conversion of 93 ± 4%	It was not possible to produce a durable, self-supporting materials without C-10 or by using I-18	88
P-A-39	-	I-21	90 ± 5	50 ± 5	HPL	HPL changed to a hybrid of H ₂ and L _α	3.74 *	3.38 *	Enhanced conductivity of the thin film via LLC templating	Conversion of 40 - 60%	The polymer showed L _α structure when it was applied on a glass substrate as a thin film	103
P-A-40	C-10b	I-13 and UV	RT	~ 15.25	H ₂	H ₂ changed to HPL structure H ₂ was retained by post-UV curing of 3D-printed sample	4.6	3.92 (for the retained H _α)	Proper structure stability toward swelling and de-swelling by ethanol	Incomplete conversion for the 3D-printed sample 1 hr exposure to UV was used to complete the reaction	Disruption of the structure was observed at C-10 contents of higher and lower than 20 w%	91
P-A-40 / P-A-41	-	UV	RT	~ 80	No structure	Formation of H ₂	-	3.2	Enhanced thermal stability due to the presence of covalently bound nanodiamond	Complete conversion	A mixture of 17 wt% DMSO and 3 wt% water was used as the solvent	80

535

536

Table 2. Summary of the reported results for synergistic LLC templating (continue).

Amphiphile	Cross-linker	Initiation system	Reaction temperature [°C]	Amphiphile concentration [wt%]	Structure before polymerization	Structure after polymerization	Lattice parameter before reaction [nm]	Lattice parameter after reaction [nm]	Application characteristics of the product	Polymerization kinetics	Remarks	Ref.
P-A-40 / P-A-42	-	UV	RT	70 ± 2	H ₂	H ₂ changed to HPL structure	3.29	-	Minor structure variations via limited swelling with water	Complete conversion	Pairs of quantum-dot core-shell particles were confined within the center of mesoscale cylinders 10 wt% of the total amphiphile was P-A-42	127
P-A-43	-	I-15	60	50	H ₂	Loss of some long-range order	6.14	5.1	The cross-linked network showed photo-responsive behavior	Conversion of 40 - 50%	P-A-43 showed thermotropic LC with columnar hexagonal structure that can be swollen by diglyme to form LLC Photopolymerization resulted in loss of structure due to isomer changes before cross-linking	128
P-A-44 / P-A-45	-	I-16	45	25	Q ₂	Retention of the structure	12.3	13.5	The polymerized LLC was soluble in organic solvents due to incomplete cross-linking but it showed higher thermal stability compared to non-polymerized LLC	-	The ratio of P-A-44/P-A-45 in LLC was 9/1	108
P-A-46	This reactive surfactant has been used for transcriptive templating. Please see Table 3/M-4 section.											
P-A-47	This reactive surfactant has been used for transcriptive templating. Please see Table 3/M-7 section.											
P-A-48	-	I-5	RT	10 - 50	Dis. Cube, L _α	Higher reaction rate results in structure retention	-	-	-	L _α had the highest polymerization rate	The LLC structure was altered with changing pH at a fixed amphiphile content	122
P-A-49	-	I-1	RT	93	H ₂	Retention of the structure	4.81	4.56	Similar activity and 10 times higher selectivity compared to industrially available catalysts for esterification reaction	Conversion of more than 90%	The ratio of P-A-49/P-A-50 in LLC was 5/1 to have pure H ₂ phase P-A-49 contained strong acid properties and P-A-50 directed the LLC assembly via amide H-bonding	129
P-A-50	This reactive surfactant was discussed in P-A-29/P-A-30 and P-A-49 sections											
P-A-51	-	I-1	RT	90 (solution in an acid)	H ₂	Retention of the structure	4.7 - 5.7	4.83 - 5.67	No enhancement of enantio- or diastereo-selectivity by polymerized LLC	Conversion of more than 90%	LLC structure depends on the nature of the acid used for LLC formation	130
P-A-52	-	γ-ray radiation	RT	a: 25 - 57 (H ₁) > 66 (L _α) b: 45 - 75 (H ₁) > 85 (L _α)	H ₁ , L _α	Retention of the structures	5.1 (H ₁)	4.83	The gel morphology was stable against temperature changes, extraction, drying, and reswelling with polar or nonpolar solvents	Complete conversion	H ₁ structure was used as a template for mesoporous silica synthesis and the structure was retained without cross-linking	101
P-A-53	-	I-1	RT	55 - 65 (H ₁) 75 - 80 (L _α)	H ₁ , L _α	Retention of the structures	6.01 - 6.59 (H ₁) 5.46 - 5.54 (L _α)	6.14 - 6.72 (H ₁) 5.61 - 5.68 (L _α)	Enhanced mechanical and thermal stability of the polymerized LLC when P-A-53 is used	-	P-A-53 cannot form LLC, but it can in combination with A-18b	81
P-A-54	-	UV	RT	50 (H ₁) 73 (L _α)	H ₁ , L _α	Retention of the structures	10.95 (H ₁) 8.34 (L _α)	10.17 (H ₁) 8.03 (L _α)	The polymerized structure was destroyed when swelled by an organic solvent, but after drying and swelling with water, the original structure was retained	Almost complete conversion	The direct UV-initiated polymerization happened due to the photosensitive cinnamoyl moieties	102
P-A-55a / A-7 / A-8	C-10b	I-1	RT	~ 26.5	L _α	Retention of the structure	12.2	11.7	Enhanced mechanical properties and preserving the structure after swelling even by organic solvents were the main characteristics of the obtained hydrogel	-	The presence of the self-assembled lipid bilayer was crucial for formation of L _α The weight ratio of P-A-55a/A-7/A-8 was 60/5/35	105
	C-10b	I-1	RT	22.8	L _α + L ₁	Packed hard sphere structure	19.5	26.5	-	Complete conversion	P-A-55a was used in this study	105
P-A-55	-	I-3 or I-9	RT	5 - 24	Dis. Cube with FCC lattice	Retention of the structure	~ 15 - 30 (depending on the surfactant content and temperature)	~ 15 - 30 (depending on the surfactant content and temperature)	Having highly viscoelastic or elastomeric behavior with excellent mechanical properties, conductivity, and mechano-electrical response through controlling the composition of the LLC was the key feature of the product The produced iono-elastomer can be used as a motion sensor as well as temperature sensor with sufficient sensitivity and accuracy	-	P-A-55b was used in these studies Partially deuterated ionic liquid ethylammonium nitrate was used instead of water to prepare the ion gel	46-48
P-A-56	C-1	I-12 or I-20	RT	25	Q ₂	Retention of the structure	-	-	-	Conversion of 95%	The LLC was used to prepare and polymerize nanoparticles with Q ₂ structure (stabilized cubosomes)	110

538 4. Transcriptive LLC templating

539 Although synergistic templating is in many cases sufficient for obtaining polymerized LLCs
540 with a variety of nanostructures for different applications, the tedious in-lab synthesis of many
541 reactive amphiphiles can be a drawback. While some recent works have used commercially
542 available formulation additives in conjunction with surfactants obtained from one-pot
543 synthesis,³⁰ the synthesis of many reactive amphiphiles can be more involved (e.g. Gemini
544 surfactants for cubic bicontinuous mesophases). This issue is also an obstacle in rapid industrial
545 adoption of polyLLCs. Therefore, there have been several efforts to use a combination of
546 commercially available surfactants and monomers instead. In this approach, a non-
547 polymerizable surfactant is usually used to direct the LLC formation followed by the
548 polymerization of the monomer. At the end of this process, which is called transcriptive
549 templating, a polymer having the structure of the parent LLC is formed. Both ternary mixtures
550 of water/hydrophobic monomer/surfactant and binary mixtures of hydrophilic monomer +
551 water/surfactant are common in this templating approach. Despite the advantages obtained
552 from easy sourcing of commercially available materials, preserving the structure of LLC
553 template during polymerization is more challenging in transcriptive templating compared to
554 synergistic templating. Because the formed polymer is not chemically bond to the surfactant,
555 polymerization-induced phase separation/inversion becomes highly probable, reducing the
556 chances of successful transcriptive templating. This issue has been addressed by addition of
557 cross-linkers in the mesophase formulation, using reactive (co)surfactants, and employing
558 block copolymer (BCP) surfactants. The first two approaches are centered around the formation
559 of a kinetically trapped cross-linked network and the last one makes phase-separation/inversion
560 process kinetically slow, enhancing the retention of the structure.³¹ Transcriptive templating is
561 very flexible since different monomers can be polymerized with the same surfactant system
562 without the need for synthesis of new chemicals. Moreover, copolymerization can also be used
563 in the process to add chemical functionality to the final product.¹³¹ As such, a wide variety of
564 surfactants, (co)monomers, and cross-linkers have been used in transcriptive LLC templating,
565 as shown in Fig. 4 and Fig. 5. A summary of the reported results for each monomer is presented
566 in Table 3. Similar to synergistic templating, we will discuss the results of transcriptive
567 templating for each type of LLC structure separately in the following sections.

568

569 4.1. Hexagonal (H_o)

570 Transcriptive templating of a variety of monomers has been reported for the hexagonal phase
571 structure. Based on the employed surfactants and LLC formulations, lattice parameters of ~ 2.7
572 to ~ 14 nm have been obtained for the templated products, a range which is quite similar to that
573 obtained for synergistic templating with H_o . As stated previously, the retention of structure in
574 transcriptive templating is a major concern, especially after removal of the template. While
575 most of the studies have used the three approaches mentioned above, Zhang et al. have also
576 tried an additional step to preserve the H_1 structure directed by A-3 or A-14 surfactants after
577 polymerization of M-24c and removal of the template.¹³² They have reported that when the
578 drying step is carried out under zero surface tension (by replacing water with CO_2) it is possible

579 to retain the structure.¹³² In another effort, they were able to retain the parent structure using a
580 regular drying method via reinforcing the polymerized LLC by an in-situ formed silica
581 network.¹³³ They have also shown that the required silica content for the structure retention can
582 be reduced from 50 to 10 wt% with respect to the total monomer content if low surface tension
583 solvents (e.g., mixture of hexane and ethanol) are used for the template extraction.¹³⁴ It is
584 noteworthy to point out that the silica present in the polymerized domains of the obtained
585 composite material not only participates in the structure preservation, but also imparts
586 relatively higher thermal stability¹³⁴ and enhanced hydrophilicity to the final product.¹³³

587 There have been several efforts to utilize transcriptive templating of H_α structures in different
588 applications. For instance, Guymon and co-workers have used this approach to prepare
589 hydrogels that possess a proper balance of water uptake, swelling/de-swelling rate, and
590 mechanical properties without compromising other properties such as stimuli-responsiveness
591 and biodegradability.³⁵⁻⁴⁵ They have also used transcriptive templating for compatibilization
592 of immiscible monomers. To do so, hydrophilic M-24c and hydrophobic M-20 are mixed with
593 the aqueous solution of A-14, resulting in the formation of an LLC with H_1 structure. The
594 polymerization of these two monomers in the LLC template results in a semi-interpenetrating
595 polymer network (IPN) structure having excellent polymer compatibility.¹³⁵

596 Templating with H_2 structure has also been applied for the fabrication of water filtration
597 membranes. In one such effort, Osuji and co-workers magnetically aligned the nanochannels
598 of a H_2 phase before polymerization to decrease the tortuosity of the produced membrane.
599 Although they were able to successfully retain the aligned structure after polymerization, the
600 study did not extend to filtration membrane fabrication.¹³⁶ Qavi et al. have successfully utilized
601 LLC templating of H_2 structures to fabricate ultrafiltration (UF) membranes that show excellent
602 permeability as well as higher fouling resistance over commercially available UF membranes.³¹
603 Successful production of antimicrobial UF membranes has also been reported by
604 polymerization of M-32 in the same LLC structure.¹³⁷

605 Fabrication of ordered mesoporous carbon (OMC) material is another application of
606 transcriptive templating of H_1 structures. Polycondensation and cross-linking of monomers
607 such as M-34, M-35, M-36 and M-37 results in a nanostructured thermoset polymer such as
608 phenol-formaldehyde. Subsequently, calcination and carbonization of the polymerized LLC at
609 high temperature (e.g., above 600 °C) is carried out to obtain OMC species.^{19,55,138-141} In the
610 reported results, OMC materials obtained via this technique show extremely high thermal
611 stability,^{19,141} excellent mechanical properties,^{19,55} enhanced electrochemical performance,¹⁴⁰
612 and promising CO_2 capture properties.⁵⁵

613

614 **4.2. Lamellar (L_α)**

615 The Lamellar phases are easily accessible structures in most LLC formulations (especially in
616 ternary systems). Several studies performed on transcriptive templating of L_α structure have
617 reported lattice parameters between ~ 2.8 to ~ 10.5 nm. In most such studies, the focus has
618 been on the investigation of fundamental/mechanistic underpinnings of retention of the L_α

619 structure during templating as well as the polymerization kinetics in nanoconfinement.
620 However, there are also studies which primarily focus on the templated products in particular
621 application scenarios. As an illustration, Qavi et al. fabricated UF membranes with transcriptive
622 templating of M-4 in lamellar structure directed by A-19c. According to the obtained results,
623 L_{α} -based membranes not only show higher permeability and fouling resistance over
624 commercially available UF membranes, but also exhibited slightly higher water flux compared
625 to H_2 -based membranes described earlier.³¹ Antimicrobial membranes with lamellar structure
626 have also been successfully fabricated.¹³⁷ In a recent trial, Bandegi et al. have produced a robust
627 ion gel with decent ion conductivity by LLC templating in the presence of 1-ethyl-3-
628 methylimidazolium tetrafluoroborate ionic liquid.¹⁴² In other demonstrations of important
629 applications of transcriptive templating in the lamellar phase, Guymon's team performed
630 compatibilization of immiscible monomers¹⁴³ and synthesis of hydrogels which have a good
631 balance of water uptake, swelling/de-swelling rate, and mechanical properties without
632 changing the chemistry or sacrificing the general biocompatibility of the biopolymers.^{45,89,144}

633

634 4.3. Bicontinuous cubic (Q_{α})

635 The Q_{α} phases have been studied less than H_{α} and L_{α} for transcriptive templating due to the
636 limited accessibility of bicontinuous cubic phase in LLC systems and difficulties in structure
637 retention after polymerization. As shown in Table 3, lattice parameters of ~ 6 to ~ 23.5 nm
638 have been reported so far for the Q_{α} structures used for the templating. In addition to the
639 fundamental studies on the transcriptive templating process with this structure,^{54,145-148} a
640 handful of works have also investigated the applicability of the final product. For instance,
641 Guymon's group has been able to produce a hydrogel with an improved water uptake and de-
642 swelling rate while keeping the mechanical properties intact by taking the advantages of
643 structural interconnectivity in Q_1 phase created by a mixture of A-13 and M-10.¹⁴⁹ They have
644 also used bicontinuous cubic structure directed by A-15 to polymerize M-9 and produce a
645 hydrogel with a faster swelling rate, higher swelling capacity, and higher compressive modulus
646 over non-LLC product.⁴³ In another trial, they have employed P-A-34, a Gemini surfactant, to
647 make Q_1 phase easily accessible. Although the retention of the structure after the template
648 removal was not possible, they observed an enhanced swelling of the polyLLC in water and 2-
649 propanol.²² Generation of a Q_1 structured OMC material with excellent thermal stability and
650 mechanical properties is another notable application of transcriptive templating via
651 bicontinuous cubic mesophase.¹⁹

652

653 4.4. Discontinuous cubic

654 The discontinuous cubic phases are the least studied structure for transcriptive templating.
655 Almost all of the studies on these mesophases, which have been conducted by Guymon and
656 co-workers, have focused on revealing the differences among LLC structures in terms of
657 polymerization kinetics^{35,36,38,39,42,43,99,150,151}. However, the observed higher water uptake in
658 prepared hydrogels with micellar cubic structure over ones with H_1 structure³⁹, as well as the

659 impressive properties of the ion gels obtained from synergistic templating within discontinuous
660 cubic structure^{46–48} indicate that there may be plenty of opportunities in transcriptive templating
661 of such structures to fabricate materials with exceptional properties.

662
663**Table 3.** Summary of the reported results for transcriptive LLC templating.* Calculated *d*-spacing for the primary reflection in the SAXS profile; SWNT: Single-walled carbon nanotube; EP: Electropolymerization; PC: Polycondensation; TEOS: Tetraethoxysilane; EISA: Evaporative induced self-assembly

Monomer	Amphiphile	Cross-linker	Initiation system	Reaction temperature [°C]	Amphiphile / oil (monomer) w/w	Structure before polymerization	Structure after polymerization	Lattice parameter before reaction [nm]	Lattice parameter after reaction [nm]	Application characteristics of the product	Polymerization kinetics	Remarks	Ref.
M-1	A-1	C-1	I-15	85	44.9 / 7	Q_{α}	-	-	-	-	-	Uniform microporous materials of arbitrary size and shape was produced	145
	A-1	-	I-15 / UV	RT	42.66-64.32 / 7.23-19.81	Q_{α}	Retention of the structure	6.01 - 10.017	Remained almost unchanged	-	Conversion of less than 100%	C-1 was also used as monomer instead of M-1 to increase the cross-linking density Q_{α} structure was obtained in surfactant/oil ratio of 30.43 / 4.99 for C-1	54
	A-2	-	I-15	70	19.4 - 37.5 / 3.2 - 6.2	Q_{α}	Q_{α} changed to L_{α}	9.4 - 18.8	8.4 - 14.2	-	-	Phase separation was observed between polymer and the template	146
	A-17	-	-	-	50 / 33 (H_1) 63 / 16 (L_{α})	H_1, L_{α}	H_1 changed to L_{α} Disordered L_{α}	-	-	-	-	-	152
	A-19f	C-1	I-15	70	45 - 65 / 10 - 30	-	H_{α} or L_{α} having some disordered domains	-	-	High mechanical properties while maintaining proper ion conductivity was the main feature of the product	Conversion of ~ 90%	1-Ethyl-3-methylimidazolium tetrafluoroborate ionic liquid was used instead of water to prepare the LLC Polymerization of M-1 was used to enhance the mechanical properties of the ion gel	142
M-2	A-1	-	I-15	RT	55 / 10	Q_{α}	Retention of the structure	-	11.8	-	-	-	145
M-3	A-3	-	I-2	RT	35 / 25 (L_1) 40 / 25 (Q_1) 45 / 25 (H_1) 65 / 25 (L_{α})	$L_1, H_1, Q_1, L_{\alpha}$	Retention of H_1	4.28 (H_1)	4.31 (H_2)	-	Polymerization rate: $L_1 \lll H_1 < L_{\alpha}$	Relative water solubility of M-3 resulted in polymerization in the polar domains of the self-assembled molecules and therefore encapsulation of the surfactant aggregates	153
	A-3	-	I-2	RT	30 / 10 (L_1) 50 / 10 (H_1) 70 / 10 (Q_1) 75 / 10 (L_{α})	$L_1, H_1, Q_1, L_{\alpha}$	-	-	-	-	Polymerization rate: $L_1 \lll H_1 < Q_1 < L_{\alpha}$	Higher reaction rate resulted in higher MW of the produced polymer	99
M-4	P-A-22 / P-A-46	C-7	I-18	RT	63.2 / 19	H_2	Retention of the structure	5.37	5.5	It is expected that the prepared membrane has high permeability as well as proper selectivity due to the low-tortuosity of the aligned nanostructure	-	To be able to preserve the structure, 6.3 wt% cyclohexane was added to the mixture as a non-reactive oil phase Nano-channels alignment was carried out via 5 - 6 T magnetic field before polymerization The reactive amphiphiles were commercially available	136
	A-19	C-8	I-9 / I-15	RT - 70	55 - 60 / 25 - 30 (H_2) 50 - 60 / 10 - 15 (L_{α})	H_2, L_{α}	Retention of the structures	10.2 - 10.4 (H_2) 7.4 - 8.5 (L_{α})	10.4 - 10.7 (H_2) 7.8 - 9.2 (L_{α})	The fabricated membrane showed excellent permeability as well as higher fouling resistance over a commercially used UF membrane	-	A-19c was used	31
	A-19	C-8	I-15	60 - 70	40 - 55 / 25 (H_2) 57 - 60 / 25 (L_{α})	H_2, L_{α}	Retention of the structures	6.6 - 7.4 (H_2) 6 - 10 (L_{α})	7.32 - 7.41 (H_2) 6 - 10.18 (L_{α})	-	Polymerization rate: $L_{\alpha} < H_2 \lll \text{non-LLC}$	A-19a, A-19c, and A-19d were used The formulation of LLC and LLC characteristics depend on m and n in the amphiphile structure	56
	A-19	C-8	I-15, I-17 or I-23	55 - 75	50 / 15 (L_{α}) 55 / 30 (H_2)	H_2, L_{α}	Retention of the structures	6.4 (L_{α}) 5.75 (H_2)	4.98 - 51 (L_{α}) 6.25 - 6.47 (H_2)	Mechanical properties of polyLLCs improved when I-17 was used	Polymerization rate: $L_{\alpha} < H_2$ I-17 resulted in faster polymerization rate in both LLC structures	A-19c was used	154
M-5	A-3	-	I-2	RT	50 / 25 (H_1)	H_1	Disordered structure	-	-	-	-	-	153
	A-3	-	I-2	RT	30 / 10 (L_1) 50 / 10 (H_1) 80 / 10 (L_{α})	L_1, H_1, L_{α}	Disordered structure for H_1	4.92 (H_1)	4.46 (H_1)	-	Polymerization rate: $L_{\alpha} < H_1 < L_1 < L_1/H_1$	Higher reaction rate resulted in higher MW of the produced polymer Phase separation was seen for LLC and polymer for H_1 structure	99
M-6	A-3	-	I-2/I-5	RT	35 / 10 (L_1) 40 / 10 (Dis. Cube) 55 / 10 (H_1) > 60 / 10 (L_{α})	$L_1, \text{Dis. Cube}, H_1, L_{\alpha}$	-	-	-	-	Polymerization rate: $L_{\alpha} < H_1 < \text{Dis. Cube} < L_1$	-	42
	A-3	-	I-2	RT	40 / 25 (Q_1) 50 / 25 (H_1) 60 / 25 (L_{α})	H_1, Q_1, L_{α}	Disordered structure of H_1	5.52 (H_1)	4.25	-	Polymerization rate: $L_{\alpha} < H_1 < Q_1$	M-6 tends to be present at nonpolar domains, so the formed polymer framework was weak, resulting in structure disruption	153

664
665

666

Table 3. Summary of the reported results for transcriptive LLC templating (continue).

Monomer	Amphiphile	Cross-linker	Initiation system	Reaction temperature [°C]	Amphiphile / oil (monomer) w/w	Structure before polymerization	Structure after polymerization	Lattice parameter before reaction [nm]	Lattice parameter after reaction [nm]	Application characteristics of the product	Polymerization kinetics	Remarks	Ref.
M-6	A-3	-	I-2	RT	30 / 10 (L ₁) 40 / 10 (Dis. Cube) 55 / 10 (H ₁) 75 / 10 (L _α)	L ₁ , Dis. Cube, H ₁ , L _α	-	-	-	-	Polymerization rate: L ₁ < L _α < Dis. Cube < H ₁	The MW of the produced polymer increased from micellar to H ₁ and then decreased in L _α structure	99
M-7	P-A-47 / A-16b	C-5	-	35	21.6 / 20	L _α	Retention of the structure	-	7.2	Anisotropic increase of the dimensions through swelling with water	Conversion of more than 95%	3.8 wt% P-A-47 was used in this study The structure was retained even after removal of the template 2 T magnetic field was used for the alignment of the structure before polymerization MW of P-A-47 did not affect d-spacing	155
M-8	A-15 or A-20	C-8	I-18	55	7 -9 / 20 -37 for A-15 30 / 7.6 for A-20	-	-	-	-	-	Complete conversion	M-8 was copolymerized with M-17 with 1:1 ratio The produced copolymer showed continuous gel structures of high connectivity, where the gel is composed of polymer strings, resembling the morphology of a marine sponge The type of surfactant had only a marginal influence on the final gel structure	131
A-1 or A-16a	C-2	I-16 / UV	RT - 55	24.3 / 10 for A-1 69.7 / 6.05 for A-16a	Q _α	Retention of the structure	-	9.3 for A-16a	-	-	-	Decane was also used in preparation of LLC with A-1	145,147
A-10 or A-12	C-2	I-14	RT	47.7 / 10 for A-10 50 / 10 for A-12	H ₁ with A-10 Q _α and L _α with A-12	Retention of the structures	4.53 (H ₁) 3.81 (L _α)	4.69 (H ₁) 3.69 (L _α)	-	-	Conversion of ~ 95% for H ₁ and L _α Conversion of ~ 75% for Q _α	Q _α was obtained from ternary system of water/A-12/decanol	148
A-5 or A-11	C-2	I-18	60	43 - 48 / 26	H ₁	H ₁ changed to L _α with A-11	-	-	-	Enhanced mechanical stability of water-swollen gels	-	The structures can be destroyed with the removal of the template The prepared gels can be chemically functionalized by incorporation of M-17, M-15, M-12, M-14 and M-13/M-21	152,156
A-14	C-2	I-18	55	6 -28 / 23 -30	-	-	-	-	-	The prepared gel showed a reduction of the moduli by only 10 - 40%	Complete conversion	Continuous gel structures of high mechanical strength was obtained due to the presence of a structure having connected spherical gel particles of ~ 500 nm diameter	131
M-9	A-15	C-2	I-5 or I-15	RT - 60	30 / 25 (L ₁) 40 - 60 / 25 (Q ₂) 70 / 25 (L ₂)	L ₁ , Q ₂ , L ₂	Retention of Q ₂	6.1 (Q ₂) *	Remained almost unchanged	Faster swelling rate, higher swelling capacity and higher compressive modulus of the structured gel compared to non-LLC one	Polymerization rate: non-LLC <<< L ₁ = L ₂ < Q ₂	Monomer concentration had a minor effect on the polymerization rate Q ₂ changed to L _α when I-15 was used to carry out the reaction at 60 °C	35,36,43,157
A-14	C-2	I-5, I-6 or I-15	RT - 80	40 / 25 (Dis. Cube) 50 - 60 / 25 (H ₁) 70 / 25 (L ₂)	Dis. Cube, H ₁ , L ₂	Retention of the structures when I-5 was used Disruption of the structures when I-15 was used for thermal polymerization	-	-	-	Anisotropic increase of the dimensions through swelling with water in the case of the LLCs polymerized via I-15 and I-5 at high temperatures Higher water uptake for the polymerized Dis. Cube structure compared to H ₁	Polymerization rate with I-5: non-LLC <<< L ₂ < Dis. Cube < H ₁ Polymerization rate with I-6: non-LLC <<< Dis. Cube ≤ H ₁ ≤ L ₂ Photoinitiation resulted in much faster polymerization rate compared to thermal initiation	Higher temperature resulted in lower reaction rate by changing structure to micellar Slow reaction rate was the reason of structure lose after polymerization by I-15	35,36,38,39
A-5 / P-A-9	C-2	I-2	RT	50 / 20	H ₁	Retention of the structure was not possible with A-5 Addition of 10-15 wt% P-A-9 resulted in the structure retention	4.53 - 4.68	5.58 - 6.04	-	Higher water swelling rate was seen for the hydrogel having H ₁ structure The water uptake decreased with an increase in hydrophobic P-A-9 content The hydrogel with H ₁ structure showed improved release properties Higher compressive modulus was seen in dehydrated state for the polymerized LLC compared to non-LLC sample	The polymerization rate increased with an increase in the content of P-A-9 due to the structure retention	-	40
M-10	A-14	C-2	I-18	55	10 - 24 / 24 -30	-	-	-	-	The moduli of the formed gels strongly depend on the frequency and the gels have a low absolute strength	Complete conversion	A "cauliflower" morphology was obtained	131

667

668

669

670

Table 3. Summary of the reported results for transcriptive LLC templating (continue).

Monomer	Amphiphile	Cross-linker	Initiation system	Reaction temperature [°C]	Amphiphile / oil (monomer) w/w	Structure before polymerization	Structure after polymerization	Lattice parameter before reaction [nm]	Lattice parameter after reaction [nm]	Application characteristics of the product	Polymerization kinetics	Remarks	Ref.
M-10	A-13	C-2	I-2	RT	50 / 20	Q_i	Retention of the structure	-	-	400% more water uptake in the temperatures less than 33 °C, similar compressive modulus despite of higher water uptake and higher de-swelling rate of templated hydrogel compared to non-LLC sample	-	-	149
	A-13	C-2	I-1	RT	50 / 40	H_i	Retention of the structure (especially at high M-29 contents)	7.18 - 7.65	7.04 - 7.18	Relatively lower water uptake, intact thermoresponsive behavior, high de-swelling rate and appropriate mechanical properties when M-29 was incorporated in LLC	Limited effect of M-29 concentration on the conversion	M-29 was incorporated in the LLC (6.7 - 50 wt% with respect to the total monomer content) to improve the mechanical properties of the produced hydrogel without compromising other properties	41
	A-13	C-2	I-2	RT	40 / 20	Q_i	Retention of Q_i at low M-16 contents Q_i changed to H_i at 4 wt% M-16 content	-	8.24 (H_i)	Dramatic increase in water uptake, shifting the thermoresponsive behavior to higher temperatures and lower de-swelling rate by incorporation of M-16 in the LLC structure	-	M-16 was incorporated in the structure of the LLC (up to 4 wt% with respect to the total monomer content) to improve water uptake while preserving other properties	37
M-11	A-14 or A-20	C-2	I-18	55	24 / 24 for A-14 28 / 14 for A-20	-	-	-	-	The prepared gel showed a reduction of the moduli by only 10 - 40%, a weak frequency dependence and low mechanical loss	Complete conversion	Continuous gel structures of high mechanical strength was obtained due to the presence of a structure having connected spherical gel particles of ~ 500 nm diameter	131
M-12	This monomer was discussed in M-9 section												
M-13	A-14 or A-20	C-8	I-18	55	24 / 24 for A-14 28 / 14 for A-20	-	-	-	-	The prepared gels had a low absolute modulus and a very high mechanical loss	Complete conversion	The obtained gel showed a morphology consisting of porous sheets	131
	A-3	C-9	I-2 / I-5	RT	40 - 45 / 20 (Dis. Cube) 50 - 55 / 20 (H_i) 60 - 65 / 20 (L_{α})	Dis. Cube, H_i , L_{α}	Disordered H_i and L_{α}	4.2 (H_i) 2.96 (L_{α})	4.4 (H_i) 3.22 (L_{α})	Lower water uptake, slower swelling rate and lower compressive modulus compared to non-LLC sample	Polymerization rate: non-LLC < H_i = Dis. Cube < L_{α}	Lower effective cross-linking density seemed to be the reason of weak hydrogel properties	42,43
	A-3	C-9	I-4	RT	47.5 / 19	H_i	Retention of the structure	3.7	3.81	-	-	The hydrophobic tails of the surfactant adsorbed to the hydrophobic SWNTs, resulting in the confinement of the nanoparticles inside the pores of H_i structure 5 T magnetic field was used to align the structure before polymerization	29
M-14	This monomer was discussed in M-9 section												
M-15	This monomer was discussed in M-9 section												
M-16	This monomer was discussed in M-10 section												
M-17	This monomer was discussed in M-8 and M-9 sections												
M-18	A-18b	-	EP	-	35 - 60 / 0.25 M	H_i	Retention of the structure even after removal of the template	6.65	-	Higher conductivity, and anisotropic absorption and conductivity of the templated film compared to the non-templated sample	-	LLC templating eliminated the need for post-polymerization methods (e.g., stretching and rubbing) to align the conductive film layer	158,159
	A-5	-	I-22	RT	Up to 0.3 M monomer was used	H_i	Limited retention of the structure	-	40 (thickness of spindle like nanostructures)	Good thermal stability (up to 200 °C) of the obtained nanostructures Higher electrical conductivity of the produced nanostructures compared to non-templated products	-	Pentanol was used as a cosurfactant Solution of M-18 in toluene was used as the oil phase	160
M-19	A-18	C-4	PC	-	50 - 70 / ~8	H_i , L_{α}	Formation of rod and sheet particles from H_i and L_{α} , respectively after about 5 days	6.37 (H_i)	6.62 (H_i) after 5 days	The particles were thermally stable while the polymerized LLCs were not	-	LLC structures were preserved after reaction. However, the structure of produced polymer changed from polyLLC to polymeric particles after ~ 5 days Slow condensation and cross-linking kinetics, gradual build-up of molecular weight, and the nonlinear architecture of the polysiloxane molecules seemed to be the reason of the particles formation	161
M-20	A-3	-	I-2, I-5, I-6 or I-8	RT	40 / 10 (Dis. Cube) 50 - 60 / 10 (H_i) 70 - 80 / 10 (L_{α})	Dis. Cube, H_i , L_{α}	Retention of H_i	2.69 - 3.9 (H_i) 3.17 (L_{α})	-	-	Polymerization rate with I-2: $L_{\alpha} \leq H_i < \text{Dis. Cube}$ Polymerization rate with I-5: $L_{\alpha} < H_i < \text{Dis. Cube}$ Polymerization rate with I-6: $H_i < L_{\alpha} < \text{Dis. Cube}$ Polymerization rate with I-8: $L_{\alpha} = H_i < \text{Dis. Cube}$	MW of the produced polymer depends on the extinction efficiency of the initiator, monomer segregation, and LLC-dependent initiation efficiency	38,42,150,151,162

671

Table 3. Summary of the reported results for transcriptive LLC templating (continue).

Monomer	Amphiphile	Cross-linker	Initiation system	Reaction temperature [°C]	Amphiphile / oil (monomer) w/w	Structure before polymerization	Structure after polymerization	Lattice parameter before reaction [nm]	Lattice parameter after reaction [nm]	Application characteristics of the product	Polymerization kinetics	Remarks	Ref.
	A-19b	-	I-10	RT	18 / 10 (L ₁) 40 / 10 (H ₁) 58 / 10 (Q ₁) 78 / 10 (H ₂) 82 / 10 (L ₂)	L ₁ , H ₁ , Q ₁ , H ₂ , L ₂	Retention of H ₁ and H ₂	7.27 (H ₁) 10.22 (H ₂)	7.33 (H ₁) 9.95 (H ₂)	Higher thermal stability of the templated sample in H ₂ structure compared to H ₁	Polymerization rate: L ₂ = H ₂ < H ₁ < Q ₁ < L ₁	-	44
M-20	A-14	-	I-5	RT	40 / 40	H ₁	Retention of the structure	-	-	The water uptake decreased, and compressible modulus and T _g increased linearly with an increase in M-20 content approving the compatibility of two polymers via LLC templating	-	This study showed that it is possible to blend two immiscible polymers via LLC templating 25 - 100 wt% M-24c was used with respect to the total monomer content along with M-20	135
	A-14	-	I-2	RT	30 - 40 / 20 (H ₁) 50 - 60 / 20 (L _α)	H ₁ , L _α	Disordered L _α	6.16 (L _α)	-	-	Polymerization rate: non-LLC < L _α < H ₁	-	151
M-21	This monomer was discussed in M-9 section												
M-22	P-A-34	-	I-2	RT	29 / 25 (H ₁) 59 / 14 (Q ₁) 64 / 25 (L _α)	H ₁ , Q ₁ , L _α	Retention of Q ₁ , H ₁ and L _α changed to Q ₁	4.7 (H ₁) 8.3 (Q ₁) 2.8 (L _α)	6.5 - 6.8 (Q ₁)	Higher 2-propanol swelling capacity of the sample which retained Q ₁ structure compared to others Water-swollen polymerized LLCs showed lower compressive modulus over less hydrated non-LLC one Enhanced swelling in water and 2-propanol even after losing the structure due to the surfactant removal	Almost complete conversion	P-A-34 can accommodate up to 37% monomer to form LLC The polymerized LLC that retained Q ₁ structure had uniform structure Retention of the structure after surfactant removal was not possible	22
M-23	A-3	-	I-2, I-5, I-6, I-7 or I-8	RT	40 / 20 (Dis. Cube) 50 - 60 / 20 (H ₁) 65 - 70 / 20 (L _α)	Dis. Cube, H ₁ , L _α	Retention of H ₁ and L _α	-	-	-	Polymerization rate with I-2, I-5, I-7 and I-8: Dis. Cube < H ₁ < L _α	-	38,42,150,162
	A-3	-	I-5	RT	50 / 10 - 30	H ₁	Retention of the structure with some structural changes at high M-23 contents	3.96 (10 wt% M-23) 3.6 (30 wt% M-23)	4 (10 wt% M-23) 3.82 (30 wt% M-23)	-	-	At 30% M-23 rod-like morphology was seen in SEM images	163
	A-3	-	I-1	RT	36.7 / 35.6	H ₁	Retention of the structure after surfactant removal under certain conditions	3.87	3.82	-	-	The retention of the structure was not possible after removal of the surfactant and drying under vacuum or via air drying When drying was carried out by CO ₂ , it was possible to retain the structure thanks to maintaining zero surface tension M-24c was used in this work	132
M-24	A-3	-	I-1	RT	36.7 / 35.6	H ₁	Retention of the structure	3.6 (0% TEOS) 3.68 (10% TEOS) 3.98 (30% TEOS) 4.61(50% TEOS)	3.9 (0% TEOS) 3.6 (10% TEOS) 3.46 (30% TEOS) 3.41 (50% TEOS)	Enhanced hydrophilicity of the product by incorporation of a silica network	-	A polymerized LLC reinforced by an in-situ formed silica network (via condensation of 0 - 50 wt% TEOS with respect to the total monomer content) was produced The presence of silica network resulted in the retention of the structure even after the surfactant removal and drying under vacuum M-24c was used in this work	133
	A-14	-	I-1	RT	40 / 35	H ₁	Retention of the structure	8.37 (0% TEOS) 8.88 (10% TEOS) 9.04 (30% TEOS) 9.39 (50% TEOS)	8.7 (0% TEOS) 8.35 (10% TEOS) 8.02 (30% TEOS) 7.5 (50% TEOS)	Relatively enhanced thermal stability of the product having silica network	-	A mixture of hexane and ethanol was used as the low surface tension solvent to first extract the surfactant and then dry the samples Drying via the low surface tension solvent mixture, reduced the content of the silica which is required for the retention of the structure M-24c was used in this work	134
	A-19b	-	I-5	RT	20 / 10 (L ₁) 44 / 10 (H ₁) 58 / 10 (Q ₁) 81 / 10 (L ₂)	L ₁ , H ₁ , Q ₁ , L ₂	Retention of H ₁	7.33 (H ₁)	7.27 (H ₁)	Enhanced thermal stability and compressive modulus of the templated gel	Polymerization rate: L ₁ < H ₁ < L ₂ < Q ₁	M-24b was used in this study	44
This monomer was also discussed in M-20 section													

672

673

Table 3. Summary of the reported results for transcriptive LLC templating (continue).

Monomer	Amphiphile	Cross-linker	Initiation system	Reaction temperature [°C]	Amphiphile / oil (monomer) w/w	Structure before polymerization	Structure after polymerization	Lattice parameter before reaction [nm]	Lattice parameter after reaction [nm]	Application characteristics of the product	Polymerization kinetics	Remarks	Ref.
M-24	A-14	-	I-9	RT	3 - 33 / 40 (L ₁ + Dis. Cube) 33 - 38 / 40 (H ₁) 38 - 42 / 40 (Q ₁) 42 - 60 / 40 (L _α)	L ₁ + Dis. Cube, H ₁ , Q ₁ , L _α	Retention of the structures	-	-	Enhanced water uptake, rate of swelling and rate of diffusion through the obtained hydrogel with a change in structure from L ₁ to lamellar	-	M-24c was used in this study	164
	A-14	-	I-2	RT	40 - 50 / 20 (H ₁) 60 - 70 / 20 (L _α)	H ₁ , L _α	Disordered H ₁	6.27 (H ₁)	7.6 (H ₁)	-	Polymerization rate: non-LLC < H ₁ (50% A-14) < L _α (70%) < L _α (60%) < H ₁ (40%)	M-24a was used in this study	151
	A-3	-	I-5	RT	30 / 20 (L ₁) 50 - 60 / 20 (H ₁) 70 / 20 (L _α)	L ₁ , H ₁ , L _α	Retention of H ₁ structure for M-24a Loss of order of H ₁ for M-24e	For M-24a: 3.72 (H ₁) For M-24e: 3.6 (H ₁)	For M-24a: 3.7 (H ₁) For M-24e: 3.8	-	Polymerization rate: L _α < H ₁ < L ₁ Higher reaction rate at L ₁ was more pronounced in the case of M-24e Polymerization rate for M-24a was higher than M-24e in H ₁ structure	M-24a, d and e were used in this study The results for M-24d was similar to M-24e	163
	A-9	-	I-1	RT	83.3 / 9.34	Q _α	Formation of hexagonal perforated lamellar (HPL) structure	-	-	Relatively low T _g , high thermal stability, and high resistance toward swelling in organic solvents and water were the important features of the product	-	M-24b was used in this study Due to the absence of a dense cross-linked network, almost 80% of ionic liquid amphiphile washed off with ethanol	88
M-25	A-14	-	I-9	RT	45 / 40	L _α	Retention of the structure after surfactant removal	-	-	Linear decrease of water uptake and linear increase of compressive modulus and T _g with an increase in M-25 content approved the compatibility of two polymers via LLC templating The rate of degradation decreased with incorporation of higher M-25 contents	-	The immiscible polymers of hydrophilic M-27a and hydrophobic M-25 was blended through LLC templating 0 - 100 wt% M-25 was used with respect to the total monomer content M-25 showed higher cross-linking density than M-28	143
M-26	A-14	-	I-9	RT	40 / 40	L _α	Retention of the structure after surfactant removal	-	-	-	Almost complete conversion The polymerization rate in LLC was faster than non-LLC phase	-	144
M-27	A-14	-	I-9	RT	40 / 40	L _α	Retention of the structure after surfactant removal	6.3	6.35	Higher water uptake, permeability and degradation rate over non-LLC sample without changing the chemistry or general biocompatibility of the biopolymer	-	-	144
	This monomer was also discussed in M-25 and M-28 sections												
	A-14	-	I-9	RT	35 / 40	L _α	Retention of the structure after surfactant removal	-	-	Higher water uptake, rate of swelling and rate of degradation while having lower compressive modulus compared to non-LLC sample	The polymerization rate in LLC was faster than non-LLC phase	-	45
M-28	A-14	-	I-9	RT	45 / 40	L _α	Retention of the structure after surfactant removal	-	-	The water uptake decreased linearly with an increase in M-28 content approving the compatibility of two polymers via LLC templating The rate of degradation decreased with incorporation of higher M-28 contents	-	The immiscible polymers of hydrophilic M-27a and hydrophobic M-28 formed interpenetrating polymer network through LLC templating 0 - 75 wt% M-28 was used in respect to the total monomer content	143
This monomer was discussed in M-10 section													
M-30	A-14	-	I-9	RT	Specific contents of A-14 and 40 wt% M-30	H ₁ , L _α	-	-	-	Enhanced water uptake of the gel obtained from the parent LLC with H ₁ structure while maintaining high compressive modulus	-	The obtained gel from H ₁ LLC structure seemed to be a perfect candidate for tissue engineering scaffolds	45
This monomer was discussed in synergistic templating/P-A-35 section													
M-32	A-19c	C-8, C-10a or C-11	I-18	≥ 5	50 / 17.5 (H ₂) 50 / 25 (L _α)	H ₂ in the presence of oil phase L _α without oil phase	Retention of the structures	9.3 (H ₂) 6.9 - 7.4 (L _α)	9.5 (H ₂) 7.3 - 7.5 (L _α)	No bacterial colony growth on the surface of the prepared membrane	-	A mixture of M-4 and C-8 was also used as oil phase to enhance the mechanical properties of the polymerized LLC	137
This monomer was discussed in synergistic templating/P-A-36b section													
M-33													

674

675

Table 3. Summary of the reported results for transcriptive LLC templating (continue).

Monomer	Amphiphile	Cross-linker	Initiation system	Reaction temperature [°C]	Amphiphile / oil (monomer) w/w	Structure before polymerization	Structure after polymerization	Lattice parameter before reaction [nm]	Lattice parameter after reaction [nm]	Application characteristics of the product	Polymerization kinetics	Remarks	Ref.
	A-4, A-5 or A-6	-	-	60 - 70	1 / 1 - 6 molar ratio	H ₁ , L _α	Disordered structure at high M-34 contents	-	2.9 for A-4 * 3.5 for A-5 * 3.7 for A-6 *	No porous carbon was obtained via LLC templating due to improper thermal stability of the structure	-	A base or acid was used to catalyze the condensation reaction	24
M-34	A-19	-	-	100	1 / 0.5 - 2.5	H ₁ , Q ₁ , L _α	Retention of the structures	-	9.8 - 14 (H ₁) 12.6 - 23.5 (Q ₁) 10.5 (L _α)	Ultrahigh thermal stability up to 1400 °C, mechanical stability up to 500 Mpa and proper high reverse electronic capacity was observed for the obtained mesoporous carbon material	-	A-19e, A-19f, and A-19g were used in this study The LLC precursor was prepared in ethanol followed by EISA to fabricate the structures L _α was not stable under surfactant removal and calcination steps A-19g was only able to produce Q _α The LLC structure and its characteristics were mainly depend on amphiphile/monomer ratio and n/m ratio in A-19	19
M-35	A-5	-	-	RT - 100	2.1 / 1.2	H ₁	Limited structure retention	-	3.7 - 4.2 *	-	-	Ordered mesoporous carbon material was not obtained after removal of the template	165
	A-19f	C-12	-	RT - 100	1 / 1	H ₁	Retention of the structure	-	-	-	Polymerization of M-36 was much faster than M-34	The LLC precursor was prepared in a mixture of ethanol and water Highly ordered H ₁ structure was achieved by controlled solvent evaporation or a shear force	138
	A-19f	C-13	I-11	RT	2 / 1	H ₁	Retention of the structure	-	9.9 - 11.8	-	Polymerization was faster in the presence of I-11 compared to the sample without initiator	EISA was carried out under mild conditions while maintaining high polymerization rate by the aid of light Highly organized H ₁ structure was obtained at high contents of I-11	139
M-36	A-19f	C-13	-	75	2 / 1	H ₁	Retention of the structure	-	9.5 - 12	The product of bio-based material showed better electrochemical performance due to the presence of a more suitable/accessible porous structure	-	It was possible to replace half of M-36 with lignin, as a less toxic and bio-derived monomer, and have the same ordered mesoporous carbon material No order was observed without M-36	140
	A-19f	C-12 / C-14	-	RT - 75	2 / 1	H ₁	Retention of the structure	-	-	The product had a robust organic framework while maintaining a promising CO ₂ capture property	-	The significant structural shrinkage during the curing and template removal was addressed by hypercross-linking the organic matrix via Friedel-Crafts alkylation reaction and C-14	55
M-37	A-19f	C-12	-	RT - 120	1 / 1	H ₁	Retention of the structure	-	12.24	The obtained highly ordered carbon material showed extremely high thermal stability and could be graphitized at 2400 - 2600°C	Highly acidic reaction conditions promoted the polymerization rate	-	141
M-38	A-19e	C-15	-	60-100	10 - 80 / 80 - 20 (L ₁) 30 - 50 / 0 - 30 (L _α) 70 - 90 / 0 - 25 (H ₁)	L ₁ , L _α , H ₁	Order-order and order-disorder changes were observed	9 - 22 *	12.4 - 19 *	-	Near complete monomer conversion	C-15 also acts as structure directing agent instead of water The structural changes continue even after completion of the polymerization	166
M-39	A-10	-	I-3 and γ-ray radiation	RT	Up to 20 wt% monomer was used	H ₁	Retention of the structure when γ-ray radiation is used	7.5 *	18.4 *	Conductivity of 10 ⁻¹ S/cm was obtained for the obtained nanofibers which was higher than the reported values in the literature	-	1-Pentanol was used as cosurfactant Micron-sized spherical particles were obtained by photo-polymerization Nanofibers were obtained by γ-ray radiation Solution of M-39 in cyclohexane was used as the oil phase	167
M-40	A-5	-	I-22	RT	Up to 0.1 M monomer can be used	H ₁	Retention of the structure	27 (diameter of the oil domain)	30 (diameter of the obtained nanowires)	The optical band gap (estimated from the absorption edge, at 550 nm) of 2.25 eV was observed for the templated product Strong absorption in the visible region was observed	-	n-Pentanol was used as cosurfactant Solution of M-40 in toluene was used as the oil phase	168
M-41	A-10	-	I-17	0	Up to 20 vol% monomer was used	H ₁	Limited retention of the structure under slow agitation of the mixture	-	100 - 200 (diameter of nanorods)	-	-	1-Pentanol was used as cosurfactant Nanospheres were produced under vortex mixing Nanorods were obtained under slow agitation of the mixture Solution of M-41 in cyclohexane was used as the oil phase	169

676

677 **5. Kinetics of polymerization in LLC templates**

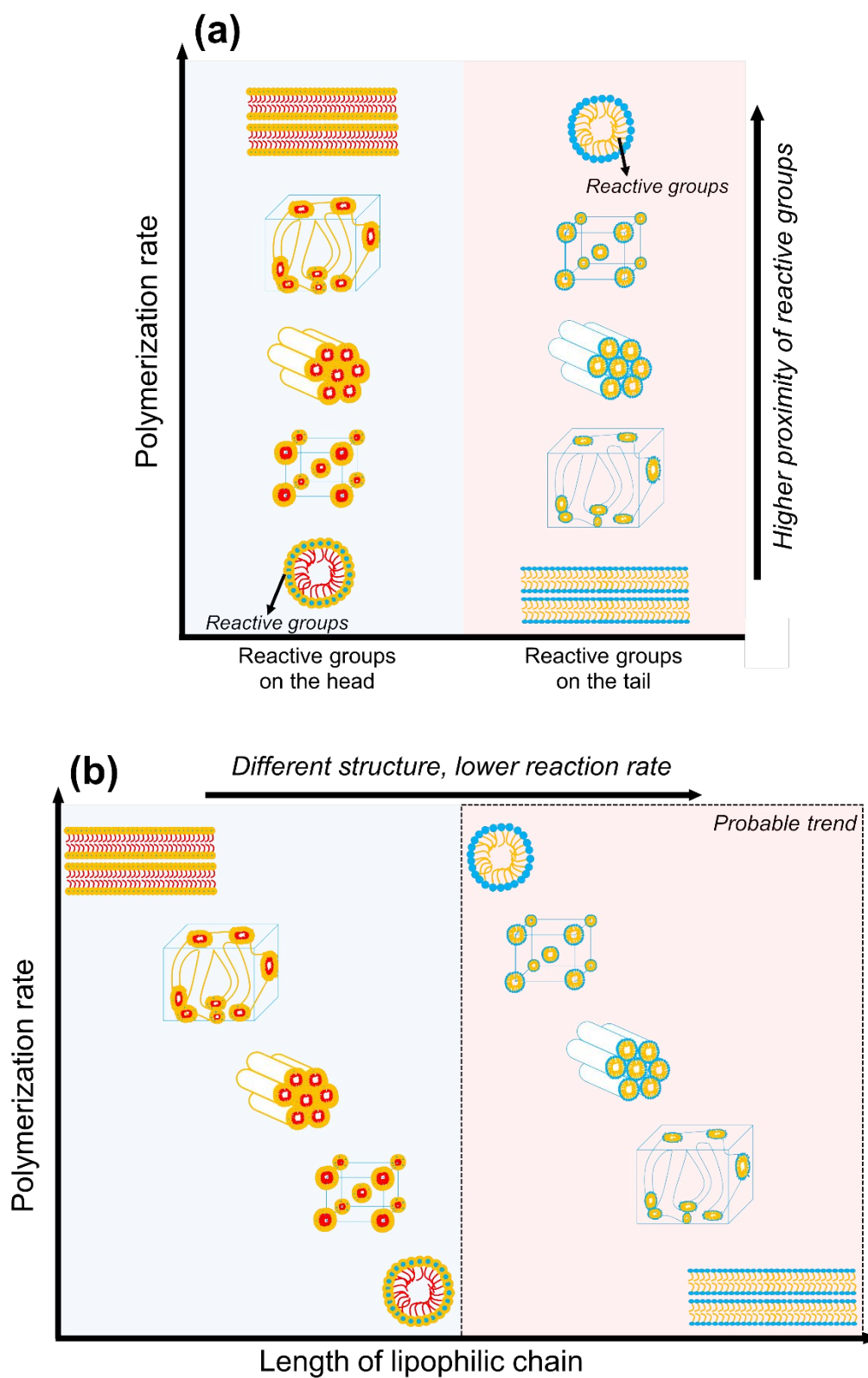
678 Studying the polymerization kinetics in nanoconfinements of LLC templates is an attractive
679 research ground not only due to the dramatic changes of the polymerization reaction rates in
680 LLC templates, but also due to the important role of kinetics in ensuring structure
681 retention during polymerization. As a rule of thumb, for both synergistic and transcriptive
682 templating approaches, the faster the polymerization rate, the higher the probability of structure
683 retention. When the reaction rate is high, the kinetically trapped cross-linked network forms
684 rapidly, decreasing the chances of phase separation/inversion. This is why
685 photopolymerization, which can often be completed in a few minutes, has been the first choice
686 in most of the studies. The self-assembly of amphiphiles is temperature dependent.^{73–75,123} In
687 addition, the polymerization reaction is exothermic. Therefore, the change in temperature
688 during non-isothermal reactions due to the heat of reaction may induce mesophase transition.⁵⁶
689 However, rapid formation of cross-linked polymer network can inhibit such phase
690 separation/inversion.

691 Polymerization kinetics in different LLC structures have mainly been studied by Guymon and
692 co-workers. They have shown that reactive sites segregation (e.g., double bond) and diffusion
693 limitations are the main factors that determine the differences in the radical reaction rate among
694 different mesophases.²⁶ The effect of the mentioned parameters will be discussed for the two
695 types of LLC templating approaches separately in the following sections.

696

697 **5.1. Synergistic LLC templating**

698 In synergistic templating, the location of polymerizable group on the reactive amphiphile and
699 the length of lipophilic chain are the main parameters that control the polymerization kinetics
700 (see Fig. 12).²⁶ The impact of polymerizable group placement on the kinetics has been
701 demonstrated by comparing the reaction rates between P-A-4 and P-A-5 in which the reactive
702 groups are located on the lipophilic tail and hydrophilic head, respectively. Based on the
703 reported results, the polymerization rate for P-A-4 increases when the LLC structure changes
704 from lamellar to micellar cubic, whereas an opposite trend is seen for P-A-5. With a change in
705 the structure from micellar cubic to lamellar, the proximity of the double bonds decreases for
706 P-A-4, resulting in fewer propagation reactions and therefore a lower polymerization rate.^{96–98}
707 It is worth noting that the effect of the initiation system cannot be neglected in this comparison
708 since applying γ -ray radiation on a similar templating formulation with P-A-5 results in a
709 slightly different trend compared to photoinitiation method (see Table 2).⁷⁶ To evaluate the
710 effect of lipophilic chain length on the reaction rate, one can compare P-A-5, P-A-6, and P-A-
711 7 in synergistic templating. Under the same conditions (e.g., surfactant content), the reaction
712 becomes slower with an increase in the chain length. The formation of LLC structures that
713 offer lower local double bond concentration (e.g., micellar cubic) is the reason why slower
714 polymerization rates are observed when lengthy surfactants are used.^{89,98}



715
 716 **Fig. 12.** The relative effect of (a) polymerizable group placement on the reactive amphiphile and (b)
 717 the lipophilic chain length on the polymerization rate in synergistic templating. Different structures
 718 are obtained with an increase in the length of lipophilic chain, resulting in lower reaction rate. Higher
 719 proximity of the reactive groups enables higher reaction rates.²⁶

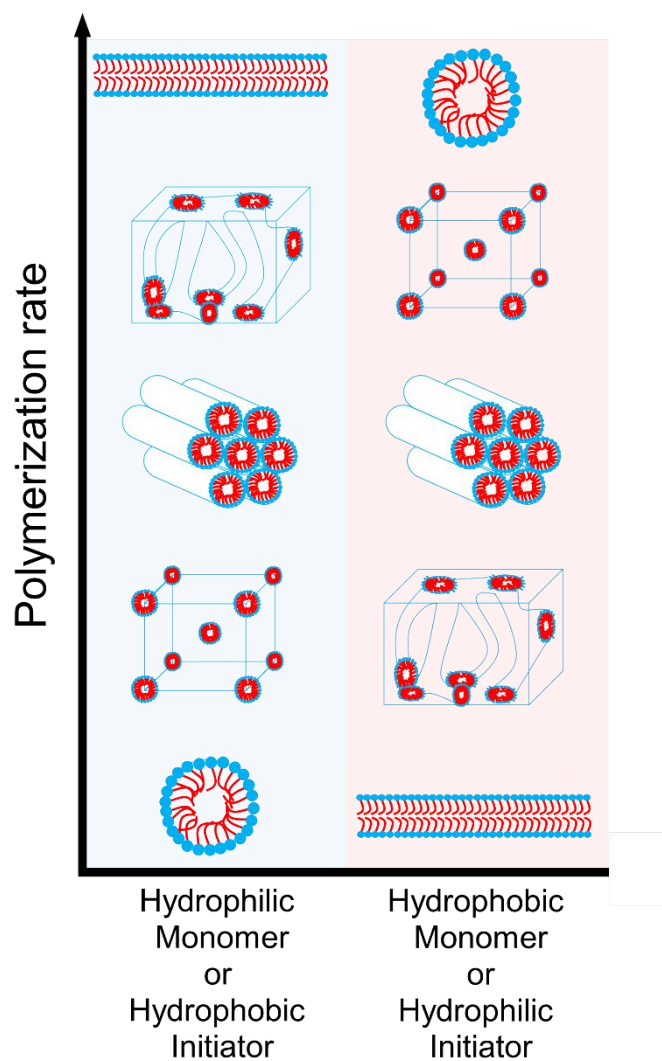
720

721 5.2. Transcriptive LLC templating

722 Studies on transcriptive templating have shown that monomer and initiator polarity are the key
723 parameters controlling the polymerization kinetics, as schematically demonstrated in Fig. 13.
724 Hydrophilic monomers tend to be present at the interface of water/surfactant. Such
725 arrangements inhibit termination reactions by limiting the mobility and diffusion of the
726 propagating polymer chains. In addition, when the LLC structure changes from micellar to
727 lamellar, the local concentration of monomer increases in the continuous polar domain,
728 resulting in higher radical propagation rates. When the limited mobility of the propagating
729 chains and higher local concentration of the monomer exist simultaneously, a dramatic increase
730 in polymerization rate is observed.²⁶ Hydrophilic monomers such as M-9,^{35,36,38-40,43,157} M-
731 13,^{42,43} and M-23^{38,42,150,162} have experimentally shown this behavior (see Table 3).

732 Hydrophobic monomers show the opposite behavior i.e. the polymerization rate decreases with
733 a change in LLC structure from micellar to lamellar. The concentration of surfactant increases
734 with a change in LLC structure from micellar to lamellar, resulting in an augment of the apolar
735 domains' volume fraction. The local monomer concentration diminishes at higher apolar
736 domain sizes which results in a lowering of polymerization rates.²⁶ Monomers such as M-4,⁵⁶
737 M-5,⁹⁹ M-6,^{42,99,153} and M-20^{38,42,44,150,151,162} are some of the hydrophobic species exhibiting
738 lowered polymerization rates at high surfactant content, as shown in Table 3. A slightly
739 different trend is seen for some of the monomers presented in Table 3. This is believed to be
740 due to phase separation, which alters the local concentration, segregation, and diffusional
741 behavior of the monomers. It is worth mentioning that M-3 exhibits unique behavior among
742 hydrophobic monomers. As shown in Table 3, this monomer shows higher reaction rates when
743 the LLC structure changes from micellar to lamellar, a behavior similar to the hydrophilic
744 species. This observation is attributed to the partial water solubility of this monomer, which
745 results in polymerization in the polar domains of the self-assembled molecules.^{99,153} In addition
746 to the monomer partitioning and mobility of the propagating chains, the effect of
747 nanoconfinement on the polymerization rates cannot be underestimated. Qavi and co-workers
748 have shown that the probability of termination steps increases when the reaction is carried out
749 in nanoconfinement, with smaller domain sizes of polymerizing phase resulting in slower
750 polymerization rates.⁵⁶

751 The effect of the photoinitiator polarity on the reaction rate is another parameter that has been
752 examined in the templating of M-20 and M-23 by Guymon and co-workers.^{38,150,162} Generally,
753 the initiation efficiency of the initiator is a measure of this effect. Higher initiator efficiency
754 leads to higher polymerization rates. The obtained results show that the efficiency of
755 hydrophilic initiators (e.g., I-5) decreases as the structure changes from micellar to lamellar.
756 The volume fraction of polar domains diminishes for this change in the structure, resulting in
757 higher proximity of the molecules of the water-soluble initiator. When the free radicals are
758 formed, radical recombination due to the cage effect occurs, usually producing nonreactive
759 components which in turn result in lower initiator efficiency. On the other hand, hydrophobic
760 initiators (e.g., I-6) are partitioned in the opposite way, resulting in lower probability of cage
761 effects and thus higher initiation efficiency.²⁶



762
763
764

Fig. 13. The relative effect of monomer and initiator polarity on the polymerization rate in transcriptive templating.²⁶

765 **6. Synergistic versus transcriptive LLC templating: a summary**

766 So far, we have discussed the two types of LLC templating approaches in detail. As a summary
767 of our discussion in previous sections, Table 4 lists the differences and
768 advantages/disadvantages of the mentioned techniques.

769

770

771

772

773

774

775 **Table 4.** The differences and advantages/disadvantages of synergistic and transcriptive LLC
 776 templating methods in summary.

	Synergistic	Transcriptive
Differences	Reactive surfactant(s) is the polymerizable species	Reactive monomer(s) is the polymerizable species
Advantages	Chemically bonding the surfactant to the structure, and thus, a higher chance of structural retention	The commercial availability of the employed components (e.g., monomers and surfactants)
Disadvantages	Unavailability of commercial reactive surfactants, and thus, requiring multi-step synthesis methods to prepare surfactants	Physically bonding the surfactant to the structure and thus lower chance of structural retention

777

778 **7. Advanced functional materials: opportunities, challenges and outlook**

779 LLC templating is an efficient “bottom-up” approach to fabricate nanostructured polymers that
 780 can be applicable in a wide variety of applications, as shown in Fig. 14. The membranes
 781 developed from the polyLLCs show enhanced permeability, selectivity, and fouling resistance
 782 compared to the current industry standard.³⁰⁻³⁴ For instance, NF membranes having a thickness
 783 of 100 nm with effective pore sizes in the 1 nm range, MWCO ~ 300 Da, and permeability of
 784 ~ 20 L m⁻² h⁻¹ bar⁻¹ have been fabricated via polyLLC technology.^{30,170} These membranes have
 785 better performance than the commercially available NF membranes like Dow FILMTEC
 786 NF90-400 which have typical permeabilities in the range of 10 to 15 L m⁻² h⁻¹ bar⁻¹. The
 787 mentioned polyLLC membranes have also an intrinsic degree of biofouling resistance thanks
 788 to the presence of water-facing quaternary ammonium groups available in the structure of the
 789 employed reactive surfactant (P-A-6). As another example, fabrication of UF polyLLC
 790 membranes with a molecular weight cut-off of about 1500 Da and a permeability of ~ 85 L m⁻²
 791 h⁻¹ bar⁻¹ (twice that of commercial control membrane, GE PT8040F30) has been reported.³¹
 792 In another effort, NF membranes with Q₁ structure have been fabricated, which outperform the
 793 commercial NF90 (Dow Filmtec) membrane in the treatment of hydraulic fracturing produced
 794 water. These PolyLLC membranes show a thickness-normalized flux of ~ 2.9 L μm m⁻² h⁻¹
 795 (about 8 times of the commercial membrane) with much higher stability against fouling
 796 compared to NF90.¹¹⁴ Additionally, the Q₁ membranes are able to recover up to 22% dissolved
 797 organic carbon while rejecting 75% of the salt which is a unique selectivity feature of these
 798 advanced materials over commercial opponents.³² PolyLLC membranes have also proven
 799 advantages in breathable barrier materials for chemical agent protection. Dense polymers such
 800 as cross-linked BR, which are the common components used in such application, can cause
 801 heat and fatigue for the wearer as they are impermeable to water vapor. However, a proper
 802 water vapor permeability (~ 500 g m⁻² day⁻¹) can be achieved without compromising the
 803 selectivity when BR incorporated polyLLC membranes are employed.¹¹²

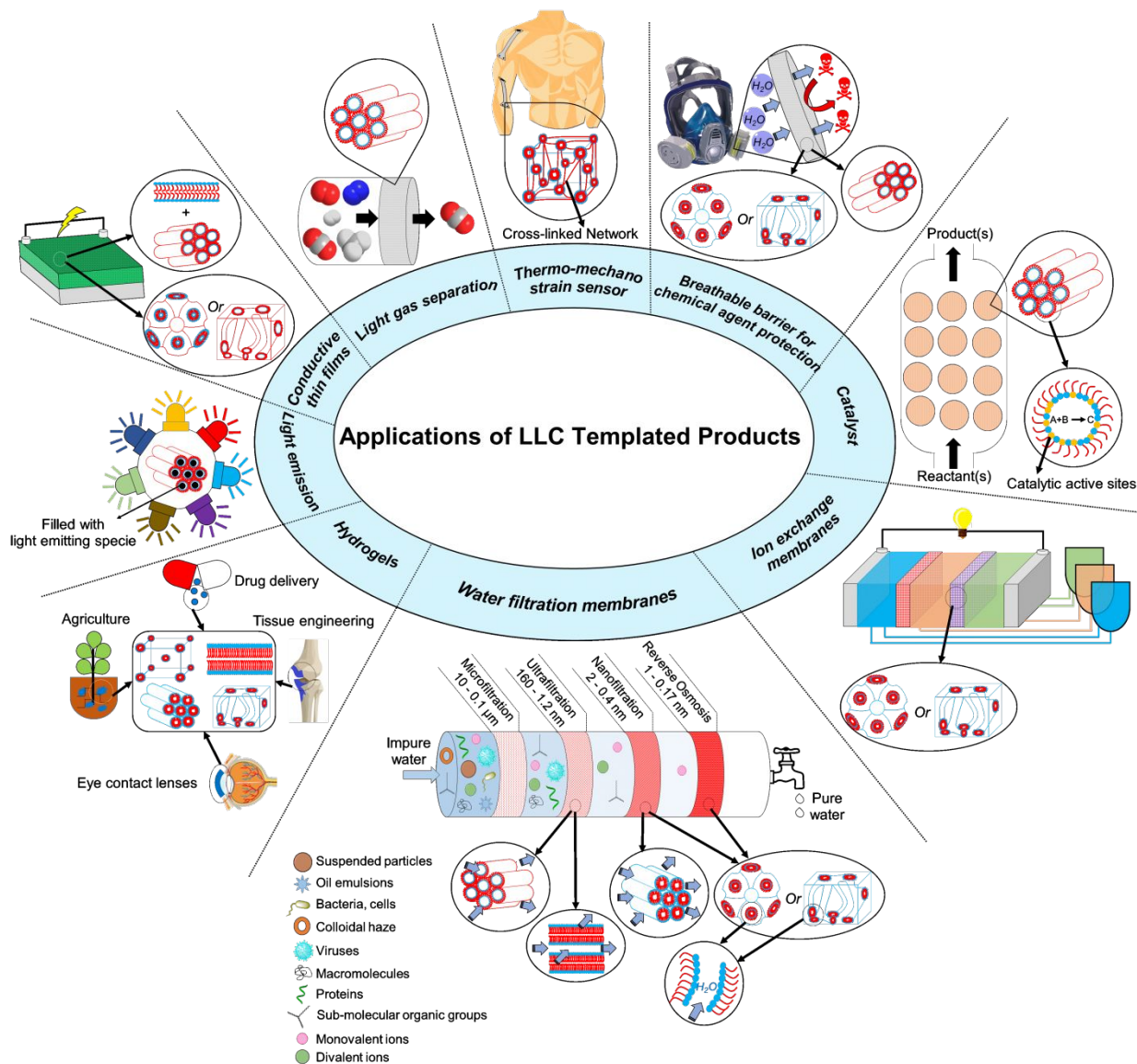
804 The hydrogels prepared through the templating processes offer a proper balance of water
805 uptake, swelling/de-swelling rate, and mechanical properties without compromising other key
806 characteristics such as biocompatibility, biodegradability, and stimuli-responsiveness.^{35–45} As
807 an example, transcriptive templating has been used to fabricate nanostructured biodegradable
808 hydrogel made of M-26 monomer, exhibiting 80% increase in network swelling and around
809 230% increase in diffusivity compared to the corresponding non-LLC polymer without
810 changing the biocompatibility of the material.¹⁴⁴ Polyacrylamide hydrogels have been
811 synthesized in LLC templates with ~ 10% higher water uptake and almost two times faster
812 swelling rate than non-LLC analogous with no change in compressive modulus.⁴³ In another
813 effort,³⁷ LLC templated poly(N-isopropylacrylamide) (PNIPAM) hydrogels have been
814 prepared, which not only show twice the equilibrium swelling of analogous non-LLC
815 counterparts but also exhibit 5 times greater dynamic range between the swollen and deswollen
816 state. In other words, the nanostructured hydrogels possess faster deswelling rates at
817 temperatures above the lowest critical solution temperature for PNIPAM. These important
818 properties have further been improved via the incorporation of about 2 wt% M-16 in the
819 polyLLC structure.³⁷

820 The templating process can also result in conductive components with excellent mechanical
821 properties compared to non-LLC materials.^{46–48} The work done by Lopez-Barron et al.^{46,48} is
822 one of the best examples in this field. They have created FCC lattice by combining P-A-55 and
823 a partially deuterated ionic liquid (ethylammonium nitrate) to fabricate a cross-linked ion gel
824 having a highly elastomeric behavior with excellent mechanical properties, conductivity, and
825 mechano-electrical responses. The produced highly stretchable iono-elastomers (exhibiting a
826 maximum elongation of 340%) are accurately and reliably sensitive to small motion as they
827 show a linear strain-resistance response. Additionally, they have a large temperature-dependent
828 conductivity (3.24 %/°C @ 30 °C) which is more than twice that of the most sensitive reported
829 materials.⁴⁷ Therefore, they have been employed as thermo-mechanical sensors to capture the
830 simultaneous/real-time strain and temperature of the human body during anaerobic exercise.
831 This tough nanostructured material can resist external damages such as rubbing, pinching, and
832 directional cutting while maintaining its functionality over 1000 cycles. Thus, it can potentially
833 be used in sports training, prosthetic, personable healthcare, and robotics applications.⁴⁷

834 It has also been shown that the nanostructured catalytic components obtained from mesophase
835 templating exhibit unique catalytic activity/selectivity over commercially used catalysts.^{28,49}
836 For example, Gin et al. have shown that a polyLLC of P-A-23 with H₂ structure can be used as
837 an effective heterogeneous base catalyst for the Knoevenagel condensation of ethyl
838 cyanoacetate with benzaldehyde in refluxing THF while maintaining faster reaction compared
839 to basic versions of zeolite-Y and MCM-41 mesoporous sieves.²⁸ In another study,
840 heterogeneous polyLLC-based catalyst with the application in aerobic oxidation of alcohols
841 has shown higher activity (~ 93% versus ~ 72% benzyl alcohol conversion) and selectivity (~
842 4.2 versus ~ 1.9 benzyl alcohol/ 3,5-bis(*tert*-butyldiphenylsilyloxy)benzyl alcohol) over the
843 industrially available TEMPO-based catalysts (e.g., Silicat[®] brand).⁷⁹

844 The distinctive light emitting behavior of LLC templated products is another advantage of such
845 materials over non-LLC ones.^{50,51} PPV-incorporated polyLLCs with H₂ structure are the best

846 example in this application. Photoluminescence quantum efficiency of about 80% has been
 847 reported for such nanostructured materials, which is much higher than 5 - 27% yields reported
 848 for the pure PPV. Additionally, the stability of PPV against oxidation can be improved by chain
 849 isolation/protection inside the polyLLC pores.⁵⁰ Polarized photoluminescence behavior can
 850 also be obtained by shear-aligning the PPV containing H₂ phase.²⁸ Moreover, metal-based
 851 luminescence can be introduced into this system by using transition-metal and lanthanide
 852 cations as the counterions.⁷⁸



853

854

Fig. 14. Potential applications of LLC templated products

855

856 Although there have been plenty of studies on the advancement of LLC templating, some
 857 challenges still exist in the field. Scalability of the templating process is perhaps the most
 858 challenging hurdle to making polyLLCs fabrication applicable on larger scales. Synergistic
 859 templating requires reactive surfactants which are currently not commercially available and are
 860 usually synthesized through relatively complicated and expensive chemistries. This issue has

861 been addressed by Gin's groups to a limited extent through the introduction of polymerizable
862 species synthesized via cheaper raw materials (e.g., P-A-33).¹¹⁸ The alternative approach is
863 transcriptive templating, although it requires a large amount of non-reactive components (i.e.,
864 surfactant) which are not chemically integrated in the polymerized phase.

865 For membrane applications, H_2 and L_α phases that are easily accessible suffer from improper
866 alignment of the nanochannels and need additional pre-polymerization steps (e.g., magnetic
867 alignment),²⁹ which are complicated and/or costly. On the other hand, no alignment is required
868 for Q_α structure, but stable polyLLC structures are not easily achieved via commercially
869 available amphiphiles. This challenge can be resolved to a large extent by using easily
870 accessible H_1 structures which do not need any alignment, as recently shown by Osuji and co-
871 workers, using a synergistic templating approach.³⁰ The accessibility of the H_1 mesophase
872 makes it a feasible structure for developing a broad range of membranes tailored for different
873 uses, including ion transport, and organic solvent nanofiltration. Recent work by the same
874 group¹⁷⁰ has demonstrated a solution-based process for rapid fabrication of ~ 100 - 200 nm thick
875 membrane selective layers over large areas using H_1 mesophases. The permeability and
876 rejection characteristics are on par with several commercial NF membranes, with effective pore
877 sizes in the 1 nm range, MWCO ~ 300 Da and permeabilities $\sim 2 \text{ L m}^{-2} \text{ h}^{-1} \text{ bar}^{-1} \mu\text{m}$. At
878 thicknesses of 100 nm, this corresponds to a permeance of $\sim 20 \text{ L m}^{-2} \text{ h}^{-1} \text{ bar}^{-1}$.

879 In the general liquid crystal literature, there are a plethora of studies on the influence of surface
880 conditions to aid the anchoring/alignment of liquid crystalline molecules or phases. In
881 commercial display devices based on nematic phases, surface modification by lecithin
882 surfactant coatings or microgrooves¹⁷¹ is used to order the nematic phases. For thermotropic
883 mesophases, Osuji et al., among others, have demonstrated the uniform homeotropic alignment
884 of hexagonal cylindrical pores by confined annealing of the pre-polymerization phase between
885 compatible substrates such as glass and PDMS.¹⁷² There are also examples in literature utilizing
886 surface anchoring techniques to align lyotropic chromonic liquid crystal phases.¹⁷³ It stands to
887 reason that surface anchoring-based alignment techniques can be utilized to resolve the
888 alignment issues for H_2 and L_α LLC structures. Foudazi et. al. have also shown that it is possible
889 to induce the alignment in LLCs simply via applying large amplitude oscillatory shear,
890 although further studies are still required.¹⁷⁴ Additionally, the thicknesses of the polyLLC
891 derived active layer in water filtration membranes have to be further decreased via industrially
892 scalable approaches to acquire higher water fluxes necessary for economic feasibility. Gin and
893 co-workers have introduced techniques to produce TFC-based membranes to address this
894 issue,^{32,114,120,121} but there is much room for further work in this area.

895 The typical molecular weight range of the amphiphiles (< 2 kDa) discussed in this review
896 necessarily limits the feature sizes of their lyotropic mesophases to the sub-10-nm, and more
897 typically the sub-5-nm regime. Recent advances in block-copolymer self-assembly have
898 enabled BCP systems which exhibit self-assembled features in the 5 - 10 nm range, thereby
899 providing a continuous spectrum of options for fabrication of self-assembled materials with
900 features in the 1 - 5 nm range templated by polyLLC, and features larger than 5 nm enabled by
901 BCP micro-phase segregation. However, there are at least two approaches based on lyotropic
902 liquid-crystalline materials to obtain features sizes near- and beyond-10 nm.

903 The first of these approaches relies on so-called ‘giant surfactants’ or ‘shape amphiphiles’,
904 which are higher molecular weight analogues of small-molecules amphiphiles. As summarized
905 by Yue et al,¹⁷⁵ giant surfactant analogues can be synthesized to mirror their lower-MW
906 polyLLC counterparts in terms of architecture i.e. single-headgroup single-tail, single-
907 headgroup multiple tail, bolaform architecture, gemini architecture and beyond. Typically, the
908 headgroup consists of a large ‘cage’ like structure, sometimes termed a molecular nanoparticle
909 (MNP). MNP headgroups in giant surfactant literature¹⁷⁶ are most often fullerene or
910 functionalized polyhedral oligomeric silsesquioxane (POSS) derivatives, although globular
911 proteins¹⁷⁷ can also be incorporated as the hydrophilic head-groups. The most commonly
912 studied tails in the literature are polystyrene tails. Work by Yu et al¹⁷⁸ has demonstrated that
913 with appropriately designed chemical structures, POSS-PS giant surfactants can display most
914 of the phases (micellar, lamellar, hexagonal, cubic) found in LLCs with 2 or 3 times larger
915 periodicities i.e. 7 - 20 nm. Given the longer tail lengths and larger headgroup radii of giant
916 surfactants compared to typical surfactants, the former provide many more atomic sites for
917 targeted/localized synthetic modifications to increase functionality for advanced applications
918 such as protein/biomolecular sensing platforms, although with the trade-off of increased
919 synthetic and purification complexity. In principle, the additional functional sites afforded by
920 the larger molecular size could be utilized to incorporate unsaturated bonds/cross-linking sites
921 in giant surfactant molecules. In one case,¹⁷⁹ a methacrylate cross-linker based on the giant
922 surfactant headgroup (M-POSS) was utilized for phase preservation in a small-molecule
923 amphiphile mesophase. However, in general, there is very little work focusing on synergistic
924 or transcriptive templating for giant surfactant mesophases at this time.

925 A second approach relies upon swelling of lyotropic bicontinuous cubic mesophases unit cell
926 sizes by addition of charged lipids. Angelov et al¹⁸⁰ reported a 50% swelling in unit cell
927 dimensions of a Diamond-type cubic bicontinuous phase consisting of an aqueous Monoolein
928 cubic phase swelled with a small amount of octyl-glucoside, resulting in a lattice parameter of
929 15.3 nm. Work by the Brooks group has shown that increasing the formulation complexity of
930 similar swollen mesophases of ternary lipid mixtures and beyond can yield even larger unit cell
931 sizes and provide additional handles for controlling the unit cell spacing. Barriga and Tyler et
932 al¹⁸¹ have shown that addition of cholesterol and charged lipids to monoolein-water
933 bicontinuous phase swell the primitive cubic unit cell spacing from ~ 10 nm to nearly 50 nm,
934 while also enabling pressure and temperature sensitivity in the phase to tune the unit cell
935 parameter. In a follow up work,¹⁸² they further elucidate the importance of the electrostatic
936 stability imparted to the swelled cubic bicontinuous phase by the added anionic lipid in the
937 ternary mixture. This additional stability allows the mesophase to surpass the theoretically
938 expected limit¹⁸³ of ~ 30 nm lattice parameter due to the effect of thermal oscillations. Recent
939 work from Leal’s group has demonstrated even larger lattice cell parameters. In glycerol
940 monooleate based mesophases,¹⁸⁴ doped with charged lipids and PEG-lipids, a gyroid phase
941 with unit cell parameter 64.4 nm was obtained, corresponding to an estimated water channel
942 diameter of 38 nm. Further work¹⁸⁵ on this composition identified the role of the PEG-lipid
943 composition as a reliable handle to switch the mesophase between diamond, gyroid and
944 primitive cubic bicontinuous morphology. The larger water channels of the swollen lipidic
945 mesophases reduce much of their suitability for selective separations such as filtration, but in

946 turn enable their use in emerging biotechnology applications such as platforms for protein
947 crystallization processes.¹⁸⁶

948 Most of the existing literature on the aforementioned two approaches focuses on the chemical
949 synthesis or formulation stability of the larger lattice parameter lyotropic mesophases. Neither
950 approach has been extensively studied for phase and feature preservation after polymerization,
951 thus presenting opportunities for future researchers to combine synergistic or transcriptive
952 templating approaches to preserve large unit cell self-assembled mesophases of giant
953 surfactants or swelled LLC phases.

954 The optimization of transcriptive templating recipes seems necessary to decrease the required
955 concentration of surfactant and thus to improve the thermal and mechanical properties of the
956 final products. Using specific types of amphiphiles which have very low CMCs (such as
957 sodium alkoxy sulfate reported by Chen et al.¹⁸⁷) might be helpful in resolving this issue.
958 Furthermore, the high porosity of polymerized LLCs after extraction/drying of non-reactive
959 component(s) results in poor mechanical properties. Although the random alignment of the
960 nanostructures overshadows this effect to some extent, incorporation of nanoparticles (e.g.,
961 carbon nanotubes) in LLC structures might be a proper approach to overcome this challenge if
962 the structure retention is not affected by the presence of nanoparticles.⁸⁰ Nanoparticles may
963 induce heterogeneity in the structure or direct the self-assembly toward formation of a different
964 LLC structure.

965 In addition to the discussed challenges, there are still some relatively unexplored application-
966 oriented opportunities available in the field. For instance, production of stimuli-responsive
967 (e.g., thermoresponsive and pH-responsive) membranes through LLC templating needs further
968 attention. To the best of our knowledge, except for the reported works on LLC templated
969 thermo-responsive hydrogels (hydrophilic polymers),^{37,41} there is only one report exploring the
970 possibility of having dynamic pore sizes in hydrophobic polymers by synergistic templating of
971 a stimuli-responsive amphiphile (P-A-43).¹²⁸ As discussed earlier, syntheses of such reactive
972 species are highly challenging; therefore, transcriptive templating of commercially available
973 monomers that result in stimuli-responsive polymers is a potentially new direction in this field.
974 According to the literature, stimuli-responsive membranes that possess inherent pore size
975 tuneability exhibit higher water flux recovery and variable permeability/selectivity.^{5,188}
976 Application of LLC templating in the production of ion gels is another fertile research ground.
977 The combination of BCPs and ionic liquids is the common approach to fabricate ion gels.^{189–}
978 ¹⁹⁵ While this method works perfectly, in some cases, to preserve the conductivity of the
979 obtained polymer electrolyte, a relatively high amount of ionic liquid is required which results
980 in deterioration of the mechanical properties over time. To address this issue, a limited number
981 of reports have used LLC templating to fabricate robust ion gels having proper conductivity.^{46–}
982 ^{48,142} Nevertheless, expanding the available formulations and using different structures are still
983 required to improve the mechanical properties beyond those offered by the current polymer
984 electrolytes.

985 LLC templating through electrochemical templating, which has already been explored for
986 inorganic species (e.g., Pt), is another unexplored research area for organic compounds. Based

987 on the available reports in the literature, this approach is simple, has low cost, and requires
988 mild conditions. Moreover, the obtained products show enhanced properties like enhanced
989 catalytic activity and stability.¹⁹⁶ Fabrication of polyLLC membranes with controlled
990 thicknesses is a potential application of electrochemical templating.

991 There has been a great deal of interest toward commercialization of energy conversion devices
992 in fuel cells and solar cells.¹⁹⁷ Therefore, it can be a great opportunity to employ polyLLCs
993 with different nanostructures to improve the efficiency of such materials and thus facilitate the
994 commercialization process. PolyLLCs and LLC templating methods offer several advantages
995 over the materials and methods currently used in this field. For instance, microemulsion-
996 templated products usually do not have anisotropic structure as L_{α} , H_1 and H_2 LLCs do.¹⁹⁷
997 Moreover, LLC templating is much more straightforward than multi-step gas bubble
998 templating approach employed to create porous structures.¹⁹⁸ Additionally, templating with
999 soft LLCs is simpler and safer than employing hard templates which not only is a complex
1000 technique, but also is not safe as harmful chemicals are used for the template removal.¹⁹⁹

1001 Successful production of inorganic nanostructures (e.g., Pt, Pd and bimetallic) in LLC
1002 templates has already been documented. According to the experimental results, the obtained
1003 nanomaterials exhibit remarkable electrocatalytic activity, high conductivity and chemical
1004 stability, and low cost of production.¹⁹⁷ Nevertheless, there are still limited works on LLC
1005 templating of organic species. In one work, Hulvat et al. used M-18 in normal hexagonal
1006 structure to fabricate nanostructured conductive materials. The obtained products have shown
1007 higher conductivity compared to the non-templated formulation.^{158,159} Similar increase in
1008 conductivity has been reported for the products obtained from LLC templating of M-18 by
1009 Ghosh et al.¹⁶⁰ In another effort, M-39 has been polymerized in H_1 structure, resulting in
1010 nanofibers with a conductivity higher than the values reported in the literature for same
1011 polymer.¹⁶⁷ M-40 has been used in LLC templating to fabricate nanostructured semiconductors
1012 with the optical band gap of 2.25 eV and strong absorption in the visible region, applicable in
1013 electronic devices or solar light harvesting applications.¹⁶⁸ Furthermore, there are some works
1014 in the literature showing that the properties of LLC-templated conductive polymers can be
1015 further enhanced by incorporation of inorganic nanoparticles in the LLC structure.¹⁹⁷ These
1016 appealing results confirm the potential of polyLLCs in this field.

1017 Another area of opportunity lies in the use of polymerized LLCs to control the synthesis and
1018 organization of inorganic nanomaterials. The use of LLCs to template synthesis of
1019 nanostructured inorganic materials is well-known and is the basis for the production of
1020 mesoporous molecular sieves such as SBA-15²⁰⁰ and MCM-41²⁰¹. These siliceous materials
1021 are valued as catalyst supports^{201,202}. The opportunity exists for templated synthesis of
1022 inorganic materials in the aqueous channels of polymerized LLCs. A simple route for example
1023 is the formation of nanoparticles by reduction of precursor species (e.g. metal ions). The
1024 resulting nanomaterial-containing nanostructured polymer membranes are of potential utility
1025 as catalytic membranes. Early work by Gin et al.,²⁰³ highlighted this potential with the
1026 formation of Pd nanoparticles in polymerized hexagonal mesophases derived from a wedge-
1027 shaped amphiphile. The concept of nanostructured catalytic polymer membranes is a
1028 compelling one. In some cases, rather than relying on the synthesis of a second phase material,

1029 the chemistry of the polar headgroup itself can be used, as demonstrated by Gin et al., for
1030 Lewis⁴⁹ and Bronsted⁹⁵ acid catalysis. In total however, well-controlled nanomaterial synthesis
1031 in polymerized LLCs can be challenging due to the difficulties in controlling the
1032 polymerization, as identified in this review.

1033

1034 **Acknowledgements**

1035 YS and RF would like to thank the support by the National Science Foundation (NSF) under
1036 grant no. 1840871. OI and CO acknowledge NSF support under DMR-1945966 and CBET-
1037 1703494

1038

1039 **References**

- 1040 1 D. Chimene, D. L. Alge and A. K. Gaharwar, *Adv. Mater.*, 2015, **27**, 7261–7284.
- 1041 2 N. M. Bardhan, *J. Mater. Res.*, 2017, **32**, 107–127.
- 1042 3 F. Iskandar, *Adv. Powder Technol.*, 2009, **20**, 283–292.
- 1043 4 J. R. Werber, C. O. Osuji and M. Elimelech, *Nat. Rev. Mater.*, 2016, **1**, 16018.
- 1044 5 D. Wandera, S. R. Wickramasinghe and S. M. Husson, *J. Memb. Sci.*, 2010, **357**, 6–35.
- 1045 6 Q. Zhang, E. Uchaker, S. L. Candelaria and G. Cao, *Chem. Soc. Rev.*, 2013, **42**, 3127–
1046 3171.
- 1047 7 D. L. Gin, X. Lu, P. R. Nemade, C. S. Pecinovsky, Y. Xu and M. Zhou, *Adv. Funct.*
1048 *Mater.*, 2006, **16**, 865–878.
- 1049 8 H. Hu, M. Gopinadhan and C. O. Osuji, *Soft Matter*, 2014, **10**, 3867.
- 1050 9 S. T. Hyde, in *Handbook of Applied Surface and Colloid Chemistry*, 2001, pp. 299–
1051 332.
- 1052 10 T. Tachibana, T. Mori and K. Hori, *Bull. Chem. Soc. Jpn.*, 1980, **53**, 1714–1719.
- 1053 11 R. Atkin, S. M. C. Bobillier and G. G. Warr, *J. Phys. Chem. B*, 2010, **114**, 1350–1360.
- 1054 12 L. A. Robertson, M. R. Schenkel, B. R. Wiesenauer and D. L. Gin, *Chem. Commun.*,
1055 2013, **49**, 9407–9409.
- 1056 13 R. Nagarajan, *Langmuir*, 2002, **18**, 31–38.
- 1057 14 V. Lutz-Bueno, S. Isabetini, F. Walker, S. Kuster, M. Liebi and P. Fischer, *Phys.*
1058 *Chem. Chem. Phys.*, 2017, **19**, 21869–21877.
- 1059 15 Y. C. Lee, T. F. Taraschi and N. Janes, *Biophys. J.*, 1993, **65**, 1429–1432.
- 1060 16 Y. Huang and S. Gui, *RSC Adv.*, 2018, **8**, 6978–6987.

- 1061 17 S. S. Soni, G. Brotons, M. Bellour, T. Narayanan and A. Gibaud, *J. Phys. Chem. B*,
1062 2006, **110**, 15157–15165.
- 1063 18 R. Rajabalaya, M. N. Musa, N. Kifli and S. R. David, *Drug Des. Devel. Ther.*, 2017,
1064 **Volume11**, 393–406.
- 1065 19 Y. Meng, D. Gu, F. Zhang, Y. Shi, L. Cheng, D. Feng, Z. Wu, Z. Chen, Y. Wan, A.
1066 Stein and D. Zhao, *Chem. Mater.*, 2006, **18**, 4447–4464.
- 1067 20 A. Jayaraman, D. Y. Zhang, B. L. Dewing and M. K. Mahanthappa, *ACS Cent. Sci.*,
1068 2019, **5**, 619–628.
- 1069 21 C. M. Baez-Cotto and M. K. Mahanthappa, *ACS Nano*, 2018, **12**, 3226–3234.
- 1070 22 J. Jennings, B. Green, T. J. Mann, C. A. Guymon and M. K. Mahanthappa, *Chem.*
1071 *Mater.*, 2018, **30**, 185–196.
- 1072 23 A. Jayaraman and M. K. Mahanthappa, *Langmuir*, 2018, **34**, 2290–2301.
- 1073 24 I. Moriguchi, A. Ozono, K. Mikuriya, Y. Teraoka, S. Kagawa and M. Kodama, *Chem.*
1074 *Lett.*, 1999, 1171–1172.
- 1075 25 H.-P. Hentze, C. C. Co, C. A. McKelvey and E. W. Kaler, in *Topics in Current*
1076 *Chemistry*, 2003, pp. 197–223.
- 1077 26 K. S. Worthington, C. Baguenard, B. S. Forney and C. A. Guymon, *J. Polym. Sci. Part*
1078 *B Polym. Phys.*, 2017, **55**, 471–489.
- 1079 27 C. Wang, D. Chen and X. Jiao, *Sci. Technol. Adv. Mater.*, 2009, **10**, 023001.
- 1080 28 D. L. Gin, W. Gu, B. A. Pindzola and W.-J. Zhou, *Acc. Chem. Res.*, 2001, **34**, 973–
1081 980.
- 1082 29 M. S. Mauter, M. Elimelech and C. O. Osuji, *ACS Nano*, 2010, **4**, 6651–6658.
- 1083 30 X. Feng, Q. Imran, Y. Zhang, L. Sixdenier, X. Lu, G. Kaufman, U. Gabinet, K.
1084 Kawabata, M. Elimelech and C. O. Osuji, *Sci. Adv.*, 2019, **5**, eaav9308.
- 1085 31 S. Qavi, A. P. Lindsay, M. A. Firestone and R. Foudazi, *J. Memb. Sci.*, 2019, **580**,
1086 125–133.
- 1087 32 S. M. Dischinger, J. Rosenblum, R. D. Noble, D. L. Gin and K. G. Linden, *J. Memb.*
1088 *Sci.*, 2017, **543**, 319–327.
- 1089 33 M. Zhou, P. R. Nemade, X. Lu, X. Zeng, E. S. Hatakeyama, R. D. Noble and D. L.
1090 Gin, *J. Am. Chem. Soc.*, 2007, **129**, 9574–9575.
- 1091 34 D. L. Gin, J. E. Bara, R. D. Noble and B. J. Elliott, *Macromol. Rapid Commun.*, 2008,
1092 **29**, 367–389.
- 1093 35 C. A. Guymon and C. L. Lester, *ACS Symp. Ser.*, 2003, **847**, 378–388.
- 1094 36 C. L. Lester, S. M. Smith, W. L. Jarrett and C. Allan Guymon, *Langmuir*, 2003, **19**,
1095 9466–9472.
- 1096 37 J. R. McLaughlin, N. L. Abbott and C. A. Guymon, *Polymer*, 2018, **142**, 119–126.

- 1097 38 M. A. DePierro, A. J. Olson and C. A. Guymon, *Polymer*, 2005, **46**, 335–345.
- 1098 39 M. A. DePierro, K. G. Carpenter and C. A. Guymon, *Chem. Mater.*, 2006, **18**, 5609–
1099 5617.
- 1100 40 B. S. Forney, C. Baguenard and C. A. Guymon, *Chem. Mater.*, 2013, **25**, 2950–2960.
- 1101 41 B. S. Forney, C. Baguenard and C. Allan Guymon, *Soft Matter*, 2013, **9**, 7458–7467.
- 1102 42 C. L. Lester, C. D. Colson and C. A. Guymon, *Macromolecules*, 2001, **34**, 4430–4438.
- 1103 43 C. L. Lester, S. M. Smith, C. D. Colson and C. A. Guymon, *Chem. Mater.*, 2003, **15**,
1104 3376–3384.
- 1105 44 D. T. McCormick, K. D. Stovall and C. A. Guymon, *Macromolecules*, 2003, **36**, 6549–
1106 6558.
- 1107 45 J. D. Clapper and C. A. Guymon, *Mol. Cryst. Liq. Cryst.*, 2009, **509**, 30/[772]-
1108 38/[780].
- 1109 46 C. R. López-Barrón, R. Chen and N. J. Wagner, *ACS Macro Lett.*, 2016, **5**, 1332–1338.
- 1110 47 Y. Xie, R. Xie, H. C. Yang, Z. Chen, J. Hou, C. R. López-Barrón, N. J. Wagner and K.
1111 Z. Gao, *ACS Appl. Mater. Interfaces*, 2018, **10**, 32435–32443.
- 1112 48 C. R. López-Barrón, R. Chen, N. J. Wagner and P. J. Beltramo, *Macromolecules*,
1113 2016, **49**, 5179–5189.
- 1114 49 W. Gu, W. J. Zhou and D. L. Gin, *Chem. Mater.*, 2001, **13**, 1949–1951.
- 1115 50 R. C. Smith, W. M. Fischer and D. L. Gin, *J. Am. Chem. Soc.*, 1997, **119**, 4092–4093.
- 1116 51 D. H. Gray, S. Hu, E. Juang and D. L. Gin, *Adv. Mater.*, 1997, **9**, 731–736.
- 1117 52 M. J. McGrath, N. Patterson, B. C. Manubay, S. H. Hardy, J. J. Malecha, Z. Shi, X.
1118 Yue, X. Xing, H. H. Funke, D. L. Gin, P. Liu and R. D. Noble, *Ind. Eng. Chem. Res.*,
1119 2019, **58**, 22250–22259.
- 1120 53 J. Herz, F. Reiss-Husson, P. Rempp and V. Luzzati, *J. Polym. Sci. Part C Polym.*
1121 *Symp.*, 2007, **4**, 1275–1290.
- 1122 54 P. Ström and D. M. Anderson, *Langmuir*, 1992, **8**, 691–709.
- 1123 55 J. Zhang, Z. A. Qiao, S. M. Mahurin, X. Jiang, S. H. Chai, H. Lu, K. Nelson and S.
1124 Dai, *Angew. Chemie - Int. Ed.*, 2015, **54**, 4582–4586.
- 1125 56 S. Qavi, A. Bandegi, M. Firestone and R. Foudazi, *Soft Matter*, 2019, **15**, 8238–8250.
- 1126 57 S. E. Friberg, R. Thundathil and J. O. Stoffer, *Science (80-.)*, 1979, **205**, 607–608.
- 1127 58 Y. S. Lee, J. T. Gleeson, J. Z. Yang, T. M. Sisson, D. A. Frankel, D. F. O'Brien, S. L.
1128 Keller, E. Aksay and S. M. Gruner, *J. Am. Chem. Soc.*, 1995, **117**, 5573–5578.
- 1129 59 C.-M. Young, C. L. Chang, Y.-H. Chen, C.-Y. Chen, Y.-F. Chang and H.-L. Chen,
1130 *Soft Matter*, 2021, **17**, 397–409.

- 1131 60 B. Soberats, M. Yoshio, T. Ichikawa, X. Zeng, H. Ohno, G. Ungar and T. Kato, *J. Am.*
1132 *Chem. Soc.*, 2015, **137**, 13212–13215.
- 1133 61 B. A. Pindzola, J. Jin and D. L. Gin, *J. Am. Chem. Soc.*, 2003, **125**, 2940–2949.
- 1134 62 S. Qavi, M. A. Firestone and R. Foudazi, *Soft Matter*, 2019, **15**, 5626–5637.
- 1135 63 M. G. Marquez Garcia, New Mexico State University, 2020.
- 1136 64 S. A. Kim, K.-J. Jeong, A. Yethiraj and M. K. Mahanthappa, *Proc. Natl. Acad. Sci.*,
1137 2017, **114**, 4072–4077.
- 1138 65 F. C. Frank and J. S. Kasper, *Acta Crystallogr.*, 1958, **11**, 184–190.
- 1139 66 F. C. Frank and J. S. Kasper, *Acta Crystallogr.*, 1959, **12**, 483–499.
- 1140 67 M. Huang, K. Yue, J. Wang, C.-H. Hsu, L. Wang and S. Z. D. Cheng, *Sci. China*
1141 *Chem.*, 2018, **61**, 33–45.
- 1142 68 D. Roux, C. Coulon and M. E. Cates, *J. Phys. Chem.*, 1992, **96**, 4174–4187.
- 1143 69 B. Angelov, A. Angelova, R. Mutafchieva, S. Lesieur, U. Vainio, V. M. Garamus, G.
1144 V. Jensen and J. S. Pedersen, *Phys. Chem. Chem. Phys.*, 2011, **13**, 3073–3081.
- 1145 70 B. Kent, C. J. Garvey, D. Cookson and G. Bryant, *Chem. Phys. Lipids*, 2009, **157**, 56–
1146 60.
- 1147 71 R. Thundathil, J. O. Stoffer and S. E. Friberg, *J. Polym. Sci. A1.*, 1980, **18**, 2629–2640.
- 1148 72 Y. Shibasaki and K. Fukuda, *Colloids and Surfaces*, 1992, **67**, 195–201.
- 1149 73 K. M. McGrath and C. J. Drummond, *Colloid Polym. Sci.*, 1996, **274**, 316–333.
- 1150 74 K. M. McGrath, *Colloid Polym. Sci.*, 1996, **274**, 499–512.
- 1151 75 K. M. McGrath, *Colloid Polym. Sci.*, 1996, **274**, 399–409.
- 1152 76 D. Pawlowski, A. Haibel and M. Tieke, *Berichte der Bunsengesellschaft/Physical*
1153 *Chem. Chem. Phys.*, 1998, **102**, 1865–1869.
- 1154 77 M. Li, W. Yang, Z. Chen, J. Qian, C. Wang and S. Fu, *J. Polym. Sci. Part A Polym.*
1155 *Chem.*, 2006, **44**, 5887–5897.
- 1156 78 H. Deng, D. L. Gin and R. C. Smith, *J. Am. Chem. Soc.*, 1998, **120**, 3522–3523.
- 1157 79 G. E. Dwulet and D. L. Gin, *Chem. Commun.*, 2018, **54**, 12053–12056.
- 1158 80 B. S. Ringstrand, S. Seifert, D. W. Podlesak and M. A. Firestone, *Macromol. Rapid*
1159 *Commun.*, 2016, **37**, 1155–1167.
- 1160 81 S. Peng, P. G. Hartley, T. C. Hughes and Q. Guo, *Soft Matter*, 2015, **11**, 6318–6326.
- 1161 82 W. Srisiri, T. M. Sisson, D. F. O'Brien, K. M. McGrath, Y. Han and S. M. Gruner, *J.*
1162 *Am. Chem. Soc.*, 1997, **119**, 4866–4873.
- 1163 83 M. A. Reppy, D. H. Gray, B. A. Pindzola, J. L. Smithers and D. L. Gin, *J. Am. Chem.*

- 1164 *Soc.*, 2001, **123**, 363–371.
- 1165 84 B. P. Hoag and D. L. Gin, *Macromolecules*, 2000, **33**, 8549–8558.
- 1166 85 B. A. Pindzola, B. P. Hoag and D. L. Gin, *J. Am. Chem. Soc.*, 2001, **123**, 4617–4618.
- 1167 86 D. Batra, D. N. T. Hay and M. A. Firestone, *Chem. Mater.*, 2007, **19**, 4423–4431.
- 1168 87 D. Batra, S. Seifert and M. A. Firestone, *Macromol. Chem. Phys.*, 2007, **208**, 1416–
1169 1427.
- 1170 88 S. Grubjesic, S. Seifert and M. A. Firestone, *Macromolecules*, 2009, **42**, 5461–5470.
- 1171 89 L. Sievens-Figueroa and C. A. Guymon, *Chem. Mater.*, 2009, **21**, 1060–1068.
- 1172 90 G. A. Becht, M. Sofos, S. Seifert and M. A. Firestone, *Macromolecules*, 2011, **44**,
1173 1421–1428.
- 1174 91 B. G. Ndefru, B. S. Ringstrand, S. I. Y. Diouf, S. Seifert, J. H. Leal, T. A.
1175 Semelsberger, T. A. Dreier and M. A. Firestone, *Mol. Syst. Des. Eng.*, 2019, **4**, 580–
1176 585.
- 1177 92 J. Jin, V. Nguyen, W. Gu, X. Lu, B. J. Elliott and D. L. Gin, *Chem. Mater.*, 2005, **17**,
1178 224–226.
- 1179 93 M. Zhou, T. J. Kidd, R. D. Noble and D. L. Gin, *Adv. Mater.*, 2005, **17**, 1850–1853.
- 1180 94 J. E. Bara, A. K. Kaminski, R. D. Noble and D. L. Gin, *J. Memb. Sci.*, 2007, **288**, 13–
1181 19.
- 1182 95 Y. Xu, W. Gu and D. L. Gin, *J. Am. Chem. Soc.*, 2004, **126**, 1616–1617.
- 1183 96 L. Sievens-Figueroa and C. A. Guymon, *Macromolecules*, 2009, **42**, 9243–9250.
- 1184 97 C. L. Lester and C. A. Guymon, *Polymer*, 2002, **43**, 3707–3715.
- 1185 98 L. Sievens-Figueroa and C. Allan Guymon, *Polymer*, 2008, **49**, 2260–2267.
- 1186 99 M. A. DePierro, C. Baguenard and C. Allan Guymon, *J. Polym. Sci. Part A Polym.*
1187 *Chem.*, 2016, **54**, 144–154.
- 1188 100 D. H. Gray and D. L. Gin, *Chem. Mater.*, 1998, **10**, 1827–1832.
- 1189 101 H. P. Hentze, E. Krämer, B. Berton, S. Förster, M. Antonietti and M. Dreja,
1190 *Macromolecules*, 1999, **32**, 5803–5809.
- 1191 102 J. Yang and G. Wegner, *Macromolecules*, 1992, **25**, 1791–1795.
- 1192 103 B. Ringstrand, S. Seifert and M. A. Firestone, *J. Polym. Sci. Part B Polym. Phys.*,
1193 2013, **51**, 1215–1227.
- 1194 104 M. Imai, K. Sakai, M. Kikuchi, K. Nakaya, A. Saeki and T. Teramoto, *J. Chem. Phys.*,
1195 2005, **122**, 214906.
- 1196 105 S. Grubjesic, B. Lee, S. Seifert and M. A. Firestone, *Soft Matter*, 2011, **7**, 9695.

- 1197 106 P. C. Hartmann and R. D. Sanderson, *Macromol. Symp.*, 2005, **225**, 229–237.
- 1198 107 B. R. Wiesenauer and D. L. Gin, *Polym. J.*, 2012, **44**, 461–468.
- 1199 108 W. Srisiri, A. Benedicto, D. F. O'Brien, T. P. Trouard, G. Orädd, S. Persson and G.
1200 Lindblom, *Langmuir*, 1998, **14**, 1921–1926.
- 1201 109 A. Mueller and D. F. O'Brien, *Chem. Rev.*, 2002, **102**, 727–757.
- 1202 110 D. Yang, D. F. O'Brien and S. R. Marder, *J. Am. Chem. Soc.*, 2002, **124**, 13388–
1203 13389.
- 1204 111 D. F. O'Brien, B. Armitage, A. Benedicto, D. E. Bennett, H. G. Lamparski, Y. S. Lee,
1205 W. Srisiri and T. M. Sisson, *Acc. Chem. Res.*, 1998, **31**, 861–868.
- 1206 112 G. E. Dwulet, S. M. Dischinger, M. J. McGrath, A. J. Basalla, J. J. Malecha, R. D.
1207 Noble and D. L. Gin, *Ind. Eng. Chem. Res.*, 2019, **58**, 21890–21893.
- 1208 113 M. J. McGrath, S. H. Hardy, A. J. Basalla, G. E. Dwulet, B. C. Manubay, J. J.
1209 Malecha, Z. Shi, H. H. Funke, D. L. Gin and R. D. Noble, *ACS Mater. Lett.*, 2019, **1**,
1210 452–458.
- 1211 114 S. M. Dischinger, J. Rosenblum, R. D. Noble and D. L. Gin, *J. Memb. Sci.*, 2019, **592**,
1212 117313.
- 1213 115 X. Lu, V. Nguyen, M. Zhou, X. Zeng, J. Jin, B. J. Elliott and D. L. Gin, *Adv. Mater.*,
1214 2006, **18**, 3294–3298.
- 1215 116 R. L. Kerr, S. A. Miller, R. K. Shoemaker, B. J. Elliott and D. L. Gin, *J. Am. Chem.*
1216 *Soc.*, 2009, **131**, 15972–15973.
- 1217 117 X. Liang, X. Lu, M. Yu, A. S. Cavanagh, D. L. Gin and A. W. Weimer, *J. Memb. Sci.*,
1218 2010, **349**, 1–5.
- 1219 118 E. S. Hatakeyama, B. R. Wiesenauer, C. J. Gabriel, R. D. Noble and D. L. Gin, *Chem.*
1220 *Mater.*, 2010, **22**, 4525–4527.
- 1221 119 E. S. Hatakeyama, C. J. Gabriel, B. R. Wiesenauer, J. L. Lohr, M. Zhou, R. D. Noble
1222 and D. L. Gin, *J. Memb. Sci.*, 2011, **366**, 62–72.
- 1223 120 B. M. Carter, B. R. Wiesenauer, E. S. Hatakeyama, J. L. Barton, R. D. Noble and D. L.
1224 Gin, *Chem. Mater.*, 2012, **24**, 4005–4007.
- 1225 121 B. M. Carter, B. R. Wiesenauer, R. D. Noble and D. L. Gin, *J. Memb. Sci.*, 2014, **455**,
1226 143–151.
- 1227 122 C. L. Lester and C. A. Guymon, *Macromolecules*, 2000, **33**, 5448–5454.
- 1228 123 K. M. McGrath and C. J. Drummond, *Colloid Polym. Sci.*, 1996, **274**, 612–621.
- 1229 124 M. H. Li, W. L. Yang, J. Qian, C. C. Wang and S. K. Fu, *Des. Monomers Polym.*,
1230 2004, **7**, 505–519.
- 1231 125 X. Feng, M. E. Tousley, M. G. Cowan, B. R. Wiesenauer, S. Nejati, Y. Choo, R. D.
1232 Noble, M. Elimelech, D. L. Gin and C. O. Osuji, *ACS Nano*, 2014, **8**, 11977–11986.

- 1233 126 C. T. Burns, S. Lee, S. Seifert and M. A. Firestone, *Polym. Adv. Technol.*, 2008, **19**,
1234 1369–1382.
- 1235 127 P. M. Welch, T. A. Dreier, H. D. Magurudeniya, M. G. Frith, J. Ilavsky, S. Seifert, A.
1236 K. Rahman, A. Rahman, A. J. Singh, B. S. Ringstrand, C. J. Hanson, J. A.
1237 Hollingsworth and M. A. Firestone, *Macromolecules*, 2020, **53**, 2822–2833.
- 1238 128 C. S. Pecinovsky, E. S. Hatakeyama and D. L. Gin, *Adv. Mater.*, 2008, **20**, 174–178.
- 1239 129 W. Zhou, W. Gu, Y. Xu, C. S. Pecinovsky and D. L. Gin, *Langmuir*, 2003, **19**, 6346–
1240 6348.
- 1241 130 C. S. Pecinovsky, G. D. Nicodemus and D. L. Gin, *Chem. Mater.*, 2005, **17**, 4889–
1242 4891.
- 1243 131 M. Antonietti, R. A. Caruso, C. G. Göltner and M. C. Weissenberger,
1244 *Macromolecules*, 1999, **32**, 1383–1389.
- 1245 132 J. Zhang, Z. Xie, A. J. Hill, F. H. She, A. W. Thornton, M. Hoang and L. X. Kong, *Soft*
1246 *Matter*, 2012, **8**, 2087–2094.
- 1247 133 J. Zhang, Z. Xie, M. Hoang, A. J. Hill, W. Cong, F. H. She, W. Gao and L. X. Kong,
1248 *Soft Matter*, 2014, **10**, 5192–5200.
- 1249 134 J. Zhang, Z. Xie, A. J. Hill, W. Cong, F. H. She, W. Gao, M. Hoang and L. X. Kong,
1250 *Polym. Bull.*, 2018, **75**, 581–595.
- 1251 135 J. D. Clapper and C. A. Guymon, *Adv. Mater.*, 2006, **18**, 1575–1580.
- 1252 136 M. E. Tousley, X. Feng, M. Elimelech and C. O. Osuji, *ACS Appl. Mater. Interfaces*,
1253 2014, **6**, 19710–19717.
- 1254 137 S. Qavi, New Mexico State University, 2019.
- 1255 138 C. Liang and S. Dai, *J. Am. Chem. Soc.*, 2006, **128**, 5316–5317.
- 1256 139 C. M. Ghimbeu, M. Sopronyi, F. Sima, C. Vaultot, L. Vidal, J. M. Le Meins and L.
1257 Delmotte, *RSC Adv.*, 2015, **5**, 2861–2868.
- 1258 140 S. Herou, M. C. Ribadeneyra, R. Madhu, V. Araullo-Peters, A. Jensen, P. Schlee and
1259 M. Titirici, *Green Chem.*, 2019, **21**, 550–559.
- 1260 141 X. Wang, C. Liang and S. Dai, *Langmuir*, 2008, **24**, 7500–7505.
- 1261 142 A. Bandegi, J. L. Bañuelos and R. Foudazi, *Soft Matter*, 2020, **16**, 6102–6114.
- 1262 143 J. D. Clapper and C. A. Guymon, *Macromolecules*, 2007, **40**, 7951–7959.
- 1263 144 J. D. Clapper, S. L. Iverson and C. A. Guymon, *Biomacromolecules*, 2007, **8**, 2104–
1264 2111.
- 1265 145 D. M. Anderson and P. Ström, ACS Symposium Series, 1989, pp. 204–224.
- 1266 146 M. Jung, A. L. German and H. R. Fischer, *Colloid Polym. Sci.*, 2001, **279**, 105–113.
- 1267 147 D. M. Anderson and P. Ström, *Phys. A Stat. Mech. its Appl.*, 1991, **176**, 151–167.

- 1268 148 R. Laversanne, *Macromolecules*, 1992, **25**, 489–491.
- 1269 149 B. S. Forney and C. Allan Guymon, *Macromol. Rapid Commun.*, 2011, **32**, 765–769.
- 1270 150 M. A. DePierro and C. A. Guymon, *Macromolecules*, 2006, **39**, 617–626.
- 1271 151 B. S. Forney and C. A. Guymon, *Macromolecules*, 2010, **43**, 8502–8510.
- 1272 152 H. P. Hentze, C. G. Göltner and M. Antonietti, *Berichte der*
1273 *Bunsengesellschaft/Physical Chem. Chem. Phys.*, 1997, **101**, 1699–1702.
- 1274 153 M. A. DePierro, K. G. Carpenter and C. A. Guymon, *Radtech Tech. Proc.*, 2006.
- 1275 154 Y. Saadat, K. Kim and R. Foudazi, *Polym. Chem.*, 2021, **12**, 2236–2252.
- 1276 155 W. Meier, *Macromolecules*, 1998, **31**, 2212–2217.
- 1277 156 M. Antonietti, C. Göltner and H. P. Hentze, *Langmuir*, 1998, **14**, 2670–2672.
- 1278 157 C. L. Lester, S. M. Smith and C. A. Guymon, *Macromolecules*, 2001, **34**, 8587–8589.
- 1279 158 J. F. Hulvat and S. I. Stupp, *Angew. Chemie - Int. Ed.*, 2003, **42**, 778–781.
- 1280 159 J. F. Hulvat and S. I. Stupp, *Adv. Mater.*, 2004, **16**, 589–592.
- 1281 160 S. Ghosh, H. Remita, L. Ramos, A. Dazzi, A. Deniset-Besseau, P. Beaunier, F.
1282 Goubard, P.-H. Aubert, F. Brisset and S. Remita, *New J. Chem.*, 2014, **38**, 1106–1115.
- 1283 161 M. N. Wadekar, R. Pasricha, A. B. Gaikwad and G. Kumaraswamy, *Chem. Mater.*,
1284 2005, **17**, 2460–2465.
- 1285 162 M. A. DePierro, A. J. Olson and C. A. Guymon, *Radtech Tech. Proc.*, 2004.
- 1286 163 M. A. Depierro and C. A. Guymon, *Macromolecules*, 2014, **47**, 5728–5738.
- 1287 164 J. D. Clapper and C. Allan Guymon, *Macromolecules*, 2007, **40**, 1101–1107.
- 1288 165 Z. Li, W. Yan and S. Dai, *Carbon N. Y.*, 2004, **42**, 767–770.
- 1289 166 D. Y. Liu and D. V. Krogstad, *Macromolecules*, 2021, **54**, 988–994.
- 1290 167 S. Ghosh, L. Ramos, S. Remita, A. Dazzi, A. Deniset-Besseau, P. Beaunier, F.
1291 Goubard, P.-H. Aubert and H. Remita, *New J. Chem.*, 2015, **39**, 8311–8320.
- 1292 168 D. Floresyona, F. Goubard, P.-H. Aubert, I. Lampre, J. Mathurin, A. Dazzi, S. Ghosh,
1293 P. Beaunier, F. Brisset, S. Remita, L. Ramos and H. Remita, *Appl. Catal. B Environ.*,
1294 2017, **209**, 23–32.
- 1295 169 S. Dutt and P. F. Siril, *J. Appl. Polym. Sci.*, 2014, **131**, 40800.
- 1296 170 Y. Zhang, R. Dong, U. R. Gabinet, R. Poling-Skutvik, N. K. Kim, C. Lee, O. Q. Imran,
1297 X. Feng and C. O. Osuji, *ACS Nano*, 2021, acsnano.1c00722.
- 1298 171 J. A. Castellano, *Mol. Cryst. Liq. Cryst.*, 1983, **94**, 33–41.
- 1299 172 X. Feng, S. Nejati, M. G. Cowan, M. E. Tousley, B. R. Wiesenauer, R. D. Noble, M.
1300 Elimelech, D. L. Gin and C. O. Osuji, *ACS Nano*, 2016, **10**, 150–158.

- 1301 173 Y. Guo, H. Shahsavan, Z. S. Davidson and M. Sitti, *ACS Appl. Mater. Interfaces*,
1302 2019, **11**, 36110–36117.
- 1303 174 S. Qavi and R. Foudazi, *Rheol. Acta*, 2019, **58**, 483–498.
- 1304 175 K. Yue, C. Liu, K. Guo, K. Wu, X.-H. Dong, H. Liu, M. Huang, C. Wesdemiotis, S. Z.
1305 D. Cheng and W.-B. Zhang, *Polym. Chem.*, 2013, **4**, 1056–1067.
- 1306 176 X. Yu, Y. Li, X.-H. Dong, K. Yue, Z. Lin, X. Feng, M. Huang, W.-B. Zhang and S. Z.
1307 D. Cheng, *J. Polym. Sci. Part B Polym. Phys.*, 2014, **52**, 1309–1325.
- 1308 177 I. C. Reynhout, J. J. L. M. Cornelissen and R. J. M. Nolte, *Acc. Chem. Res.*, 2009, **42**,
1309 681–692.
- 1310 178 X. Yu, K. Yue, I.-F. Hsieh, Y. Li, X.-H. Dong, C. Liu, Y. Xin, H.-F. Wang, A.-C. Shi,
1311 G. R. Newkome, R.-M. Ho, E.-Q. Chen, W.-B. Zhang and S. Z. D. Cheng, *Proc. Natl.*
1312 *Acad. Sci.*, 2013, **110**, 10078–10083.
- 1313 179 W.-J. Yoon, K. M. Lee, D. R. Evans, M. E. McConney, D.-Y. Kim and K.-U. Jeong, *J.*
1314 *Mater. Chem. C*, 2019, **7**, 8500–8514.
- 1315 180 B. Angelov, A. Angelova, M. Ollivon, C. Bourgaux and A. Campitelli, *J. Am. Chem.*
1316 *Soc.*, 2003, **125**, 7188–7189.
- 1317 181 H. M. G. Barriga, A. I. I. Tyler, N. L. C. McCarthy, E. S. Parsons, O. Ces, R. V. Law,
1318 J. M. Seddon and N. J. Brooks, *Soft Matter*, 2015, **11**, 600–607.
- 1319 182 A. I. I. Tyler, H. M. G. Barriga, E. S. Parsons, N. L. C. McCarthy, O. Ces, R. V. Law,
1320 J. M. Seddon and N. J. Brooks, *Soft Matter*, 2015, **11**, 3279–3286.
- 1321 183 R. Bruinsma, *J. Phys. II*, 1992, **2**, 425–451.
- 1322 184 H. Kim, Z. Song and C. Leal, *Proc. Natl. Acad. Sci.*, 2017, **114**, 10834–10839.
- 1323 185 S. S. W. Leung and C. Leal, *Soft Matter*, 2019, **15**, 1269–1277.
- 1324 186 A. Zabara, J. T. Y. Chong, I. Martiel, L. Stark, B. A. Cromer, C. Speziale, C. J.
1325 Drummond and R. Mezzenga, *Nat. Commun.*, 2018, **9**, 544.
- 1326 187 C. Chen, S. Wang, B. P. Grady, J. H. Harwell and B.-J. Shiau, *Langmuir*, 2019, **35**,
1327 12168–12179.
- 1328 188 J.-Y. Choi, T. Yun and S.-Y. Kwak, *J. Memb. Sci.*, 2018, **554**, 117–124.
- 1329 189 P. M. Simone and T. P. Lodge, *Macromolecules*, 2008, **41**, 1753–1759.
- 1330 190 A. Panday, S. Mullin, E. D. Gomez, N. Wanakule, V. L. Chen, A. Hexemer, J. Pople
1331 and N. P. Balsara, *Macromolecules*, 2009, **42**, 4632–4637.
- 1332 191 N. S. Wanakule, A. Panday, S. A. Mullin, E. Gann, A. Hexemer and N. P. Balsara,
1333 *Macromolecules*, 2009, **42**, 5642–5651.
- 1334 192 M. Singh, O. Odusanya, G. M. Wilmes, H. B. Eitouni, E. D. Gomez, A. J. Patel, V. L.
1335 Chen, M. J. Park, P. Fragouli, H. Iatrou, N. Hadjichristidis, D. Cookson and N. P.
1336 Balsara, *Macromolecules*, 2007, **40**, 4578–4585.

- 1337 193 M. L. Hoarfrost, M. S. Tyagi, R. A. Segalman and J. A. Reimer, *Macromolecules*,
1338 2012, **45**, 3112–3120.
- 1339 194 J. M. Virgili, M. L. Hoarfrost and R. A. Segalman, *Macromolecules*, 2010, **43**, 5417–
1340 5423.
- 1341 195 W.-S. Young, W.-F. Kuan and T. H. Epps, *J. Polym. Sci. Part B Polym. Phys.*, 2014,
1342 **52**, 1–16.
- 1343 196 S. Akbar, J. M. Elliott, A. M. Squires and A. Anwar, *J. Nanoparticle Res.*, 2020, **22**,
1344 170.
- 1345 197 S. Ghosh, L. Ramos and H. Remita, *Nanoscale*, 2018, **10**, 5793–5819.
- 1346 198 X. Fan, Z. Zhang, G. Li and N. A. Rowson, *Chem. Eng. Sci.*, 2004, **59**, 2639–2645.
- 1347 199 A. Thomas, F. Goettmann and M. Antonietti, *Chem. Mater.*, 2008, **20**, 738–755.
- 1348 200 X. Wang, K. S. K. Lin, J. C. C. Chan and S. Cheng, *J. Phys. Chem. B*, 2005, **109**,
1349 1763–1769.
- 1350 201 X. S. Zhao, G. Q. (Max) Lu and G. J. Millar, *Ind. Eng. Chem. Res.*, 1996, **35**, 2075–
1351 2090.
- 1352 202 F. das C. M. da Silva, M. J. dos S. Costa, L. K. R. da Silva, A. M. Batista and G. E. da
1353 Luz, *SN Appl. Sci.*, 2019, **1**, 654.
- 1354 203 J. H. Ding and D. L. Gin, *Chem. Mater.*, 2000, **12**, 22–24.
- 1355